The modified Q-cycle: A look back at its development and forward to a functional model

Antony R. Crofts

PII: S0005-2728(21)00050-5

DOI: https://doi.org/10.1016/j.bbabio.2021.148417

Reference: BBABIO 148417

To appear in: *BBA - Bioenergetics*

Received date: 6 January 2021

Revised date: 28 February 2021

Accepted date: 11 March 2021

Please cite this article as: A.R. Crofts, The modified Q-cycle: A look back at its development and forward to a functional model, *BBA - Bioenergetics* (2021), https://doi.org/10.1016/j.bbabio.2021.148417

The modified Q-cycle: A look back at its development and forward to a functional model

by

Antony R. Crofts, Professor Emeritus

Department of Biochemistry, 417 Roger Adams Laboratory, 600 South Mathews Avenue,

Urbana, IL 61801

Abstract

On looking back at a lifetime of research, it is interesting to see, in the light of current progress, how things came to be, and to speculate on how things might be. I am delighted in the context of the Mitchell prize to have that excuse to present this necessarily personal view of developments in areas of my interests. I have focused on the Q-cycle and a few examples showing wider ramifications, since that had been the main interest of the lab in the 20 years since structures became available, - a watershed event in determining our molecular perspective. I have reviewed the evidence for our model for the mechanism of the first electron transfer of the bifurcated reaction at the Q_o-site, which I think is compelling. In reviewing progress in understanding the second electron transfer, I have revisited some controversies to justify important conclusions which appear, from the literature, not to have been taken seriously. I hope this does not come over as nitpicking. The conclusions are important to the final section in which I develop an internally consistent mechanism for turnovers of the complex leading to a state similar to that observed in recent rapid-mix/freeze-quench experiments, reported three years ago. The final model is necessarily speculative but is open to test.

1. Introduction

Since my PhD work with Brian Chappell starting in 1961, a lifetime of research in respiratory and photosynthetic energy conversion has provided excitement, disappointment, and fulfillment, and even some achievements that have stood the test of time. It is, of course, painful to recognize that a career must end (at least in terms of practical research), but after six years of failure to obtain any support, I gave up trying two years ago, happy to have brought my last three students successfully to substantial PhDs, through the kind support of the Department. This brief review will therefore necessarily be retrospective. Rather than rehash everything from those 59 years, I want to look back at a few significant achievements, to show how they subsequently played out, to speculate on what is still missing, and to offer some lessons I have learned from the controversies involved. Although a substantial fraction of our work involved green plant photosynthesis, I will concentrate on the work on the bc_1 complex, since that has occupied the lab for the last two decades.

A. PhD and post-doctoral work

Intellectual credit for my PhD work obviously belongs to Brian, but it is worth noting that the 4 papers [1-4] summarized in [5], spawned three areas of research still identifiable as mainstream themes. Brian started me off in the library trying to understand a paper by Mitchell [6], "- a bit wild, but there's maybe something in it…", - which launched the chemiosmotic hypotheses, and this introduction then steered the enterprise. The work on atractylate inhibition [3] revealed the adenylate and, in parallel, the phosphate exchange enzymes [5], to establish the first of the carrier mechanisms allowing exchange of matrix with the cytoplasmic metabolites critical to Mitchell's hypothesis; the work on gramicidin-induced K^+ transport [2] introduced the ionophoric mechanism, and by extension, that of other ionophores, including valinomycin and protonophoric uncouplers; the work on Ca^{2+}-uptake, and the swelling it induced [1, 4], can be seen as opening in the chemiosmotic context the discussion on Ca^{2+}-induced swelling of mitochondria and cellular disruption, important for example in response to reperfusion after ischemia. The role of a mitochondrial permeability pore, and outer membrane permeabilization in release of cytochrome *c* and the apoptosis inducing factor (AIF) to initiate programmed cell death through apoptosis, necrosis, autophagy, and cellular recycling, are now important areas of research, but unknown then. More generally, the work provided some of the first experimental evidence supporting wider aspects of Mitchell's hypothesis. Another feature of the research was exploitation of the permeability of NH_3 in experiments to show, through the co-transport of ammonium salts, the presence of neutral substrate antiporters, initially that for phosphate [5]. In my post-doctoral work in Les Packer's lab, I showed that the differential permeability of the NH_3/NH_4^+ species provided a mechanism for amine uncoupling in chloroplasts [7-11]. This was made possible by a eureka moment; while dawdling along the corridor worrying about artifacts when using the K^+-electrode to measure ion transport, it occurred to me that the electrode might be sensitive to NH_4^+. It was, making possible direct measurement of the kinetics of NH_4^+-uptake on illumination.

B. Early work on photosynthetic bacteria

On my return to Bristol in 1966, I became interested in work on photosynthetic bacteria through the happy co-location of Owen Jones and Trevor Griffiths in neighboring labs in the same corridor; they were looking at pigment development in photosynthetic systems, including the photosynthetic bacteria *Rhodospirillum rubrum*, *Rhodobacter sphaeroides* and *Rb. capsulatus*. On mechanical disruption of the bacteria, the invaginating cell membrane containing the photosynthetic apparatus was pinched off to form sealed vesicles, the chromatophores, trapping cytochrome (cyt) c_2, to yield robust preparations with a fully functional cyclic electron transfer chain [12]. Over the years before I moved to Urbana in 1978, the

chromatophore systems had proved to be a wonderful vehicle for mechanistic studies. In those early years, we developed protocols to measure light induced absorbance changes, initially on continuous illumination, but, later, on flash excitation. In this work, initially by Baz Jackson [13-17], some of it in an early collaboration with Les Dutton in Chance's group at the Johnson Foundation in Philadelphia, later by Hilary Evans [18-20], Richard Cogdell [21-23], Roger Prince [24-27], Nigel Holmes [28-30], and David Crowther [31-33], we used these experiments to separate the contributions to absorbance changes from the cytochromes *b* and c_2 of the photosynthetic chain, the reaction center changes, and the carotenoid and bacteriochlorophyll changes. Our studies of H^+ uptake and release in which the mechanism of action of ionophores valinomycin, nigericin, and the similarly acting dianemycin were sorted out, built on the gramicidin studies of my PhD work, [16]. The ionophores became essential tools in all later studies. An important step, inspired by the parallel work on chloroplasts by Wolfgang Junge in Horst Witt's group [34, 35], was the demonstration that absorbance changes associated with bacteriochlorophyll and carotenoids of the light harvesting apparatus were electrochromic band shifts, induced by the field generated across the chromatophore membrane through electrogenic processes in the photochemical reactions and on electron transfer through the cyclic chain. By inducing membrane potential changes of known values using valinomycin and K^+ gradients, we could show that the absorbance change was proportional to the membrane potential [14, 15]. Mutant strains from Owen's lab which truncated the pathway for carotenoid synthesis were important in simplifying the carotenoid spectrum [28-30], leaving a window for the cytochrome α-bands free. In parallel, we also showed that by judicious choice of pH indicator dyes, we could minimize artifacts and measure changes in pH on a faster time scale than accessible using electrodes. Following a visit to the Johnson Foundation, the timescale accessible was extended to the µs range when using flash activation [13, 16, 21-23, 36]. Using these tools, we were able to demonstrate the close coupling between redox events of the photosynthetic chain, proton uptake, and electrogenic processes indicated by the carotenoid signal, interpreted on the context of a chemiosmotic mechanism.

C. Work on chloroplast – Colin Wraight

Over this same period, Colin Wraight took on the green side of photosynthesis, and largely on his own initiative developed two important new themes. On a brief visit to Stacy French's group at the Carnegie Institute at Stanford, he was introduced to Norio Murata, and became interested in the energy dependent fluorescence quenching Murata had discovered [37], - a lowering of fluorescence yield independent of the photochemical quenching the redox state of photosystem II acceptors, but dependent on the "high-energy state" associated with coupling to ATP synthesis. On returning to Bristol, Colin set out to test the relation between this state and the chemiosmotic expectations using the tools above and was able to show from the sensitivity to inhibition by dianemycin, nigericin, or NH_4Cl, and the weak inhibition by valinomycin, that the ΔpH component of the proton gradient was more important than the $\Delta\psi$ component. Independently, and unbeknown to us, Hager [38] had discovered that a light dependent decrease of pH in chloroplasts triggered an enzymatic interconversion of violaxanthin to zeaxanthin, an effect later studied in detail by Yamamoto [39]. These two themes have come together since in the field of non-photochemical quenching and its important role in protection of plants against damage in strong light (cf. [40, 41]).

The second theme of Colin's thesis was his exploration of the enhancement of delayed fluorescence (DF) by the proton gradient [42]. Construction of a Becquerel phosphoroscope allowed us to study the ms DF of chloroplasts. DF comes from fluorescence from chlorophylls in the pigment bed in equilibrium with P* generated on reversal of the photochemistry. Quantification of contributions of $\Delta\psi$ and ΔpH to enhancement of DF showed that photosystem II transferred charge across the membrane in an

electrogenic photochemistry, and that electron transfers reopening the reaction center were linked to uptake (on the acceptor side) and release (on the donor side) of protons. Further analysis in collaboration with Darrell Fleischman led to a simple physicochemical explanation of the effect, in which the thermodynamic contributions to reversal of the photochemistry could be partitioned into that from stored redox free-energy and that from the two components of the proton gradient [43, 44]. We incorporated this explanation and a topological model of photosystem II in a chemiosmotic framework, and could then quantify the enhancement of DF by the proton gradient, and allow further consideration of the efficiency of photosynthesis with respect to the Carnot treatment of the overall process as a heat engine. By including the contribution of the proton gradient, the work stored was shown to approach the Carnot limit of ~0.7 expected from Duysens' treatment [45].

Satham Saphon [46] then showed by direct measurement using indicator dyes the period 4 oscillation associated with the S-states [47], yielding the pattern 1, 0, 1, 2 protons release (inside) (when starting in S_0) as a function of flash number, and the period of 2 oscillations associated with the two-electron gate for proton uptake (outside). Later, Jane Bowes, by presetting the state using flash activation, found with the phosphoroscope, a period four pattern of DF enhancement involving the partial reactions of the S-states [48-50]. By development of protocols for measurements of rapid fluorescence rise and DF decay in the µs range with Shigeru Itoh, these studies were extended to dissection of a similar pattern as a function of pH, interpreted as showing that the reactions were in equilibrium with the proton gradient [48, 51]. The 1, 0, 1, 2 pattern of proton release, and our explanation through the S-states, are still widely accepted, though now appreciated in a more sophisticated molecular context (cf. [52]).

2. The modified Q-cycle

In 1975, Mitchell [53] had suggested a Q-cycle mechanism for the bc_1 complex. The seeds of the Q-cycle were planted by Wikström and Berden [54] in studies of the reduction of cyt *b* in mitochondria on addition of oxidant in the presence of antimycin, which they suggested to show a bifurcated reaction. On oxidation of cyt *c* by external oxidant (O_2), cyt *b* was *reduced* by QH_2 in one chain, yielding QH•, which could then reduce cyt *c* in the other chain. This mechanism for "oxidant induced reduction of cyt *b*" was incorporated by Mitchell in his initial Q-cycle, and opened a discussion that evolved so rapidly that by the time he reviewed the field in 1976 [55], half-a-dozen different versions could be recognized. However, the data then available did not allow a clear preference among these. A major advantage of studying these reactions in the photosynthetic bacteria was the unique facility for dissection of partial process of the cycle through excitation of the reaction center by flash activation and measurement of the return to a pre-flash state as discussed above. We interpreted our own results as precluding a Q-cycle mechanism, based on a mismatch between reduction kinetics of heme *b* and heme *c* under the above conditions. From the bifurcated reaction one might have expected the kinetics to match [33], but following flash excitation in the presence of antimycin, heme *b* went reduced several fold faster than cyt c_2. However, our knowledge of redox players was then primitive, and based on absorbance changes; the involvement of the Rieske iron sulfur protein (ISP) and its Fe_2S_2 cluster was unknown, and only cyt b_H and cyt c_2 were identified. Although it was clear that the intermediate enzyme of the cyclic chain was like the mitochondrial bc_1 complex, it was only over the period 1975 – 1983 that this similarity was fully fleshed out. We and others characterized previously unrecognized functional roles for three components, - the ISP [56-58], cytochrome c_1 [59] (earlier identified by Paul Wood [60, 61]), and the low potential cytochrome *b* (cyt b_L, $E_{m,7}$ = -90 mV) [62-64]. From the close analogy of these to the components of the mitochondrial bc_1 complex, and the similarity of their function, it seemed likely that the *Rhodobacter* enzyme reflected a common bacterial ancestry. Elucidation of their roles was greatly aided by John Bowyer's demonstration of the site of action of a new inhibitor, UHDBT which we showed

blocked reduction of oxidized cyt c_2 by the Rieske center [57, 58, 65]. This was the first demonstration of this function, and provided a mechanistic basis for the parallel finding of Trumpower [66], by extraction and reconstitution, that the iron sulfur protein (ISP) was essential to function. When amplified by Steve Meinhardt's work [67] on the recently discovered myxothiazol [68], where we demonstrated that myxothiazol allowed oxidation of reduced ISP (nowadays known to be the neutral $ISPH^{\bullet}$) by oxidized cyt *c*, but blocked its re-reduction, clearly acting at a different site than UHDBT. In combination, these results showed that ISP functioned by transferring electrons from QH_2 to cyt c_1, with myxothiazol blocking electron transfer from QH_2 to the Rieske center of ISP but not the oxidation of $ISPH^{\bullet}$ by cyt *c*, and UHDBT blocking both electron transfer to the ISP, and the oxidation of $ISPH^{\bullet}$. ISP was shown now to be a necessary component in the high potential chain to heme c_1. It was clear that myxothiazol bound in a different site than UHDBT, a hint to the complexity of what is now known as the Q_o-site. A third important inhibitor characterized shortly after was stigmatellin [69], showing similar behavior to that seen with UHDBT [58]. With both, binding induced the appearance of a band in the EPR spectrum of ISPH around g_x ~1.800 on interaction with the reduced form, and an apparent shift in E_m value, - in this case from 290 to 540 mV, more mark than the shift we had earlier demonstrated, from 280 to 350 mV on binding of UHDBT [58]. When crystallographic structures later became available, they confirmed the two binding modes inferred from these early studies.

In comparing schemes in late 1980 [65], John Bowyer and I had concluded that neither a simple linear scheme nor a simple Q-cycle model could account adequately for all the observations, but while John preferred the Q-cycle, I leaned towards the linear. I have described elsewhere [70] the epiphany that released me from what I now realize was a hypothesis-induced myopia favoring the linear mechanism. About 10 months after the 1980 paper, Kevin Jones, a bright undergraduate working in the lab, asked me again to explain why the Q-cycle was wrong, and as I began my spiel, I realized to my chagrin that I had not thought through the change in perspective from the past few years of work; neither the implications in terms of the equilibrium constants involved, nor the stoichiometric consequences of quantification. From a frantic few days of review of the Q-cycle literature in light of the advances discussed above, it became obvious that we had demonstrated a perfectly plausible Q-cycle, albeit one that, in contrast to those being currently considered, was highly constrained by the data, and I recognized that it had been anticipated in outline six years earlier by Garland et al. [71]. The Q-cycle scheme Mitchell had first suggested [6], required input of an electron from the dehydrogenases to complete reduction of Q on the matrix side, and this feature was still preferred in the 1976 review [55]. What Garland had realized shortly after its introduction was that, since mitochondrial bc_1 complexes had been isolated and shown to function independently, Mitchell's scheme had to be modified [71]. A stand-alone functionality could be introduced by having the bifurcated reaction on the cytoplasmic side turn over twice, to provide, through the *b*-heme chain, both electrons needed to reduce Q to QH_2 on the other side of the membrane [70]. The modified Q-cycle we rediscovered was now fleshed out by extensive kinetic, thermodynamic, and stoichiometric data. It accounted with satisfactory economy for all the experimental findings and accounted also for the kinetic characteristics which had previously seemed anomalous [72-75]. Measurement of electrogenic processes in reaction centers and the bc_1 complex was a key feature. With a stoichiometric ratio of 2:1 for reaction centers to bc_1 complex in chromatophores, each flash should activate formation of $2P^+$ and (in the mean) $1QH_2$, available for turnover of the bc_1 complex. The electrochromic change showed equal electrogenic contributions from reaction centers and the complex. Since the photochemical reaction spanned the membrane, the fast phase showed the change due to 2 reaction centers, and the slow phase indicated that the oxidation of $1QH_2$ by the two P^+ through one bc_1 complex led to movement of two electrons/QH_2 across the membrane. The Q-cycle explained this through two consecutive turnovers of the Q_o-site, and regeneration of 1 QH_2 at the Q_i-site. However, the

thermodynamic properties of the high-potential chain meant that in the first turnover, most of the electrons from QH_2 re-reduced the 'invisible' Fe_2S_2 cluster rather than heme c_1, so its contribution was not apparent in kinetic measurement of the total cyt *c* through absorbance changes, thus accounting for the mismatch in kinetics. In addition, reduction of heme b_L required more work than reduction of heme b_H, and after reduction of ISP, not enough was available in the high potential chain until after another flash, ISPH was re-oxidized. The model also suggested that the bc_1 complex behaved as a stand-alone complex, as required by Garland. This was later demonstrated *in situ* through the second order nature of the reactions of both substrates with the complex, with QH_2 diffusing in the membrane and cyt c_2 diffusing in the aqueous chromatophore interior [76-80]. The thermodynamics of the bifurcate reaction at the Q_o-site also provided severe constraints on choice of mechanism, and these were further explored in preliminary experiments to probe the energy landscape [81]. These studies showed some important features: i) from measurement of activation barriers for separate partial processes, the rate limiting reaction was transfer of the first electron from QH_2 to the Fe_2S_2 cluster of ISP to generate an intermediate semiquinone (SQ); ii) that the reaction was strongly endergonic; and iii) that in order to outcompete the back reaction, the SQ would have to be rapidly removed by oxidation via the *b*-heme chain. We pointed out that the minimal model would involve the SQ intermediate state at the top of the activation barrier and proposed a set of kinetic equations through which this and other models could be explored and tested against the observed kinetics. The modified Q-cycle that we demonstrated in 1982, as refined in [75], and extended with substantial additional refinements from more recent work in the context of structures [70, 81-85], has become the consensus mechanism for the bc_1 complex. Fig. 1 shows the mechanism set against a model of the structure from MD simulation containing substrates QH_2 and Q at Q_o- and Q_i-sites, respectively.

A. Prediction of structure of cytochrome b

It had become obvious that any substantial further progress towards a molecular understanding could only come if we had structural information. At that time, no membrane proteins had been solved crystallographically, so we looked at the possibly of modelling. Howie Robinson and I developed two software packages, PDV (a Protein Data Viewer) allowing an IBM PC (or compatible computer) to be used for viewing structures from the Protein Data Bank, and SEQANAL, for sequence analysis. The transmembrane function of the bc_1 complex had obvious structural implications, but, although the reaction center structures came out in 1984 [86] no other structures were yet available. However, mitochondrial DNA was an early target for sequence analysis, so that sequences of several mitochondrial cytochrome *b* subunits were available quite early. Alignment of sequences by Widger et al. [87], and by Saraste [88] in 1984 showed four conserved histidines suggested to be the ligands for the two *b*-hemes, two each in separate helices. Hydropathic analysis had suggested nine transmembrane helices as the supporting scaffold and showed that the histidines were in pairs separated by ~20 Å across the membrane in two of the helices. These were assigned as ligands to the two hemes to provide a preliminary structural model. The transmembrane distribution was interpreted as supporting electron transfer between hemes as expected from the electrogenic process identified in our kinetic work [74].

B. The 8-helical model of cytochrome b

In addition to structural prediction and hydropathic analysis, routines were written to analyze sequences for amphipathic character. Information from amphipathic analysis strongly suggested that one of the putative transmembrane helices of the Widger et al. and the Saraste structures (helix IV) was an amphipathic surface helix. From this, we suggested an 8-transmembrane model that reversed the direction of helices across the membrane downstream of III, including helix V, one of the histidine-bearing helices), with important structural implications [89]. Around this time spontaneous mutations that

rendered the yeast complex resistant to antimycin or funiculosin (Q_i-site inhibitors), or mucidin (a Q_o-site inhibitor) were identified in yeast [90], and sequenced. In the 9-helix model, the residues introducing resistance at a particular site clustered on both sides of the membrane, but in the 8-helix model, all Q_i-site resistance mutations were on the N-side, and all Q_o-site resistance mutations on the P-side [89, 91]. In collaboration with Bob Gennis and his group (see ***C.*** below), we found strong support for this folding pattern from assignment of histidines to specific hemes using directed mutagenesis [92], and by *pho*A-fusion analysis [93]. When structures eventually became available, this new folding model was shown to be correct [94, 95]. The SEQANAL package was later extended to include information on amino acid propensities revised to take account of the effect of hydrophobic forces in determining secondary structure, and the asymmetry of conservation in secondary structures (the "mutability moment") as an indicator of tertiary structure (the PSAAM (Protein Sequence Analysis and Modelling) suite [96]). We used these programs to develop more refined models of the cytochrome *b* subunit, including location of the Q_o- and Q_i-sites [97], later validated in its main features by crystallographic structures.

Although in retrospect these structures from predictions pale in comparison with the crystallographic models, it was nevertheless gratifying to see how well our predicted cytochrome *b* structure anticipated the latter.

C. Site-directed mutagenesis of the bc_1 complex

Techniques for molecular engineering of cyt c_2 in *Rb. sphaeroides* were developed by Donohue, McEwan, and Kaplan [98], and extended for the bc_1 complex by Gabellini and Sebald [99], and by Davidson and Daldal [100] for *Rb. capsulatus* in 1987. The Kaplan and Gennis labs shortly after developed similar protocols for molecular engineering in the three main subunits of the bc_1 complex in *Rb. sphaeroides*, and in collaboration with them we tested the protocols by characterizing several engineered mutants [101]. With the *fbc* operon encoding the three major subunits of the bc_1 complex cloned and sequenced, a battery of molecular engineering techniques was developed to allow specific mutation at any site. Initially, we used the strains engineered in Bob's group to investigate the role of conserved amino acids in the structure and catalytic mechanisms of the bc_1 complex, including the liganding histidines above, but later made our own contributions [92, 93, 102-106]. In the iron-sulfur protein (ISP), we developed protocols for expression of the subunit in *E. coli* [105] and used specific mutagenesis to establish that putative ligands to the Fe_2S_2 cluster were essential to function [104]. The collaboration with Bob Gennis has continued since, and I am happy to acknowledge the fun we had, and the increasing debt I have owed him over the years.

Isolation and characterization of the bc_1 complex of Rhodobacter sphaeroides

The *Rb. sphaeroides* bc_1 complex was purified as an active enzyme in high yield using conventional chromatographic methods [107]. The isolated enzyme had essentially the same thermodynamic and spectroscopic properties as the enzyme *in situ*, contained the same prosthetic groups, but had an activity somewhat lower than that measured *in situ*. The enzyme had four subunits, three of which, cytochrome *b*, Rieske-type iron sulfur protein (ISP), and cytochrome c_1, contain the centers associated with redox active prosthetic groups. N-terminal sequencing data indicate that these three subunits are the proteins coded by the *fbc* operon. Later, we constructed an *fbc* gene with a coding sequence for a $(His)_6$ tag at the C-terminal end of cytochrome *b* (BH6) or cyt c_1 (CH6) and expressed these in *Rb. sphaeroides* [108]. The complexes synthesized was fully active and could be rapidly isolated and purified using a Ni-affinity column. The isolated complex was obtained in high yield and had properties similar to the native complex but with a somewhat reduced activity compare to that *in situ*. We used this preparation to synthesize protein for structural studies, and detailed spectroscopic investigations.

We have continued to do our molecular engineering in this background to allow ready isolation of the mutant complexes.

3. Status of research on bc_1 complex before structures became available

The modified Q-cycle mechanism provided a satisfactory explanation for the overall reaction and the main kinetic features studied [75], and provided clues as to the architecture of the protein housing the mechanism, as summarized in the models published [81, 96]. Although the seminal papers [72-74] are seldom cited, the change from Mitchell's model was necessary to further advances. The difference was critical because the modified version was so highly constrained. No other Q-cycle model combined the high explanatory value with the parsimony introduced by the high degree of constraint; these features, the qualities most highly valued by Popper [109], opened the hypothesis to rigorous experimental test, and the survival of the essential elements through subsequent evolution is testimony to its strength.

From the dependence of rate on the degree of reduction of the Q pool, properties of the *ES*-complex could be derived from Michaelis-Menten considerations but provided no other structural context beyond our models [77-81, 110]. There was strong evidence from the isolated enzyme that the complex was dimeric [107, 108], but no suggestion as to why. The structural model of cyt *b* provided distances for electron transfer across the membrane between the hemes, and between the catalytic sites [81, 96] that allowed us to exploit the development by Moser, Dutton and colleagues [111-113] of a simplified Marcus treatment.

$$\log_{10} k_{et} = 13.0 - \frac{\beta}{2.303}(R - 3.6) - \gamma(\Delta G^{o\prime} + \lambda)^2/\lambda$$

The first two terms on the right transformed a densely quantum mechanical treatment of the pre-exponential term to a simple dependence on distance, accessible to the mathematically challenged, so that once structures were available, measured distances could provide a basis for estimation of rate constants between centers, and *vice versa*, opening a wider perspective on mechanism. The value of γ has more recently become controversial; the Marcus value of (4×2.303RT), or 4.23 at 298 K, is classical, but Moser et al. chose a value of 3.1, reflecting the Hopfield approximation to introduce a quantum mechanically modified dependence of rate on temperature. We have preferred the former choice (see **5, A.** j), and [114]).

An important study by Ding and Dutton [115-117] had shown that the g_x line at 1.800 of the ISP EPR spectrum was lost on reduction or changed on extraction of the quinone pool. They interpreted these phenomena as interaction of the reduced ISP with two distinct quinone species Q_{os} and Q_{ow} involved strongly and weakly binding components. They suggested that the Q_o-site operates through a double-occupancy of Q species, in which the weakly binding species associated with the g_x 1.800 signal was modelled as a complex with ISP. Trumpower [66, 118] had demonstrated that the ISP could be detached (with loss of overall function) and reconstituted (with regain of function), and John Bowyer and I had demonstrated from the inhibition by UHDBT that the ISP had a functional role as reductant for cyt *c* [56, 57], and, in collaboration with the Dutton group, that the inhibition involved a binding of UHDBT and ISP [58], taken as a quinone analogue. After he moved to Trumpower's lab, they developed a strong case for a Q-cycle based on the effects of UHDBT [119, 120], albeit still Mitchell's model requiring an input of one electron from the dehydrogenases at the Q_i-site. However, there was no hint from any of this work of the movement of the ISP extrinsic domain discover from the structures (see **4.** below).

In the preamble above, my intention has been to set up both the adequacy of the Q-cycle before structures were available, and set the scene for the importance of the new structural information to an

understanding of mechanism at the molecular level; the modified Q-cycle provided an economical model before the structures, but evolved as details became available, with the main features of the original form still providing the framework for subsequent evolution.

4. Crystallographic structures

Before structures were available, extensive spectroscopic work had identified two histidine ligands stabilizing the ISP cluster [121, 122]. A high resolution structure of the solubilized head group of the Rieske iron-sulfur protein (ISP) was published early in 1996 [123], showing an egg-shaped structure, with the cluster liganded as expected from spectroscopy, in a domain at the narrower end. The first more complete structures of the bc_1 complex from a collaboration between Chang-An Yu, and Xia and Deisenhofer of mitochondrial bc_1 complexes (bovine) was published in a preliminary report in 1996, with a more detailed structure in 1997 [94, 124], and showed a dimeric structure. The cytochrome *b* subunit showed the 8 transmembrane helices and location of the *b*-hemes predicted from our model [89, 96, 125]. In the complex containing myxothiazol, cyt *b* showed density for the inhibitor close to heme b_L, thus indicating the location of the Q_o-site, and structures binding antimycin showed location of the Q_i-site, both situated as predicted in our model, but now shown at atomic resolution (2.9 Å), providing details critical to an understanding of many mechanistic features. The cytochrome c_1 subunit was a new structure, but unfortunately, a key player was missing from the overall structure, - the extrinsic domain of the Rieske iron-sulfur protein. However, density was assigned to the Fe_2S_2 cluster of ISP, and in discussion at meetings, they had hinted at the possibility of mobility based on distance changes of this density compared to the other redox centers.

The first complete structures were solved by Ed Berry and colleagues in 1998 [95], and showed as the main new feature, the extrinsic domain of the ISP, missing from the Xia et al. model. Structures with stigmatellin bound showed the Fe_2S_2 cluster domain binding at the Q_o-site of the cyt *b* subunit, H-bonded to the inhibitor. In structures with myxothiazol bound the cluster binding domain was closer to heme c_1, with the whole extrinsic domain moving without major change of its structure except in a linker span connected to the helical membrane anchor (already known from the Xia et al. structure). From this we inferred that substantial movement between interaction sites would be needed to complete the catalytic cycle. Berry also solved structures for the native complex without occupants of the catalytic sites (and with the ISP head in an intermediate position), and with ubiquinone or antimycin in the Q_i-site. Structures with myxothiazol bound showed the same location as in the Xia structure, but in the stigmatellin bound structure, the inhibitor was in a volume overlapping the myxothiazol site, but more distal from heme b_L. Stigmatellin was liganded to ISP through a H-bond between the -C=O of the ring and N_ε of one of the histidine ligands, His-161, of the cluster. The position of the ISP extrinsic domain in the stigmatellin structure was different than that in other structures with myxothiazol, or with a vacant Q_o-site, and protein occupancy (from electron density) of the extrinsic domain was higher [126]. This suggested that the H-bond from stigmatellin to His-161 of ISP stabilized the extrinsic domain [126] in a configuration likely mimicking its interaction with ubiquinone species. Structures with ubiquinone in the Q_i-site showed ligands to His-217 and Asp-252, which mutagenesis had shown to be critical to turnover [102]. No quinone species were seen at the Q_o-site, but stigmatellin provided an obvious model. During the next few years, additional structures were published showing other positions of the ISP, and other inhibitors.

A. Lessons from the structures

Early in 1997, Berry had generously invited me to participate in the publication of his structures to provide a functional perspective. As structures became available, he sent them along to us, so we had the unique privilege of a series of marvelous revelations, many showing details of binding of new

inhibitors at the Q_o- and Q_i-sites. The structures were of enormous help in extending our understanding of function. In the context of the structures, we publish in 1999 a series of papers in Biochemistry [126-128] exploring in great detail the structure/function implications of the architecture revealed. Several critical new features of the structures allowed is to extend our understanding of the Q-cycle mechanism [129-131], discussed in the next section.

B. Electron transfer by movement of the extrinsic domain of ISP

Resolution of the ISP subunit proved to be critical to a new understanding the Q_o-site mechanism. In particular, the binding of stigmatellin suggested where QH_2 must bind in formation of the *ES*-complex. Since the Q-cycle would not be competent in all partial reactions of quinol oxidation in any of the single static structures provided by crystallography, we had suggested that a movement of the ISP extrinsic domain must occur between the interaction domains [95]. Movement allowed the Fe_2S_2 cluster binding domain to connect to widely separated reaction interfaces during turnover of the Q_o-site [95]. We suggested that the movement itself was a spontaneous diffusional process with an expected timescale in the sub-microsecond range [126, 128]. In collaboration with the Schulten group, we demonstrated the feasibility of this scenario through molecular dynamic (MD) simulations [130]. The MD model was based in Berry's avian mitochondrial complex, incorporated into a POPC membrane separating two aqueous phases. It was among the largest MD models attempted at the time and use of the technique of steered molecular dynamics in this study tested the computational resources available. We also noted that in setting up the model, equilibration of the protein with the water phases populated some interesting water chains in cytochrome *b*, some of which provided important clues as to the pathway for H^+ release from the Q_o-site reaction [129, 130]. The mechanism proposed for proton exit in [129] included a movement of the intermediate semiquinone from the stigmatellin occupied domain distal from heme b_L to the myxothiazol occupied proximal domain, to allow more rapid oxidation of SQ by the heme. This incorporated a displacement of the sidechain of a glutamate in the conserved -PEWY- sequence (seen in the myxothiazol structure), to connect it to a water chain leading to the P-phase, thus providing a path for proton exit, and a role for the glutamate. Much of our subsequent research has been devoted to testing and refining this model.

C. Stigmatellin binding as a model for the ES-complex

None of the structures have shown any quinone species at the Q_o-site, but structures were solved with different inhibitors present. The structures with inhibitors provided clues to mechanism. In particular, the structure with stigmatellin showed a complex at the Q_o-site in which the inhibitor was H-bonded to N_ε of His-161 of ISP (avian numbering); the other imidazole N of this histidine serves as a ligand to the Fe_2S_2 cluster [95, 127]. This interaction with ISP recalled the earlier information on UHDBT and stigmatellin binding from EPR studies [58, 69], showing that binding involved the reduced cluster (ISPH). We suggested that a similar H-bond might be involved in formation of the *ES*-complex, but between OH- of ubiquinol (QH_2) and the same His-161 of the oxidized ISP [127, 129]; it is now generally accepted that the *ES*-complex forms at or close to the site shown by stigmatellin binding and involves such a H-bond.

D. The bifurcated volume of the Q_o-site

The structures showed that the Q_o-site of the complex has a bi-lobed volume. It is accessed from the lipid phase by a relatively narrow tunnel through which substrates, products and inhibitors must diffuse. Contrary to the expectations of double-occupancy models, the native structure showed no evidence for occupancy by any quinone species, much less a tightly bound quinone at this site ([127] and see above). In co-crystals with inhibitors, stigmatellin occupied the lobe distal from heme b_L, and

myxothiazol or MOA-type inhibitors occupy the proximal lobe. The volume also has an opening to the P-side aqueous phase, which is occluded by the cluster domain of ISP in structures showing it bound through a H-bond to the inhibitor.

E. Functional significance of the different Q_o-site conformations

The configuration of the site undergoes substantial rearrangement depending on the occupant [84, 128]. In the stigmatellin complex, the volume between the inhibitor in the distal site and heme b_L is occupied by sidechains of conserved residues (including the -PEWY- glutamate), but in the myxothiazol structure these were displaced to allow occupancy of this proximal domain by the inhibitor. For the most part, these displacements were by simple rotation of the side chain; the configuration of the backbone atoms was not changed. However structural displacements conserving backbone orientations are important in redistribution of volume to accommodate inhibitors in the different lobes. The volume occupied by myxothiazol would obviously be available and suitable for hosting the head-group of quinone species in the absence of the inhibitor, but only by similar side-chain displacements. Structures of the inhibitors overlap in the common volume of the access tunnel, which, absent substantial expansion, constrains occupancy to a single species, Q, QH_2 or an inhibitor. However, some inhibitors showed little occupancy of the tunnel (no tails), and evidence from bypass reactions suggests that QH_2 then can form an (incompetent) *ES*-complex, albeit with a reduced affinity, generate SQ and form superoxide (SO). We suggested that this complicated design had a functional significance. The products of the first electron transfer are a semiquinone (SQ) and ISPH, which would be constrained to the distal domain, and would have to dissociate from the intermediate product complex before the reaction could proceed forward. From kinetic data and an analysis of mutant strains we suggested that a movement of the semiquinone from the distal domain in which it is formed to the proximal domain of the binding pocket must occur during catalysis to take advantage of the 1000-fold increase in rate constant for reduction of heme b_L that the 5.5 Å decrease in distance would provide. Analysis of the functional consequences of mutation around the Q_o-site volume, in the context of related effects on inhibitor binding, strongly supported the idea that this movement is essential for function of the bifurcated reaction [84, 128]. These two mobile features would clearly be linked; dissociation of any intermediate complex would be required before the ISPH could move away to donate its electron to heme c_1, and before SQ movement in the site could occur.

5. Complexes of ubiquinone species with ISP

A. The nature of the g_x = 1.800 species.

The structures provided new insights into the nature of interactions of ISP with quinone species shown by changes in the EPR spectrum of reduced ISP [126-129]. The evidence for double occupancy model of Ding, Dutton and colleagues [115, 117] had depended heavily on interpretation of features of the EPR signal detected by the line at g_x = 1.800 from ISPH, which was modified by interaction with Q_o-site occupants [58, 69]. In the absence of inhibitors, and with the Q-pool initially oxidized, redox titrations showed that the g_x 1.800 signal titrated out on reduction of the pool and was replaced by a weaker band at g_x 1.77. This suggested that the g_x 1.800 band showed binding to Q, and the g_x 1.777 to QH_2. Both disappearance of the 1.800 band and appearance of the 1.777 band titrated with the midpoint of the Q-pool at $E_{m,7}$ ~90 mV indicating no preferential binding of the quinone over quinol. However, extraction of the ubiquinone pool changed the signal, through an intermediate line shape with a weaker signal displaced from 1.800 to 1.783, further displaced to poorly defined g_x= 1.765 feature on complete extraction. The differential shifts were interpreted as coming from strongly (Q_{os}, the g_x 1.783 species) and weakly binding species (Q_{ow}, g_x 1.800 species).

When structures became available, they showed no evidence for any quinone species at the Q_o-site. They showed a quinone species binding at Q_i-site with significant occupancy, but Ding et al. had indicated that the strongly binding Q_{os}-site species should by much more tightly bound than this, so the failure to see any occupancy was anomalous. In effect, the structures provided no explanation for the Q_{os} phenomena. Since the strong the g_x 1.800 signal was seen only when ISP was reduced and the quinone pool oxidized, we suggested that the simplest interpretation was that it represented a complex between the reduced ISP and ubiquinone (Q) through the same His-161 as seen in the stigmatellin complex [127], but with relatively weak binding.

B. Complexes with ISPH: the g_x 1.800 species, UHDBT and stigmatellin.

The g_x 1.800 species figured prominently in a later study, in which the Daldal and Dutton groups collaborated in an interesting exploration by Elisabeth Darrouzet of consequences of mutation in the tether region of the ISP connecting the extrinsic head to the membrane anchor to explore its role in movement [132-136]. Examination of the structures [128] had shown us that the linker region was helical in structures containing myxothiazol, in which the cluster domain had no H-bonding interactions, and extended in the stigmatellin containing structures, apparently pulled out to accommodate the movement of the extrinsic domain associated with binding. In the Darrouzet et al. studies, the g_x 1.800 line was used to assay binding of ISP, and the results showed that binding led to a change in the E_m of the cluster, which increased dramatically when the tether was extended by insertion of 1-3 alanines, and less dramatically by other mutations in the linker span. From our previous work on the changes at this spectral band on binding of UHDBT, and our recognition of the g_x 1.800 species as a complex of ISPH with Q, we could reinterpret their data in terms of the complex with Q. Rather than an *intrinsic* change in the E_m, the change was only apparent. It could be attributed to a preferential binding of the reduced form, an interpretation previously used in the studies of inhibitors which showed that that binding with ISPH led to a change in the E_m of ISP (cf. [58, 69]), and that the extent of change reflected the binding constant for the inhibitor. This was most obvious in the presence of myxothiazol, which displaced the relatively weakly binding UHDBT, prevented its interaction, and eliminated the E_m shift by the inhibitor. The change in E_m in the linker mutations was also lost in the presence of myxothiazol, but in that case by preventing ISPH from interacting with quinone. We suggested that the change in E_m was a measure of the strength of binding with quinone, changed on extending the linker, providing a value for the binding energy. In light of the structures, this could be explained through a "spring-loaded" hypothesis: in wild-type, the binding to a Q_o-site occupant pulled the ISP extrinsic domain from the relaxed configuration observed in the presence of myxothiazol (with the linker span in a helix), to a strained configuration (with the linker span extended). Extension of the tether on forming the complex pulled the helix (a "chemical" spring) apart, required a force to break H-bonds stabilizing the helix. This force and the binding force acted against each other. As a consequence, the binding force assayed through the apparent ΔG was weaker than that measured when the tether was pre-extended on mutation [137]. Mutation of the linker region led to a tighter binding with Q because it extended the linker, removing the tension. The hypothesis could also account for the change in E_m of ISP by -30 mV in wild type on addition of myxothiazol, which eliminated the interaction with Q (seen by loss of the g_x= 1.800 signal). The -30 mV change in E_m showed the *loss* of the binding force with Q [138] in the uncomplex state. It will be obvious from this discussion that the properties of the different complexes are determined by specific properties of both species contributing to the H-bond, and an important component of our work has been in characterizing those properties for each complex. We will revisit this "spring-loading" question in greater detail later.

C. Accounting for catalysis in terms of the kinetic and thermodynamic characteristics of the Q_o-site reaction

In order to give some idea of the kinetic data from which we can determine rate constants and equilibrium constant, Fig. 2, taken from [139], shows kinetic traces for mutant E295D, annotated to demonstrate how measurement of kinetic and thermodynamic parameters can be made (see legend). The curve defined by open triangles shows the difference of redox potential (*E'*) between the high potential and low potential chains (given by the scale on the right), determined from the poise of reactants measured from the traces at select time points, - shortly after each flash for flashes 1, 2, 3, 5 and 6, and then at points during the return towards equilibrium.

a) ***Formation of the ES-complex***.

We estimated a relative binding force for QH_2 in formation of the *ES*-complex from redox titration of the rate of QH_2 oxidation in the presence of antimycin, assayed through heme b_H reduction. The rate, and hence the occupancy of the *ES*-complex, titrated in with a mid-point ~130 mV [74, 77, 79, 80]. At that E_h, the Q-pool was 90% oxidized, so the displacement showed a 10-15-fold tighter binding of QH_2 than expected from the equal binding with Q in formation of the g_x 1.800 complex [117]. A comprehensive study of temperature dependence showed that the activation barrier was in the first electron transfer [81, 131]. These studies characterized the energy landscape of the reaction as starting from an *ES*-complex populated by preferential binding of QH_2, followed by formation of an activated state showing (at least in the low temperature range) a barrier of 65 kJ.mol^{-1} [131] before formation of products, the reduced ISP and semiquinone (SQ). The SQ was removed by electron transfer to heme b_L and then to heme b_H. We later showed that in formation of the *ES*-complex, a similar value for the binding constant could be derived from the change in p*K* of ISP between the free (pK_{ox1} = 7.6) and bound (p*K* = ~6.5 in the *ES*-complex from the dependence of electron transfer rate), as expected from the contribution of QH_2 *and* ISP_{ox} to its formation [82].

b) ***The oxidation of QH_2 was several orders slower than expected from distance***.

Several anomalies were obvious from comparing the apparent rate constant from kinetics with that expected from the structures. The H-bond with *H-161* (avian numbering) in the *ES*-complex must be close to the same length as that with stigmatellin. This gives a distance for the electron transfer process of ~ 7Å. We noted that application of Dutton's ruler to determine a rate constant for the first electron yielded a value several orders of magnitude faster than the observed rate [128, 131].

c) ***The rate limiting step and the high activation barrier are in the first electron transfer***.

We analyzed the activation barriers of partial processes in the high-potential chain and compare these with the turnover of the Q_o-site as determined by the kinetics of reduction of heme b_H in the presence of antimycin [131]. In confirmation of earlier work [81], the highest activation barrier and the rate limiting step were identified as in the first electron transfer, with a rate-constant varying with pH and temperature. The straight-line fit to the points showed ~47 kJ/mol; however, the activation energy for the limiting reaction taken over the low temperature range was higher (~65 kJ/mol) than over the higher range (~35 kJ/mol), and higher than previously reported, likely because over that range, the temperature was not well controlled in the early experiments. The change in slope from low to high ranges suggested a distributed kinetic limitation, with the components of faster rate but lower E_{ac} contributing more in the high range.

d) ***Binding of inhibitors at the Q_i-site did not affect the rate limiting step at the Q_o-site***.

We had earlier demonstrated that the oxidation of QH_2 in the absence of antimycin, determined from the electrogenic events associated with turnover, occurred at the same rate as that in the presence of antimycin, determined from the rate of reduction of heme b_H [74], and confirmed this

in more extensive work [85, 127]. This result was important because it precluded any mechanisms in which physicochemical properties affecting turnover at the Q_o-site were modified by binding of antimycin at the Q_i-site.

e) ***Most of the lag before reduction of heme b_H begins is accounted for by the time to deliver oxidizing equivalent from the reaction center***.

The Q_o-site reaction can be assayed through reduction of heme b_H, the terminal acceptor in the presence of antimycin. Reduction started only after a lag of ~120 μs [65, 74]. The 120 μs lag was mostly accounted for by the time needed to get the oxidizing equivalent generated in the reaction center to the Q_o-site (by transfer of the oxidizing equivalent from P^+ through cyt c_2, to heme c_1 and ISP, including its movement) [85, 128, 131].

f) ***The 20μs residual lag limits occupancy of intermediate steps of the second electron transfer to <0.02***.

The unaccounted lag value was <20 μs [85, 127, 128, 131], which would have to include all processes associated with intermediate states (SQ, heme b_L) before reduction of heme b_H. Since population of intermediate states occurs at the limiting rate (~1000 s^{-1}), this would allow a maximal occupancy of ~0.02 for the sum of all intermediates; the lifetime of the SQ must be less the this. The result was important because the constraints eliminated all reaction mechanisms in which a SQ intermediate (SQ-ISPH, $QH^{\bullet}$, $Q^{\bullet-}$) accumulates significantly in normal forward chemistry. Essential the same lag is seen in the rapid-mix/freeze experiments of Zhu et al. [140].

A similar constraint on lag in heme b_H reduction (<30 μs) was also seen in experiments from Millet's group [141], when cyt c_1 was oxidized within 1 μs by photoactivation (via a ruthenium dimer and $[Co(NH_3)_5Cl]^{2+}$ used as a sacrificial electron acceptor) and re-reduced by ISPH with rate constant 80,000 s^{-1}. The pool of 10-bromodecylQH$_2$ was maintained reduced by succinate and succinate-Q reductase, so the 30 μs lag would include at least one transit of the ISP head between heme c_1 and the docking interface on cyt *b*, and the formation of the *ES*-complex. In these experiments, they used famoxadone to inhibit the Q_o-site, which has a curious binding mode seen in Berry's structure of the avian complex with famoxadone (PDB 3L74) [142]; it has a similar H-bond to the backbone >NH of E295 as the MOA-type inhibitors, but its odd lumpy structure distorts the volume of the Q_o-site so as to allow the "trap-door" tyrosine [84] to reach out to H-bond with His-152 of ISP, so as to hold it close to the cyt *b* docking interface (discussed in more detail in Section **10 A** below). This same structural constraint is also seen for the equivalent Tyr-302 in the *Rb. sphaeroides* bc_1 complex with famoxadone (PDB 5KKZ). Although the inhibitor does not form a H-bond to the histidine (as stigmatellin and UHDBT do) the Tyr-His H-bond does substantially inhibit the oxidation of ISPH [141]. The consequence of this constraint on ISP movement is that, in contrast with myxothiazol and MOA-type inhibitors, the reduction of heme c_1 by ISPH is inhibited, and the rapid kinetic phase lost on addition of famoxadone reflects the true kinetics of ISPH oxidation in the uninhibited complex. Taking account of these additional processes of the first step, the fraction of lag attributable to intermediate states of the second electron transfer is reduced and hence also the maximal occupancy.

g) ***The low occupancy of SQ shows an endergonic reaction***.

Since the reaction is measured at close to saturating QH_2 as substrate, and the kinetically estimated occupancy is close to that later measured directly [143, 144], transfer of an electron in the first step, $QH_2.ISP_{ox} \rightleftarrows SQ.ISPH$, must occur in a strongly endergonic process in which the rate constant for the back-reaction is much higher than for the forward reaction. The reaction for removal of SQ must compete with the back-reaction, and would therefore need at full-occupancy to involve a

rate >>100-fold more rapid than that of the limiting step, and a rate constant many-fold higher at the low occupancy suggested in the previous paragraph.

h) ***The H-bond acceptor from ISP_{ox} on binding QH_2.***

By reference to the structure with stigmatellin bound, the *ES*-complex from which the oxidation of QH_2 occurs was modeled with QH_2 bound to ISP_{ox} through a H-bond. The physical chemistry of this bond has been of critical importance in understanding mechanism. We suggested that the QH_2 acts as H-bond donor to the N_ε of His-161 (in avian, *H-152* in *Rb. sphaeroides*). In formation of this bond, the p*K* of the histidine is critical. The pH dependence of E_m on redox titration of ISP suggested that this group is responsible for the pK_{ox1} at 7.6 measured on the oxidized ISP [145, 146]. This assignment has now been confirmed directly by NMR [147], and was interpreted by the authors as validating our model for the cycle of reactions involved in turnover of the Q_o-site. However, in generating that model, we depended in extensive studies of the pH dependence of kinetic and thermodynamic characteristics of the functional system, in which the nature of the *ES*-complex provided only the starting point.

i) ***The equilibria determining the formation of the ES-complex.***

A critical initial consideration in developing our hypothesis was that the *ES*-complex involves binding of two substrates, QH_2 and ISP_{ox} [84, 129, 148]. The dependence on concentration for each of the two substrates could be estimated separately while keeping the other constant [82, 84, 129]. For QH_2 this was done by varying the degree of reduction of the Q-pool at fixed pH; at pH 7 the half maximal rate is observed at ~130 mV, 30-40 mV higher than the mid-point of the Q-pool, showing a 10-15-fold preferential binding of the reduced form. Since QH_2 can donate to the H-bond only if ISP_{ox} is in the dissociated form, the binding of ISP_{ox} can be assayed by varying the pH with QH_2 constant. The occupancy of the *ES*-complex depends on pH over the range of the pK_{ox1} of the group involved. That the dependence of electron transfer rate on pH, with the p*K* of ~6.5, was shifted from the pK_{ox1} of 7.6 measured by titration of the proteolyzed head group, could be accounted for by the work invested in the H-bond on formation of the *ES*-complex [82]. Since the two approaches gave close to the same value for an apparent binding constant, K_{app}, they represented a common process iso-energetic for the two sequences (QH_2 then ISP_{ox} or vice versa).

j) ***Proton-coupled electron transfer accounts for the slow first electron transfer.***

A second critical point to establish was an explanation for the slow rate of the first electron transfer. The p*K* of *His-161* of ISP_{ox} contributes two separate effects. The first of these is in the pH dependence of formation of the *ES*-complex noted above. To understand the second effect, it is important to appreciate that the properties of the *ES*-complex determine the behavior of the first electron transfer that starts from this state. Several paradoxical features had to be explained; the high activation barrier, the slow rate of the reaction, and the short distance for electron transfer (~7 Å). From the latter, the expected rate constant was in the range <1 μs, at least 3-orders faster than the rate measured. This latter paradox could be resolved by recognizing that the Moser-Dutton treatment assumed a simple electron transfer, but that the reduction of ISP_{ox} by QH_2 involves both an electron and a H^+. Since ISPH shows a pK_{red} ~13, on receiving an electron, the ISP_{ox} would become protonated. The stigmatellin structures show that the interface around the H-bond to ISPH is anhydrous, so, assuming the structure of the ISP/cyt *b* interface around the *ES*-complex is similar, reduction of ISP_{ox} could not involve a H^+ from the bulk phase. However, transfer of a proton together with the electron along the H-bond from QH_2 to His-161 could serve this role without any need for an extrinsic proton. The reaction would effectively be neutral, - a H-transfer, - but thermodynamic

description would require additional equilibria to those implicit in the Moser-Dutton equation to accommodate the involvement of the H^+. H-transfer could occur by a proton-first-then-electron or by an electron-first-then-proton mechanism. Representing these by a thermodynamic square using estimates for work terms from the literature (see Fig. 3, taken from [84, 146]), it was obvious that the *proton-first mechanism was the most probable* [84, 145, 146], even though it involved a weakly populated state. The probability for electron transfer would then depend on the probability of finding the H^+ close to the histidine. The second effect of the pK_{ox1} on ISP_{ox} therefore comes from its involvement in determining this distribution. The probability distribution of the proton along the H-bond is determined by the *pK* values for dissociation of QH_2 (pK >11.3) and pK_{ox}^{app} for ISP_{ox}. The latter is determined by two contributions, the pK_{ox1} of 7.6 in the isolated complex, lowered to ~ 6.5 by the binding energy of QH_2. The distribution of the H-bond proton close to ISP would be quite improbable and would contribute part of the energy barrier determining the rate of electron transfer. In effect, the rapid rate constant expected from the short distance is slowed by the low probability of finding the proton in the right place. This type of mechanism was first proposed to explain the behavior in chemical models by Nocera and colleagues [149, 150].

k) ***A Marcus-Brønsted equation describes the reaction.***

From the above, we suggested that the electron transfer rate constant would be given by a Marcus-type treatment incorporating the distance dependence of electron transfer (Dutton's ruler, the first two terms on the right in the equation below), a classical activation barrier, and the weak probability for the proton from a Brønsted term, given by the ΔpK of the groups contributing to the H-bond (the right-most term) [82, 148, 151]. The kinetic behavior of WT could then be economically explained in terms of standard probability theory. With probabilities in $\log_{10}$ form, this gives:

$$\log_{10} k_{et} = 13.0 - \frac{\beta}{2.303}(R - 3.6) - \gamma(\Delta G^{o\prime} + \lambda)^2/\lambda - \Delta pK_{(QH_2-his)} \qquad (eq.\ 1).$$

Here the value 13 is $\log_{10}$ of the limiting rate constant ($10^{13}\ s^{-1}$) from bond vibrational frequency of a typical H-bond (3.6 Å), and β is an empirically determined slope for dependence of rate on distance from a sampling of measured rates in the context of structural distances (in the seminal work, mainly from bacterial reaction centers). In summary, the first two terms then represent in $\log_{10}$ form the intrinsic rate constant (the pre-exponential term), the next term is $\log_{10}$ of the activation barrier in Marcus' form, and the Brønsted ΔpK term is the $\log_{10}$ probability of finding the H close to the histidine along the H-bond.

In the experiments leading to the equation above, temperature dependence was explored in the range above 0^o C and was treated classically. Marcus' treatment was a refinement of the classical activation energy approach and he used $\gamma = F/(4\times2.303RT)$, or 4.23 at 298 K. However, γ is treated differently by Dutton and colleagues (cf. [111]) through a value of γ=3.1, originally from empirical fits, but justified by using the Hopfield [14] approximation in which $\hbar\omega/2\ \coth[\hbar\omega/2k_BT]$ is substituted for k_BT, originally suggested to account for temperature independence of electron transfer at low temperature. Justification for this treatment is controversial [114]. Marcus [152] treated λ is a composite term, dependent on dielectric response in two ranges; D_{op} in the refractive index range, and D_S representing the mobility of dipolar and charged groups from the outer sphere. Matyushov [153] has pointed out that dielectric response, and therefore λ, depends on the nature of the process, and he investigated the density of such states as a function of response time over seven orders of magnitude. One obvious point that comes from this is that a value for λ appropriate to a particular process will depend on how fast it occurs; the dielectric response to the picosecond processes of the reaction center

will reflect D_{op} processes, which will be independent of temperature. The slowing down of rate as temperature is lowered will represent a mixture of effects, part classical activation barrier, and part a freezing out of the dielectric response; it is by no means obvious that Hopfield took account of these, or that quantum mechanical effects are usefully applied in this part of the equation. Since $\log_{10}k_{et}$ scales with γ, calculates rate constants will be more than 10-fold higher than the classical values.

D. The role of the two histidines binding the Fe_2S_2 cluster.

As noted above, eq. 1 introduced thermodynamic values for the ISP in two different processes: through the role of $E_{m,pH}$ in determining $\Delta G^{o'}$, and through the value of pK_{ox1} in the Brønsted term. Electron and proton affinities for both redox centers are included in $\Delta G^{o'}$, but in the ΔpK term, the proton affinities alone. Looking at the equation as the summary of a hypothesis, the involvement if these work terms for ISP could clearly be tested in terms of properties of the ISP, and changes in those properties on mutation.

Following early redox titrations by Prince and Dutton [154] showing a pK ~8 on the oxidized ISP, Link [155] had shown using cyclic voltammetry [156] and CD spectroscopy [155] that this could be resolved into two pK values at 7.6 and 9.2. Structures of the solubilized extrinsic domain [123] had confirmed the ligation by two histidines, and Berry's complete structures [95] showed which of the histidines was likely involved in formation of the *ES*-complex in the full bc_1 complex. We had shown using CD spectroscopy on isolated bc_1 complex or chromatophores from *Rb. sphaeroides* [145], results similar to those of Link for the mitochondrial complex with pK_{ox1} of 7.6, pK_{ox2} of 9.8, and could then interpret these results in relation to the complete structure [95]; the stigmatellin-bound structure showed a complex with ISP through a H-bond from His-161 (avian numbering), which we suggested might indicate the location of similar complexes with ubiquinone in Q or QH_2 forms formed through a similar bond.

Our understanding of the first electron transfer in terms of the Marcus-Brønsted equation is outline above [129, 145, 148]. The overall reaction involves transfer of an electron and a proton from QH_2 to ISP_{ox}, and the probable sequence of the proton-coupled electron transfer could be calculated from a thermodynamic square (see Fig. 3) which strongly favored a proton first then electron sequence. With the bc_1 complex initially with Q.ISPH at the Q_o-site (the g_x=1.800 complex), the sequence [85] involves dissociation of the complex, domain movement, oxidation of ISPH, domain movement back, and then formation of the *ES*-complex and the processes leading to the intermediate product state given by the following scheme:

1. *Dissociation of His-161 (at pH >7.6)*: $ISP_o\text{-}NH^+\ldots(\text{cyt } b) \rightleftarrows ISP_o\text{-}N\ldots(\text{cyt } b) + H^+$
2. *Binding of QH_2:* $ISP_o\text{-}N\ldots(\text{cyt } b) + QH_2 + \rightleftarrows ISP_o\text{-}N\ldots Q_oH_2.(\text{cyt } b)$
3. *Equilibria in the ES-complex*: $ISP_o\text{-}N\text{---}H\text{-}O\text{-}Q_oH_2.(\text{cyt } b) \rightleftarrows ISP_o\text{-}N\text{-}H\text{---}O\text{-}Q_o.(\text{cyt } b) \rightarrow$ electron transfer, to yield the intermediate product state, $ISPH^{\bullet}.Q_oH^{\bullet}$.

(The scheme here is an elaboration of that in [85], with $\text{-}NH^+$ and -N representing different dissociation states of the N_ε atom of His-161 (His-152 in *Rb. sphaeroides*) , and N---H-O-Q_oH_2 and N-H---O-Q_oH_2 representing the H-bond from quinol -OH to N with the H-atom distal and proximal to the histidine, respectively.)

Most of this work, including several collaborations through structural, thermodynamic, kinetic, and spectroscopic studies using both wild type and specifically engineered strains, was reported before 2004. The results strongly support a detailed hypothesis for the mechanism for turnover of the Q_o-site, and in particular provided a detailed description and the characterization of the first electron transfer,

summarized in the Marcus-Brønsted equation above. However, the results also strongly support certain features of the second electron transfer of the bifurcated reaction: the need a rapid removal of the SQ and hence for movement of the SQ in the site. This hypothesis was fleshed out over the rest of the decade.

6. Detailed characterization of the first electron transfer

The changes in E_m and pK_{ox1} on mutagenesis of sidechains contributing to binding of the Fe_2S_2 cluster. Previous work on mutagenesis of ISP had shown that the both E_m and pK value were modified on elimination of H-bonds to the cluster or its ligands [104, 145, 157, 158]. The study by Mariana Guergova-Kuras, Richard Kuras and Natalia Ugulava was on mutations at Y156 to H, L, F, and W [157] (see scheme below), and had demonstrated changes in ISP properties induced by mutation that were important then, but took on new significance after our understanding of the PCET reaction in terms of the Marcus-Brønsted equation. In general, changes in activity were correlated with substantial changes in thermodynamic properties. The Y156H mutation had little effect on thermodynamic or EPR properties, perhaps because the H-bond to Cys-129 could still be made. The largest effects were in the Y156W mutant, were the rate of the Q_o-site reaction was substantially inhibited (to 7.2%), and this was linked to a change in the limiting E_m at pH below pK_{ox1} (from 312 mV in wildtype to 198 mV in Y156W), and of pK_{ox1} (up from 7.6 to 8.5). In addition, substantial shifts of the g=1.80 band in the presence of ascorbate (ISP reduced, but the Q-pool largely oxidized (the ISPH.Q signal) or in the presence of stigmatellin.

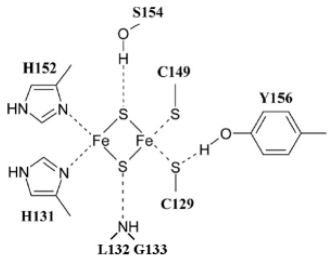

Derrick Kolling and Sanghoon Lhee [159] built on this preliminary work by detailed studies of the following mutant strains, newly constructed when necessary: S154T, S154C, S154A, Y156F and Y156W. We identified the structural basis of changes in the H-bonding of the Fe_2S_2 cluster using ESEEM spectroscopy in collaboration with Sergei Dikanov [160, 161], and, in collaboration with Satish Nair, by solving structures for mutant strains at high resolution (1-1.4 Å) [162]. These showed that, apart from the small changes in distance associated with the liganding atom, the mutations resulted in minimal structural distortion, so that the altered properties could be attributed to the H-bond changes, and pleotropic effects could be excluded. The exception was for Y156W, where the bulk of the tryptophan led to some displacement in surrounding residues. In a collaboration with Judy Hirst, Derrick had visited Cambridge to learn about protein film voltammetry [146], and brought the technique back to the lab where we developed our own apparatus and used it to characterize the thermodynamic properties of the mutant ISPs through redox titration as a function of pH over a wide range, and by characterizing the changes in kinetic behavior [159, 160, 162]. For the S154 and Y156 mutants, we performed extensive kinetic studies to show that the measured kinetic behavior could be accounted for by the Marcus-Brønsted equation simply by substituting the changed thermodynamic parameters [159].

We also constructed several mutants at G133 to P,Y,S, for which we did not characterize thermodynamic properties as extensively, but (with Satish Nair), did solve structures. The structures show that the backbone ψ, ϕ-angles in the native protein lie in the area of Ramachandra plots normally accessible only for glycine. As a consequence, all mutations at this residue flipped them to a more conventional range. This removed a weak H-bond with an S-atoms of the cluster through the backbone >NH, which could no longer be made in the mutants (Lhee, S. and Nair, S. unpublished). In the structures of the complete complex, the volume around the L132 - G133 span is open, so mutation to larger residues is tolerated. We had previously shown that the G133D mutation leaves an active bc_1 complex, but with the rate 20-fold slower than in wildtype [104], which was in line with the behavior in a spontaneous mutation in the yeast bc_1 complex with this residue change [163].

This body of work established rigorously that the oxidation of QH_2 by ISP_{ox} is dependent on the thermodynamic properties of His-152 as expected from a proton-coupled electron transfer occurring in a proton-first-then-electron sequence. The rate constant using the Marcus-Brønsted equation was smaller than that calculated from the Moser-Dutton equation by the ΔpK of 5 in the right-most term, and the thermodynamic properties then accounted for the slow rate of the reaction compared to that expected from simple electron transfer through the distance shown by structures. The endergonic nature keeps the occupancy of the SQ product low (to minimize SO production) but requires a rapid rate constant for removal to ensure the observed forward rate. This in turn necessitates a movement of the SQ closer to heme b_L. This second electron transfer is also proton coupled, as detailed in the next section, but through separate steps. The mechanism proposed for the first electron transfer accounts economically for the observed behavior over a wide range of changes in the critical properties explored using many mutant strains. Since this is the rate determining step, our mechanism also explains much of the subsequent behavior of the complex.

7. Pathway for reduction of heme b_H on transfer of the second electron and exit of the proton.

We had suggested in 1999 [129] that a movement of the SQ in the Q_o-site site from a domain distal, to one more proximal to heme b_L might be essential. This was based on occupancy of the latter domain by myxothiazol, the displacement of the side-chain of the highly conserved glutamate in the -PEWY- span of cyt *b* observed in the structures, a water chain populated in MD simulation [130] of the ISP movement. This displacement brought the glutamate sidechain into contact with a water chain connecting to the P-phase and providing an obvious path for proton exit. From a detailed analysis of mutant strains in terms of differential effects in inhibitor resistance, differential effects on partial processes, and on their location in structures [127, 128], it was also obvious that residues in the proximal domain were important to function. Hunte and colleagues independently suggested a similar role in H^+ exit of the equivalent glutamate (Glu-272 in their yeast bc_1 complex structure), but based on crystallographic waters; these showed a water chain similar to the one we had anticipated from our MD simulations [130].

A. Tyr-147 provides the H-bond to QH_2 in formation of the ES-complex.

The pathway suggested in [129] was based on an *ES*-complex modelled on the complex between ISP and stigmatellin, in which the -PEWY- glutamate served as a second ligand to the inhibitor. The stigmatellin resistance seen in E295 mutants supported the crystallographic model. We also noted that these same mutant strains showed a weak increase in K_m for QH_2, that might indicate a weak liganding of QH_2 by the glutamate. On the other hand, many structures with other quinone analogues bound later became available, which show several different configurations for the site, and other possible coordinating residues. Our recent MD simulations in *Rhodobacter* complexes [164, 165] have suggested that Tyr-147 (in *Rhodobacter* numbering) forms the immediate H-bond to QH_2. A similar configuration had been seen previously by Esser et al. in the bovine complex with UHDBT [166], and compared there with structures containing complexes to stigmatellin, myxothiazol and several other similar compounds. Since the role of Glu-295 in proton transfer had been clearly established (see ***B*** below), Barragan et al. [167], included this as a secondary ligand to the Y147 -OH group in the model used for QM calculations. They suggest that E295 could serve as the acceptor of the H^+ released by relay through Y147. The glutamate could then function to facilitate H^+ exit as suggested in the original scheme, by rotation of the side chain -COOH down to the water chain leading to the P-phase.

B. Further characterization of the role of the -PEWY- glutamate. The first electron transfer from QH_2 is a neutral process involving transfer of an electron and a proton to ISP_{ox}, and generation of $QH^{\bullet}$, as discussed above. In the endergonic process involved, the back-reaction would be much more rapid than the forward, and to achieve efficient forward chemistry, the removal of SQ would have to out-compete the back reaction. The SQ is initially generated in the neutral form, so oxidation would involve transfer of both an electron and a H^+, with the latter likely exiting via the -PEWY- glutamate. Earlier work [129] had shown that all strains mutated at E295 showed inhibition of heme b_H reduction (E295D at 11%, E295G at 4.9%, E295Q at <4%). We also showed that E295D and G led to stigmatellin resistance, and noted a small increase in K_m for QH_2, consistent with the *ES*-complex modelled on the stigmatellin structure showing involvement of E295 in binding the inhibitor. This earlier work had been criticized by Osyczka et al. [168] on the basis of work on additional mutations at this site. All mutant strains showed substantial inhibition of heme b_H reduction in the presence of antimycin. Unexpectedly, E295V showed a relatively weak inhibition (83%), but the others were in line with our earlier results, ranging from 88% for E295H down to 98% for E295Q, measured at pH 7. Importantly, they showed that none of these mutations affected binding of stigmatellin or formation of the g_x 1.800 complex, or had any obvious effect on the E_m values of redox centers, or in the reduced - oxidized ATR-FTIR difference spectra. In view of the high degree of conservation of the -PEWY- span, and the substantial inhibition of the reduction rate for heme b_H, their main conclusion was that Glu-295 had no specific catalytic function, and they specifically excluded the role in proton exit we had previously proposed.

To address this critique, in more recent work [139], we constructed additional E295 mutants and showed that in all mutated (strains E295D, G, Q, K, T and W) the strongly inhibited turnover was consistent with the essential role in H^+ exit we had earlier proposed. As observed previously [129], E295D retained a considerable rate (~11%), consistent with its carboxylate nature, but the still substantial inhibition suggested that the greater "reach" of the glutamate side chain was essential to maximal function, but all other strains showed inhibition >90%. We extended the conclusion that the binding reactions between ISP and occupant were not affected by mutation to include the equilibria associated with formation of the ES-complex. However, the lack of effect on the parameters associated with the first electron transfer, left open the important role in proton exit we had proposed in the second electron transfer. It was obvious from our measurements of the pH dependence of electron transfer in wild-type and mutant strains that the effects on the rate limiting step associated with p*K* values of His-152 and QH_2 described in the Marcus-Brønsted equation were not observed in the mutant strains, from which we concluded that the rate-determining step was no longer in the first, but now in the second electron transfer. Furthermore, in determining the degree of inhibition, we now had to compare these rates to the uninhibited rate of the second step, with rate constant necessarily orders of magnitude higher than the first.

C. With the rate limiting step in the second electron transfer, the pH dependence reveals a new pK at ~8.5, leading to increased rate.

We characterized the kinetics of electron transfer through the Q_o-site by measuring hemes (c_2 + c_1), heme b_H, heme b_L, and the reaction center (RC) to study the pH dependence over a wide range [139]. In wildtype, the rate of turnover increases over the range pH 6 to 8 with an apparent p*K* ~6.5 (pK_{ox1} convoluted with the binding energy for QH_2 in formation of the *ES*-complex, see above), followed by a decrease reflecting pK_{ox2}. In contrast, the more strongly inhibited strains all showed a relatively flat pH dependence in the range pH 6 to 7. Because the rate was so slow, reflecting the high degree of inhibition, (<7 s^{-1} at pH 7 compared to ~700 s^{1} in wildtype), the increase in rate with pH over this range seen in wildtype was mostly lost in the noise, but as the pH was increased we then saw a more substantial

increase in rate (to as high as 70 to 80 s^{-1} in E295G, K, Q) over the range pH 7.5 to 9, with a pK ~8.5 ± 0.3; the wildtype showed the decrease in rate over this range associated with pK_{ox2}.

D. Binding of QH_2 is independent of pH over a wide range in wildtype and mutant strains.

Even in the severely crippled mutants, the increase in rate on reduction of the pool (to vary [QH_2]) was sufficient to determine values over a wide range of pH for the binding of QH_2 in formation of the *ES*-complex. This effect can be expressed in terms of the shift in E_m dependence of rate compared to the E_h of the Q-pool (see **5 *A*** above and [74, 84]), and used to calculate K_m values. In wildtype, the shift is 30 to 40 mV, showing a 10 to 15-fold tighter binding of QH_2. Within noise levels, the same shift was seen in the mutant strains, independent of pH over the range 6 to 8. However, when expressed in terms of K_m, the scatter was substantial, and led us to conclude that the small effect of mutation of E295 on binding of QH_2 previously reported [129] was not significant. In addition, it was unlikely that the pK at 8.5 could reflect effects on the formation of the *ES*-complex.

E. Candidates for the pK at~ 8.5 and possible roles in the dissociation of $QH^{\bullet}$ to release H^+.

Which dissociable group contributes the pK? This is a complicated question, because several groups might be involved, and pK values can be changed by coulombic effects and local dielectric behavior. One simple answer comes from consideration of the species providing the electron, the $QH^{\bullet}$ of the first electron transfer. The initial product of the 1st electron transfer is the complex ISPH.$QH^{\bullet}$. The question is then how rapidly this complex dissociates, and by what path. If dissociation of the intermediate state were rapid, and independent of dissociation of $QH^{\bullet}$, and the ISPH moved away (to reduce heme c_1) releasing the free $QH^{\bullet}$, that could be a mobile species, and inhibition in the E295 mutants might reflect loss of the facilitation of dissociation and H^+ exit later in the process. Another scenario is that dissociation of the ISPH.$QH^{\bullet}$ complex might depend on transfer of the proton from the bound $QH^{\bullet}$ to E295-COO^-, and that only then could $Q^{\bullet-}$ become mobile, and able to serve as donor to heme b_L. In this second scenario, absent E295-COO^-, both $QH^{\bullet}$ and ISPH would be tied up so as to prevent movement. In either of these pictures, the forward flux would require eventual transfer of the H^+ from $QH^{\bullet}$ to the glutamate. In the E295 mutant strains, since the H^+ acceptor is lost, the SQ would be left in the neutral $QH^{\bullet}$ form. If the pK at 8.5 is from dissociation of this group, the increase in rate in this range could then be attributed to dissociation of that species. The still inhibited rate would then have reflected loss of *catalysis* of the H^+ exit pathway. In any scenario in which $QH^{\bullet}$ passes a H^+ to an acceptor, the suitability of the two pK values has to be addressed. If $QH^{\bullet}$ had a pK in the ~8.5 range, the acceptor would be expected to be in the same range or higher. Although glutamic acid has a pK_a ~4.3 in aqueous solution, when buried in a protein, the pK can be much higher (cf. E286 in cytochrome oxidase, with pK >9 [169, 170]. If such is the case here, the pK would have to change dramatically in the dissociation leading to release to the aqueous phase. This seems unlikely, - in the cytochrome oxidase case, the high pK reflects electrochemical equilibrium with the aqueous in which a proton well effect leads to a large contribution of the membrane potential component, and any such effect at the Q_o-site would likely be smaller and have the wrong sign. There are other potentially dissociable groups in the reaction volume, in particular Tyr-147, and His-276, either of which might have a pK in that range. However, since the histidine is replaced by aspartate in bovine or avian complexes, it seems unlikely that the pK at 8.5 would apply there. This leaves the tyrosine as the most plausible contender. We will discuss this pK later in the context of H^+ exit pathways.

One conclusion previously noted above was that in the E295 mutants, the rate limiting reaction had been shifted from the first electron transfer to the second electron transfer. We had previously shown in wild type that the rate constant for removal of the SQ intermediate must by very substantially higher

than the ~10^3 s^{-1} rate limiting the first electron transfer. The substantial inhibition of the overall rate in E295 mutants means that, when compared to the rate constant for oxidation of SQ, the 90% inhibition represents a massive change in this rate constant.

F. Occupancy of the intermediate semiquinone state allows calculation of a rate constant for its removal.

We determined an occupancy of SQ (0.03) at the Q_o-site in wild-type under conditions in which its removal was blocked by inhibition of the Q_i-site by antimycin, confirming the findings of Cape et al. [143]. We extended measurements to the most strongly inhibited mutant, E295W, which showed a higher occupancy (0.06) [139]. The results allowed us to estimate the rate constant for oxidation of SQ by heme b_L in E295W, based on $k_{cat} = v / ([SQ])$. In the scenario above, in the E295W strain, the loss of the dissociable carboxylate on mutation of the glutamate and the bulk of tryptophan, would prevent both any role in proton exit, and, if the bulk impeded rotational displacement, movement into the proximal domain. From the pattern of behavior, the rate limiting step was no longer in the first electron transfer to generate the SQ, but now in the pathway for oxidation of SQ. Using the occupancy of 0.06 for SQ in E295W, and the maximal inhibited rate of ~60 e^-/s/bc_1 (from the rate at pH 9), we determined a maximal k_{cat} <10^3 s^{-1}. In contrast, given the endergonic nature of the reaction, the uninhibited rate constant would need to be >10^6 s^{-1}, more than 1000-fold greater than the maximal turnover rate of ~10^3 s^{-1}, to outcompete the backreaction. A similar value can be calculated using the 11.5 Å for an edge-to-edge distance from an occupant of the distal domain to heme b_L and reasonable values parameters in the Moser-Dutton equation, to give a value for k_{cat}(distal) of ~10^6 s^{-1}. On the other hand, the 6.5 Å distance from the proximal position gives k_{cat}(proximal) of ~10^9 s^{-1}, so that, at the occupancy observed in wildtype, oxidation of $Q^{\bullet-}$ by ferriheme b_L would not be rate determining.

8. Why is the Q_o-site so complicated? The need to limit by-pass processes

The success of the modified Q-cycle in explaining the normal forward pathway of electron and proton transfer in the absence of structural information begs the question of why the Q_o-site revealed by the structures is so much more complicated than might have been expected. The answer lies in the by-pass reactions and the damage they do. Early work from Boveris and Chance [171, 172] showed that under conditions in which the bc_1 complex becomes backed-up in the low potential chain (antimycin inhibition, or back-pressure from the proton gradient) the complex generated reactive oxygen species, attributed to reduction of O_2 to O_2^- by SQ. Much of the argument about mechanism above had been framed in terms of the need to limit SQ occupancy to minimize such reactions, reviewed in [173]. Under aerobic conditions similar effects are seen in the bacterial complex. Under anaerobic conditions and photosynthetic turnover, on antimycin inhibition the complex turns over at a similar rate, about 1% of the uninhibited complex through slippage in the Q_o-site attributed to other by-pass reactions. In our collaboration with Dave Kramer's group, Florian Muller in 2002 discussed several mechanisms in which a SQ intermediate was important [174], all in the context of Q-cycle mechanism in which, under backed up conditions, SQ could accumulate but under conditions restricting occupancy.

The need to limit bypass reactions introduces complicating features arising from the need for gating [139, 175, 176]. In particular, as noted in [177], the movement from distal to proximal domains would not by itself eliminate bypass processes (see next section). Recently we have been able to explore these conditions using a microfluidics based rapid-mix followed by rapid freeze-quench experiments. We have been able to observe a free radical signal in the g=2.00 region of the EPR spectrum, which might suggest SQ accumulation at the Q_o-site in the first few ms after adding oxidized cyt c to an anaerobic mixture of QH_2 and bc_1 complex in the presence of antimycin [165, 178]. With heme b_H initially oxidized,

we could detect no SQ until after the first turnover of the site needed to reduce heme b_H (~ 1 ms); as heme b_L became reduced, the SQ began to accumulate but only if acceptor (cyt c^+) was present in excess to pull the second electron transfer over. However, with hem b_H initially reduced, SQ accumulated over the first ms, with a hysteresis associated with reduction of heme b_L. In the E295 mutants, this rapid appearance of SQ was independent of the redox state of heme b_H. The results support a model in which deprotonation of $QH^{\bullet}$ to form $Q^{\bullet-}$ is the rapid event, likely lost in the E295 mutants, and must precede migration of $Q^{\bullet-}$ from distal to proximal domains of the Q_o-site to facilitate rapid electron transfer. Consideration of the changing occupancies of charged species (E295-COO^-/–COOH, $QH^{\bullet}/Q^{\bullet-}$, heme b_L^+/b_L(H)) opens the discussion of the coulombic consequences introduced on coordination SQ oxidation with proton exit with the redox changes of heme b_L, and the possibility that this could allow coulombic gating important to frustration of by-pass reactions [82, 83, 139, 165, 175, 176, 178-180]**.** We will return to this discussion later (**16, F)**.

A. Mechanisms for coping with by-pass reactions in the Q_o-site

In an important paper in 2005, Osyczka et al. [177] argued that, in a model configured so that distances for the Q_o-site reactions were those shown in the structures, massive by-pass rates would be expected from the modified Q-cycle, and suggested that the Q-cycle needed fixing to deal with this. Their model was somewhat limited by a treatment in which all Q_o site reactions were restricted to the distal domain, and redox reactions were treated as electron transfers with rate constants determined by the Moser-Dutton equation. They have an extended and sophisticated discussion of possible mechanisms that included our model requiring SQ movement suggested in two earlier papers suggesting [127, 129], but they dismissed it (correctly in the context of their model) by pointing out that the rate constants for reverse reactions would be even higher for SQ on the proximal domain. However, they had ignored all publications from the Crofts lab over the intervening five years establishing the characteristics of the rate limiting first electron transfer. Consequently, although speculation on the role of waters in equilibration with H^+ was included, no account was taken of the important features of the first electron transfer summarized in the Marcus-Brønsted equation where, in the coupling of electron transfers to protons, the proton has a controlling role. The important question of occupancy in determining rate was not seriously considered. In the earliest of the post-structural papers, we had pointed that SQ was likely formed at such a low occupancy that even with quite high rate-constants calculated, it would have to move to expedite rapid forward reaction [84, 121, 151]. In their model for the second electron transfer, all rate constants for forward and reverse reactions involving heme b_L were determined by the same 11.5 Å distance. As a consequence, without gating, the bypass reactions that came from back reactions from the reduced heme b_L to Q or SQ would occur with rates determined by similar Moser-Dutton parameters as for the forward reaction. The massive de-coupling they predicted was based on this simplistic model; since no such effect was observed experimentally, their discussion of possible mechanisms for their prevention, - the fixing of the Q-cycle of their title, - was impoverished by its exclusion of alternative scenarios involving movement of the SQ.

They suggested two types of mechanism: either that the two steps of the bifurcated reaction must be concerted so as to eliminate SQ generation, or that they must be so strongly controlled that the first step could occur only under conditions in which SQ was rapidly removed. The first of these alternatives was physico-chemically unrealistic. Their concerted case was in effect a model considered by Crofts and Wang [81] in which the intermediate state generating SQ would have to be that of the activation barrier. In light of the 65 kJ/mol activation barrier shown by Hong et al. [131], the occupancy would be so low that no realistic value for a rate constant for electron transfer to heme b_L from the distal domain could

provide the observed rate. In the case invoking strong control, the mechanisms suggested were largely speculative, involving gating of H^+ transfer by configurational changes of H_2O molecules, following an idea from Wikström et al. [181] who had suggested this type of mechanism in cytochrome oxidase where it was justified in the context of detailed structures and innovative physical chemistry. Among the important features they missed were that a mechanism with a mobile SQ opened many possibilities for control that were unavailable for any process constrained to reaction from the distal domain, and that Dutton's ruler, although useful for simple electron transfers, was inadequate in calculation of rate constants involving proton-coupled electron transfers of the type involved in the first step of oxidation of QH_2. Other critical points ignored were the argument constraining occupancy of *all* intermediate states before heme b_H to ≤0.02, and the need for a rate >>100-fold greater than the limiting first electron transfer so as to out-compete the more rapid back reaction from the strongly endergonic nature, together indicating a need for mobility.

With hindsight, their failure to recognize or address these difficulties left their argument somewhat empty. The main theme of the paper could be restated as showing on important point, - that the simple model resulting from treatment of all electron transfer reactions through the Moser-Dutton equation with fixed distances given by crystallographic structures must lead to the massive by-passes, and that these can be avoided only if additional complexities are considered.

Our early discussion had not adequately dealt with need for specific gating pointed out in [177], and out subsequent efforts were addressed at correcting this deficit in the light of the mobility of the SQ. This could be most economically achieved if the SQ was, in the backed up case, constrained to the distal position [176]. We discussed mechanisms in terms of coulombic interactions between $Q^{\bullet-}$, the proton released, and the carboxylate form of E295, changes in the local electrostatic field on reduction of heme b_L, and protonation of the propionates, and pointed out possibilities for gating. In the later extension of the E295 work, we suggested a kinetic model of the Q_o-site reaction in the presence of antimycin, and showed that we could account for the behavior both in wildtype and in the glutamate mutants discussed above, in terms of the parameters for the first electron transfer provided by the Marcus-Brønsted equation, and a model for the second electron transfer including movement of the SQ [139], with all rate constants justified experimentally or derived by calculation and explored through the model to reveal plausible values, but with a bias between k_f and k_b for SQ movement introduced by coulombic fields. Although recent developments show that the model needs to be refined (see **16 *F*** below), our general conclusions still stand. "…The results are consistent with a plausible mechanism for this second step of the bifurcated reaction, and suggest a molecular ballet, with E295 as the prima ballerina, whose choreography is directed by coulombic interactions that implement control functions. In the mechanism we propose, and in contrast to previous proposals…the participation of E295 lowers energy barriers for the forward reaction as in the conventional view of catalysis, but raises them towards the bypass reactions by exploiting separate pathways for electron and proton, the spatial separation between the distal domain (at which SQ is generated) and the proximal domain (close enough to the acceptor (heme b_L) for rapid oxidation), the mobility of the SQ, and the potential for gating in the flexibility of conformation in the Q_o-site, and a dance, frozen in the (crystallographic) structures, whose step-by-step choreography remains to be explored…".

B. Simplified models derived from the structures by application of the Gillespie algorithm

Essentially the same problem with a static Q_o-site mechanism arose in an interesting exercise in speculative modelling by Ransac et al. [182, 183]. They asked what the outcome would be if they simply took the structures, calculated rate constants from distances, and asked the Gillespie algorithm [184] to sort out the probable pathways. With values chosen to ensure that binding and unbinding of substrates and

products did not limit, and some minor fudging to accommodate the movement of ISP, the mechanism that emerged was a simple modified Q-cycle, essentially that previously chosen by Osyczka et al. [177] in discussing how to fix the Q-cycle. The common features were use of structures to determine distances for electron transfer, restriction of reactants to the distal volume of the Q_o-site shown by stigmatellin, calculation of rate constants determined by crystallographic distances and use of the Moser-Dutton equation. These entailed all the inadequacies pointed out above; such models ignore the proton coupling equilibria, our Marcus-Brønsted treatment [82], and complexities from movement. The problem was revealed when they extended their kinetic model to consider antimycin inhibition; they rediscovered the Osyczka problem, - a massive decoupling so that antimycin failed to inhibit [183]. To overcome that deficit, they increased the complexity of their kinetic model to include both monomers, a substantial flux across the dimer interface, and feedback from the two-electron gate of the Qi-site [183]. However, from our own work ([175] and see below), we had concluded that no flux comparable to that of normal forward chemistry could be detected across the dimer interface. From that perspective, their more complex model was not satisfactory.

The Ransac et al. model [182] was used later by Springett and colleagues [185] in a neat spectroscopic approach to measurement of membrane potential in intact cells. The basis of the measurement was the exploitation of the positions of hemes of b_L and b_H in the axis perpendicular to the membrane, and the fact that electron transfer occurs across the membrane through the hemes to generate the membrane potential, $\Delta\psi$. The potential was then "felt" by the electron so that the measured redox difference between the two hemes changed with $\Delta\psi$, as given by $\Delta G^{b_L-b_H} = -\left(E_h^{b_H} - E_h^{b_L}\right) + \beta\Delta\psi$, where β is the fraction of the dielectric distance of the insulating phase between the two hemes. By quantifying the redox potentials of the two b-hemes, they could calculate $\beta\Delta\psi$, and use the structures to determine β. The results reported looked sensible and therefore seemed to indicate that the simple treatment was realistic. As in the Ransac et al. treatment, rate constants were based on distances and application of the Moser-Dutton equation, and no attention was paid to the complications introduced by proton coupling. From this, the Springett model should have shown the bypass reactions anticipated in [177, 182, 183]. This then raises an obvious question. Since the $\Delta\psi$ provides a back-pressure on forward electron transfer, under conditions in which the value approaches the maximal ~180 mV, why does this not lead to massive decoupling as electrons back-up in the *b*-heme chain, as seen by Ransac et al. in the presence of antimycin? The parameters of the model were discussed in somewhat general terms in [185], mainly by reference to the Ransac model [182], but was based on a monomeric mechanism. Consequently, the dimeric interactions used to explain away the antimycin decoupling would not have been available.

The resolution to this paradox is given in a more recent paper from the Springett group [186]: "…However, contrary to the enzyme, the model showed substantial short circuiting under *in vivo* conditions. To prevent the short circuiting, we artificially constrained the model to precisely bifurcate by omitting the short circuit elementary reactions…". Removing essential rate constants clearly is *not* in the spirit of the Gillespie algorithm. The general idea of using the measured $\Delta G^{b_L-b_H}$ to estimate $\Delta\psi$ is neat, but before it can be more generally applied, it needs a mechanistic context that avoids the shortfalls of the Osyczka/Ransac model.

9. Electron transfer across the dimer interface

The Q-cycle mechanism in its simplest form is functionally monomeric, but the structures show a homodimer, with one monomer rotated 180° about the vertical axis with respect to the other so that the dimer interface involves the same face but complementary surfaces. In fact, the interface involves relatively little area. In terms of mechanistic interest, the interface between the volumes containing the

two b_L hemes is the most interesting, discussed at length below, and, below that, the "clamps" constraining the ISP anchors. The structure above the interface between the b_L hemes in all crystallographic structures is an 'empty' volume, open to the lipid phase on two sides, likely occupied by disordered lipid side chains, but defined by trans-membrane helices on the closed sides, forming a cone with the wide end at the top. There, a pair of horizontal helix-turn-helix motifs, one from each cyt *b*, provide an upper scaffolding, in which interaction between the turn and the ends of membrane helices of the other monomer form two other interface between the cyt *b* subunits. The volume is open at the sides to the insulating phase, and at the top to the aqueous N-phase.

One function requiring a dimeric structure is the electron transfer by domain movement of the ISP. The membrane anchor for ISP is bound in one monomer while the interactions of the cluster binding domain with its partners were all in the other. In both subunits, as noted above, the structure linking head to membrane anchor is clamped at the dimer interface so that the movement does not get unhinged.

Are there other functional requirements for the dimer? Application of the Moser-Dutton equation suggested that electron transfer across the dimer interface at the level of heme b_L should be rapid. With closest distance of 10.54 Å, rate constants in the range from $4.08\ 10^5\ s^{-1}$ up to $6.51\ 10^6\ s^{-1}$ could be justified [175]. (The range of values depends on choice of parameters (see *eq*. 1 and discussion); in particular, choice of a value of 3.1 for γ gives rate constants substantially higher than choice of 4.23, the classical value.). These compare with a distance of 7.02 Å between heme b_L and heme b_H, and rate constants for transfer about 100-fold higher, so that path should normally out compete the intermonomer flux [187]. However, in antimycin inhibited conditions, with myxothiazol present to block half the Q_o-sites, reduction of heme b_H should still occur rapidly in most dimers (see Fig. 4). All such inter-heme rate constants are much more rapid than the rate-limiting first electron transfer of $\sim 10^3\ s^{-1}$, and several groups had claimed to demonstrate inter dimer electron transfer expected from this. However, we had earlier explored this question experimentally in some detail, and concluded from several arguments that no significant flux of electron transfer across the dimer interface could be detected [175]. The path of closest approach includes a pair of tyrosine residues (Y199 in *Rb. sphaeroides*, or phenylalanines in most mitochondrial complexes), one from each monomer configured in opposite directions on either side of the vertical axis of symmetry that passes between them (Fig. 4, C), defining the interface. We constructed mutant strains Y199T, L, S and W, each of which would substantially change the physical chemistry of the interface and any putative pathway for electrons. All showed rapid turnover of the bc_1 complex, comparable to wildtype. We also constructed a strain to mimic the chain in the chloroplast cyt b_6f complex, in which a threonine was inserted between His-198 (the heme b_L ligand) and Tyr-199, which was also functional, but with a somewhat reduced rate. To test for electron transfer across the interface (see Fig. 4A), we analyzed the shape of the curve for all these strains when rates were titrated by incremental additions of myxothiazol. Kinetics were measured with saturating antimycin to block the dimer at both Q_i-sites. Reduction of heme b_H can then occur either through the monomeric mechanism, or, to the extent that electron transfer can occur across the dimer interface, by that route. Titration using myxothiazol to progressively inhibit the Q_o-sites will result in a linear curve for monomeric mechanisms, and a convex curve if transfer between heme b_L can occur. For example, when half the Q_o-sites are inhibited, in the inter dimer model, heme b_H in the myxothiazol-inhibited monomer could still receive electrons from the uninhibited Q_o-site. With excess substrate, the amplitude of b_H reduction would show both hemes going reduced because the uninhibited site could turnover more than once. This simple picture is complicated by the statistics of binding. Assuming equal affinity for myxothiazol at both sites, when half the sites are inhibited, 25% of dimers will have neither Q_o-site blocked, 50% one or the other blocked, and 25% will have both blocked. If the mechanism is monomeric, any monomer blocked would be unable to reduce the b-hemes, so the fraction of heme b_H reduced would be proportional to the fraction

of Q_o-sites blocked, generating the linear titration. The behavior in the intermonomer transfer case could be modeled to show what degree of convexity of the titration curve to expect (cf. [188]), always substantial. Our titrations with wildtype and all the mutant strains, showed strictly linear behavior [175]. We concluded that no rapid flux across the dimer interface could be seen, even when in a second turnover, the unblocked Q_o-site would generated maximal redox pressure (in equilibrium with a strongly reduced heme b_L) for transfer across the interface to reduce any *b* hemes still oxidized in the myxothiazol-blocked monomer [175, 188]. We discussed earlier suggestions from Covian et al. [189, 190] that electron transfer across the dimer interface could occur rapidly, and pointed out that the modified Q-cycle accounted naturally in a monomeric context for several of the effects interpreted as showing this. We also pointed out that the convex titration curves they found could be explained by "pool" effects previously seen by Kröger, and Klingenberg [191, 192].

We went on to consider consequences of the dimeric structure that did not involve electron transfer across the interface [175]. Effects could be expected from coulombic interactions. It had earlier been recognized that within a monomer such effects are to be expected most obviously between hemes b_H and b_L, where redox titration will show heme b_H titration unaffected by reduction of heme b_L, but heme b_L titration always reflecting the charge on the reduce heme b_H. This was demonstrated by Yun et al. [92] in strains mutated to eliminate binding of heme b_H, leading to a higher observed E_m for heme b_L. Other effects can be explored kinetically (cf. [193]). We pointed out that similar coulombic affects would be expected across the dimer interface. We demonstrated that, on careful analysis of redox titrations, the curves could be better interpreted as showing two components titrating with slopes n=1, with E_m values separated by coulombic interaction.

Another important feature of the interface between the two cyt *b* monomers is the clamping of the membrane anchors of the two ISP subunits over the short span as each transitions to the linker connecting it to the mobile head. Although the clamps for the two are separated, there are possibilities for interaction between them through chemo-mechanical forces. It is still an open question as to whether these possibilities for coulombic and mechanical interactions are exploited in coordinating the activities of the two monomers.

Although we could explain previous data from Covian et al. data [189, 190] suggesting intermonomer redox traffic, and had demonstrated that none could be discerned in the kinetics, somewhat surprisingly, a number of other groups have since claimed that rapid intermonomer electron transfer can be demonstrated. The most experiments from which this is most strongly advocated [194-196] have shown turnover in heterodimeric constructs of the bc_1 complex in which differential mutation in the two monomers enforced function through electron transfer across the interface at the level of heme b_L.

In the Świerczek et al. paper [194] from the Osyczka group, the authors claim to have demonstrated that: "…Electrons moved freely within and between monomers, crossing an electron-transfer bridge between two hemes in the core of the dimer. This revealed an H-shaped electron-transfer system that distributes electrons between four quinone oxidation-reduction terminals at the corners of the dimer within the millisecond time scale of enzymatic turnover…". Since these results would not be possible without rapid electron transfer across the dimer interface, they were clearly in conflict with our earlier work [175], which had been cited but dismissed in a disparaging phrase. In their protocol, heterodimeric complexes were synthesized in *Rb. capsulatus* by replacing the *fbc b* gene by a gene coding for two cyt *b* sequences, joined by a linker span. Different strains were generated in which mutations H212N and G158W were constructed in the two copies in different combinations (Fig. 4B). The H212N mutation eliminates a ligand to heme b_H to block electron transfer beyond heme b_L (see [92] for rationale), and the G158W mutation replaces a glycine in the Q_o-site in the volume where the ring of

Q/QH_2 is found, by a bulky tryptophan to block the binding of QH_2, either mutation inhibiting flux in the homodimeric complex. By judicious placement in the two copies, the heterodimeric complex could be blocked so as enforce transfer across the interface. The authors represented different configurations in a useful shorthand, for example, in $_{W}$B-B^{N}, by showing one monomer, $_{W}$B, mutated to block the Q_o-site by G158**W**, and the other, B^{N}, with H212**N** to prevent binding of heme b_H, and thus block transfer of electrons to the Q_i-site (see Fig. 4B for location of mutations). In $_{W}$B-B^{N}, neither monomer could function monomerically, but flux through the Q-cycle could occur by turnover of the Q_o-site in monomer B^{N} and transfer across the interface to reduce heme b_H in monomer $_{W}$B. The subscripted W and superscripted N roughly indicate the positions with respect to cyt *b* (B) in the membrane, with the N-phase at the top as seen in Fig. 4B.

In order to explore the system, we developed similar protocols to generate such heterodimers in *Rb. sphaeroides* [188] , and were surprised to be able to reproduce the Świerczek et al. behavior. However, in our hands, the appearance of rapid electron transfer in such systems turned out to be the outcome of an endogenous corrective process. We demonstrate a local genetic mechanism, leading, in strains enforcing interdimer flux, to reconstruction of the homodimeric wildtype sequence at the DNA level by crossover recombination between the two copies of the gene encoding cyt *b*, to eliminate the mutations and generate the wildtype sequence, now expressed in homodimeric complexes [188]. Interestingly, in strains with the constructed DNA encoding complexes with one monomer fully functional, although most of the DNA analyzed was that encoding wildtype homodimers, a fraction of the DNA encoding the heterodimer could still be detected in substantial amounts. We suggested that heterodimers with one functional monomer were active enough to compete. When we explored different stages of the mutagenesis protocol, we found with constructs encoding $_{W}$B-B^{N} strain, that cross-over could be seen already in *E. coli* in the preliminary phase of the engineering protocol, as detected by similar levels of short 'monomeric' DNA and double length 'heterodimeric' DNA. On growth under aerobic conditions in the dark, both DNA classes were expressed at similar levels in *Rb. sphaeroides*, but it was clear that under photosynthetic growth requiring an active bc_1 complex, the DNA encoding the heterodimeric strains could no longer be detected, and the population that survived was homodimeric and wildtype.

Surprisingly, no difficulties of this sort had been discussed by Świerczek et al. [194]. However, after we had shown our results at a Gordon Conference, several additional papers were quickly published in which it became obvious that they were well aware of the problem and had taken substantial efforts to ameliorate it. All their genetic manipulations and samples for experiment had involved growth under dark, aerobic conditions in which the selective pressure of photosynthetic growth was avoided. The suppression of this information in the original publication was certainly not in the interests of science.

One substantial new experimental result was shown in a later publication [197], where the authors succeeded in isolating bc_1 complex from heterodimeric strains B-B, $_{W}$B-B, ^{N}B-B, $_{W}{}^{N}$B-B, and $_{W}$B-B^{N} strains, and assayed their decyl benzohydroquinone (DBH_2):cyt *c* reductase activity as a function of increasing concentration of cyt *c*. I have included the kinetic traces from their paper so that the reader can understand the point I want to make (Fig. 5). On examination of the titration curves, it will be seen that, with one exception, all showed the same dependence on [cyt *c*] and, to a good approximation, gave maximal rates (V_{max}) proportional to the concentration of active monomers. With respect to the order above, values report were 408, 267, 223, and 173 s^{-1}. The exception to this pattern was strain $_{W}$B-B^{N}, for which they reported a V_{max} of 69.8 s^{-1}. However, the titration curve shows that, within the scatter, the same rate was detected at the lowest concentration of cyt *c* (~1-2 μM) as at the highest (80 μM), so this is clearly not a V_{max}, but some non-enzymic process independent of [substrate].

The obvious take-home message from this paper was that these results were entirely consistent with those from our earlier kinetic analysis [175] and cross-over data [188]; each monomer acts more or less independently and at maximal rate, and no electron transfer across the dimer interface occurs "…within the millisecond time scale of enzymatic turnover…". However, the authors instead claimed that their V_{max} value of 69.8 s^{-1} for $_{W}$B-B^{N} proved that electron transfer across the dimer interface occurred at a substantial rate.

In Lanciano et al. [195], similar mutations (also in *Rb. capsulatus*), H212N and Y147A, were constructed, but using two separate versions of the gene, modified so as to allow selective expression using differential antibiotic resistance, and/or separate isolation of different mixtures by differential epitope-tagging. This more sophisticated approach likely reflected a response to difficulties encountered in earlier work in the Daldal lab similar to those discussed above. The H212N removes the same heme b_H ligand as in [194], but the Y147A mutation used to block the Q_o-site, was selected on the basis of earlier mutagenesis at this site showing nearly complete inhibition of Q_o-site turnover in this strain [198]. This mutation is closer to the heme b_L, and blocks electron transfer through a different mechanism than the steric effect of G158W mutation in the distal lobe. As noted briefly above, Y131 (the equivalent residue in the bovine sequence) is seen as a ligand to UHDBT in crystallographic structures (PDB file 1SQV) [166]. A similar liganding function was seen in our MD simulations in the *Rhodobacter* structures, which showed that the hydroxyl group of Y147 was a ligand to QH_2 on formation of the *ES*-complex [164, 165, 178]. As discussed below (**10, A**), this liganding function, which might have been inferred from earlier work from the Daldal lab on mutagenesis at Y147 [198], would be lost in Y147A. These experiments will be discussed in greater detail below.

The selection of strains giving heterodimeric complexes with enforced intermonomer electron transfer was enabled by including in the encoding a carboxyl-terminal epitope-tagged with S (Streptactin) or F (FLAG) tags, and kanamycin and tetracycline resistance genes in the plasmids. This approach could minimized the sort of cross-over seen in our experiments, and in the Methods section [195], the authors detail procedures to isolate differently tagged complexes, and to characterize their cytochrome content by UV-VIS and by EPR spectroscopy, and also to show that neither mutation affected formation of the g_x 1.80 complex (Q.ISPH). Apart from the test of photosynthetic growth, two different sorts of experiment to look for inter-dimer traffic were performed; the first by measurement *in vitro* of Michaelis-Menten kinetics with solubilized complexes, the second using spectrophotometric measurement *in situ* of kinetics on flash excitation in chromatophores. Their discussion is not helped by the nomenclature for these strains, which is bewildering, so I have adapted the Świerczek notation to simplify the operational features, so that, for example, $_{A}$B-B^{N} represents a strain enforcing intermonomer electron transfer.

In order to generate heterodimeric complexes, two different genes encoding monomeric cyt *b* subunits must be expressed in a single cell. The different versions used were pED2(S) (or pHY103(S)) carrying Y147A, represented by $_{A}$B, and pED3(F) (or pHY101(F)) carried H212N, represented as B^{N}, with the S and F denoting the different epitope tags. Antibiotic resistance associated with each mutation were pED2, Kan^{R}; pED3, Tet^{R}; pHY103, Kan^{R}; pHY101, Tet^{R}. For any choice of two copies, cyt *b* can be incorporated into a dimeric bc_1 complex in several different combinations, with equal probability: $_{A}$B-B^{N}, ^{N}B-B$_{A}$, ^{N}B-B^{N}, and $_{A}$B-B$_{A}$ (in the simplest case). The first two (heterodimeric complexes) would be appropriate for testing traffic across the interface, and adding their activities would give ~50% of the population in chromatophores. The last two (homodimeric complexes, ~25% each) would both be inactive in turnover, but both would show some activity on flash excitation in chromatophores: in $_{A}$B-B$_{A}$, only in the high potential chain; but in ^{N}B-B^{N}, in full Q_o-site turnover including reduction of heme b_L, as demonstrated in the seminal paper introducing mutation of the histidine ligands to prevent binding of the

heme [92]. The behavior for different combinations was tested either through growth under photosynthetic conditions (Ps^+, requiring a functional bc_1 complex), or by measuring DBH_2:cyt *c* reductase activity.

In general, cells expressing only homodimeric complexes showed no growth (Ps^-) under photosynthetic conditions, but cells expressing heterodimeric complexes showed a weak photosynthetic growth. The activity of different preparations was measured through their DBH_2:cyt *c* reductase activity. However, it is not clear if particular complexes were pre-isolated or whether a mixture from solubilized chromatophores was tested. The Table of data seems to suggest the latter. Samples expressing only homodimeric complexes showed weak activity (~10%) but no growth, and cells expressing heterodimeric complexes showed ~20% activity and "slow" growth.

Assays of cytochrome and reaction center kinetics on flash excitation *in situ* in chromatophores showed more ambiguous results. The kinetics were measured in wildtype, in homodimeric strains pED2 ($_AB$-B_A) and pED3 (^NB-B^N), and in strains expressing both mutations, pED2 + pED3, 50% $_AB$-B^N plus ^NB-B_A, and 25% each $_AB$-B_A and ^NB-B^N) (their Fig. 5). The kinetics in the latter showed more or less the behavior expected from the mixture of behaviors discussed above, including a substantial (~0.33 of wildtype) heme b_H reduction in the presence of antimycin, interpreted as showing intermonomer electron transfer. However, in a subsequent figure (their Fig. 6), they show better resolved kinetics, including for the pED2 + pED3 case (with the same mixture as above), in which the heme b_H reduction was of similar amplitude, but much slower rate, with a similar behavior in the (pHY101 + pHY103) case (also with the mix above). On the other hand, in the (pED2 + pHY101) or (pHY103 + pED3) cases (same mix), the amplitude was much higher, both ~0.58 that of the wildtype, - and the traces show comparable halftimes. This latter behavior would certainly not have been expected from the DBH_2:cyt *c* reductase activities (0.22 of wildtype for (pED2 + pED3); 0.19 for (pED2 + pHY101); 0.18 for (pHY103 + pED3); 0.15 for (pHY101 + pHY103)), or from the growth rates implicit in lawn densities in their Fig. 3. The authors invoke "…better electronic couplings in the membranes harboring heterogeneous cyt bc_1 subpopulations…", but whatever was intended the mismatch of kinetics for the (pED2 + pED3) seen in their Figs. 5 and 6, the amplitude of 0.58, greater than the fraction of heterodimeric complexes, for the heterogeneous populations B and C in their Fig. 6, and the halftimes comparable to wildtype seen from the *in situ* kinetics compared weak DBH_2:cyt *c* reductase activities, all raise worrying questions.

Whenever two copies of a gene bearing different deleterious mutations are present in a cell, there is a possibility for cross-over recombination at the genetic level that will restore the wildtype sequence. However, the authors did not discuss such a possibility. They reported that reversion to wildtype was rare (0.01%), and that "…cultures that occasionally yielded larger numbers of Ps^+ revertants (>0.01%) were discarded…". However, the % referred to appears to have been based on counting of colonies (their Fig. 3A), with rare dense colonies representing strains with wildtype sequence. It is not possible to estimate accurately the relative numbers in each colony, but it is obvious that if integrated over all colonies, the fraction of wildtype cells would have been far higher than the fraction of dense colonies. In liquid culture under photosynthetic growth, given the difference in growth rate shown by the difference in density of lawns for pMTS1 and pED2 + pED3 segments, the wildtypes would quickly swamp the original heterodimeric strains. The authors mention, but not explicitly as a required condition, growth under semi-aerobic conditions in the dark; expression of the photosynthetic apparatus can be suppressed to an extent dependent on the how vigorous the aeration, but the "semi-aerobic" implies this was not a problem. Nevertheless, this reader found it difficult to assess how these factors might have been tuned, and whether the variability in kinetic assays *in situ* might reflect some variability in cross-over recombination. On the other hand, none of the homodimeric mutant strains could grow photosynthetically, and therefore

presumably had to be grown semi-aerobically in the dark. On flash excitation, pED2 ($_{A}$B-B$_{A}$) cultures generated kinetic changes in the high potential chain showing a normal bc_1 complex / RC ratio and partial function (their Fig. 5), so perhaps all cultures were similarly grown, and therefore not subject to selection pressure. Somewhat surprisingly, pED3 (^{N}B-B^{N}) cultures showed no evidence of any significant turnover of the Q_o-site; the *c*-hemes went oxidized following the flash, but remained oxidized with little effect on adding myxothiazol or stigmatellin. If the only mutation was the H212N change, the high potential chain and the Q_o-site reaction including reduction of heme b_L should have been observable (see for example Yun et al. [92] where on similar mutation to the other ligand to heme b_H, H111N, a rapid heme b_L reduction was seen on the first flash in the absence of antimycin).

Space does not permit a detailed analysis of the Castellini et al. paper [196], but there is no indication in the paper that they were aware of, or appreciated, the cross-over problem, and their protocol would certainly have allowed it to occur.

The take-home message from this section is that none of the reported results unambiguously support the claim to have demonstrated that electron transfer occurs across the dimer interface. The Czapla et al. [197] experiments exclude that that any substantial electron transfer occurs across the interface "…within the millisecond time scale of enzymatic turnover…". The data from Daldal's lab are the more credible, but are ambiguous.

On the theme of simplified models, in an interesting exercise from Beratan's group, Yuly et al. [199] have sought a common theme for discussion of bifurcated reactions in a wider context, but included comments on the Q-cycle mechanism. In trying to understand bypass reactions they discussed the free-energy gradients operating to process the products of the bifurcated reaction; in the Q-cycle, these would be the high potential chain oxidizing $ISPH^{\bullet}$ and the low potential chain oxidizing $QH^{\bullet}$. Their preferred arrangement for successful electron bifurcation (G in their Fig. 2) has the low potential chain catalyzing a thermodynamically "downhill" path, while the high potential chain has an "uphill" path. The bc_1 complex scheme on which they base their model has ISP, cyt c_1 and cyt *c* as the "uphill" path, where the E_m values conform to this expectation. In the reaction *in situ*, the Q-cycle pumps H^+ across the membrane, but they do not discuss in any detail the electrogenic nature of the reactions from $QH^{\bullet}$ through the *b*-heme chain to the Q_i-site, so do not include the work done against $\Delta\psi$. These two features set up a model that corresponds in essentials to that used by Zhu et al. [140] in experiments in which they followed kinetics of components over the first few ms after mixing excess QH_2 with the fully-oxidized isolated bc_1 complex. Two types of experiment were done: the first using conventional stopped-flow apparatus measuring cytochromes optically, and the second using their ultra-rapid mix/freeze quench with EPR-detectable free-radical species assayed over the first 3 ms. These later are $ISPH^{\bullet}$, $SQ^{\bullet}_i$, and the ferrihemes of b_H, b_L, and c_1. In the stopped-flow experiment, they describe their results as showing "…the early reduction of heme b_H, starting before 1 ms, followed by the reduction of heme c_1 after 3 ms. The reduction of b_L is completed within the dead time of stopped-flow apparatus…". There is some ambiguity in the last statement, but from their ultra-fast experiments, they would have seen no kinetics for b_L in optical measurement after the dead time because the initial 10% already reduced by then would not have changed over the time of their measurement. These results are what the modified Q-cycle predicts [74, 85]; electrons arrive at the highest potential component of each chain in the first turnover of the Q_o-site; heme b_H in the low potential chain goes reduced (via heme b_L) before cyt c_1 in the high potential chain because electrons must first reduce the (unseen) ISP, which has the a higher E_m, before they spill out to heme c_1. The Q-cycle is then backed up until heme b_H can pass its electron on to Q at the Q_i-site, as it becomes available from QH_2 oxidation at the Q_o-site. This allows a second turnover to complete the reduction of heme c_1, but heme b_L never gets significantly reduced because by then there is not enough

work available from the (now full) high potential chain. This conjectured sequence can be readily observed on flash-activation of turnover in chromatophores. Their ultra-fast experiments essentially confirmed this sequence. They compared the EPR spectra generated on premixing the reagents (presumably after equilibration), with spectra generated at selected times over the first 3 ms after mixing, now with a deadtime ~60 μs, and found as a new feature the rapid reduction of a small fraction of heme b_L and ISP_{ox} in the first 300 μs, assumed to reflect an intermediate state, and discussed more extensively below.

The point I want to make in this context is that the bc_1 complex jams up unless the reducing equivalents in the high potential chain are removed. The functional complex necessarily includes a high potential oxidant as acceptor, - the P^+/P couple of the reaction center (E_m ~450 mV) in chromatophores, excess cyt *c* in our own ultra-fast experiments (below), or cytochrome aa_3 in respiratory chains. This then comports more with model C in Fig. 2 of Yuly et al. [199].

Before going on to discuss mechanistic features in detail, it might be worthwhile to summarize the energy landscape of the overall reaction (Fig. 6). The basic outline dates back to our early studies of activation barriers in which we identified the first electron transfer as the rate determining step [81, 131], and to early studies characterizing the thermodynamics of formation of the *ES*-complex [129]. These features have not changed much, except insofar as the activation barrier is now more complex. It has to include the low probability of finding the H^+ in a favorable configuration for electron transfer, as summarized in the Marcus-Brønsted equation [179]. The partition of energy levels associated with the reactions on the other side of the barrier is still somewhat conjectural, and the version shown here, taken from [165], had evolved to include the intermediate product state of our recent experiments. The profile (left) is compared here with a similar profile from quantum chemical calculations (right), to be discussed later.

10. Roles for specific residues

A. Glu-295, Asn-279, and Tyr-147

Returning to less contentious issues, I now want to address experimental evidence that allows a better understanding of the process through which the intermediate SQ is oxidized in the second electron transfer of the bifurcated reaction.

Saribas et al. [196] made an extensive study of mutations at Tyr-147 mentioned briefly above. Y147F showed a relatively weak inhibitory effect on rate, but when changed to smaller residues in Y146V, S and A, much more complete inhibition was observed. None of the mutations prevented the binding of Q by ISPH (g_x 1.800 EPR line), or stigmatellin from binding as assayed through the g_x=1.786 EPR line [198], so the tyrosine is not likely to be involved in those complexes. In contrast, on titration of the rate of heme b_H reduction on lowering the E_h of the Q-pool, a shift of the E_h at which the half maximal rate occurred to lower values could be interpreted as a change in K_m suggesting formation of the *ES*-complex was weaker in strains mutated at Y147. This effect in strains with different mutations correlated with the degree of inhibition, supporting the role for Y147 in binding QH_2 [198]. However, the relatively weak inhibition in Y147F is unexpected given the role in stabilizing the *ES*-complex suggested in our MD studies (below). In the more strongly inhibited stains, Y147S and A, second site revertant strains relieving this inhibition showed Met-154 mutations to M154I or M154V.

Our earliest MD studies [130] had identified a water "chain" reaching into the protein from the P-phase to the Q_o-site that might be involved in exit of the H^+ released on oxidation of SQ, and we noted the participation of the -PEWY- glutamate (E272 in avian sequence), a tyrosine (Y274) and asparagine

(N249), and of the heme b_L propionates in H-bonding to the chain, and incorporated a role for the glutamate in proton exit in the model introducing SQ movement proposed in [129]. Expanding on this simple picture, if Glu-295 (in *Rb. sphaeroides* numbering) was in carboxylate form (E295-COO^-) before flash activation of turnover and was protonated by the H^+ from $QH^\bullet$ after its formation, the E295-COOH could rotate away to deliver the proton to the water chain and regenerate E295-COO^- to participate in the next cycle. In a paper from a later phase of this collaboration on MD simulation with the Schulten group, using an earlier *Rb. sphaeroides* model to explore mechanistic features [180], we looked at the waters around the Q_o-site and heme b_L, and polar residue that might be involved in H-bonding interactions, and identified additional residues, Tyr-147, Asn-279, Arg-94, Ser-79 (in *Rb. sphaeroides* numbering) and the heme propionates as of interest. We also showed data from experiments with strains mutated at Asn-279 to give N279D, I and F, which suggested a role of this residue in facilitating H^+ exit on dissociation of E295-COOH. We measured kinetics of redox changes of heme b_H, heme b_L, hemes c_2+c_1, and reaction center (RC) (at pH 7) following a train of flashes spaced at 20 ms in the presence of antimycin (see Fig. 2). Of special interest were the rates of reduction of heme b_H, detected after the first flash, and of heme b_L, detected after the second flash (see Table 1). The aim here was to test the hypothesis that mutation of N279 would interfere with stabilization of the water chain needed to regenerate E295-COO^- as an acceptor for the H^+ from the $QH^\bullet$ generated on a second flash. Since antimycin was present, the electron from the first QH_2 would reduce heme b_H, and that from the second, heme b_L, so, from this hypothesis, a change of behavior on the second flash would suggest a role in H^+ processing. This is just the behavior shown in Table 1. In all mutant strains, although the heme b_H reduction rate was somewhat inhibited, the rate of heme b_L reduction was more severely inhibited, in particular in N279I and F, the strains with apolar sidechains. This inhibition in all strains, with an effect of polarity of side chain, is certainly in line with the role in catalysis of H^+ transfer suggested, from E295-COOH to a water chain stabilized by H-bonding with Asn-279. However, no detailed mechanistic model can be constructed from this limited information.

We had noted in earlier discussion of Berry's structures, that -PEWY- glutamate was in different configurations in stigmatellin and in myxothiazol containing structures [127]. Other structures made available showed several other inhibitors bound, including MOA-stilbene at the Q_o-site, which showed the same rotation of the glutamate. This rotation allowed >C=O of the methoxyacrylate (MOA) group (or of the methoxyacrylamide of myxothiazol) to H-bond with the backbone amide >NH of the glutamate. Further clues to function can be gleaned from these and other structures of the bc_1 complex containing different inhibitors; comprehensive sets at the Q_o-site are from Berry's group (3H1H-L series, 3L70-5 series, each with a different Q_o-site inhibitor, including famoxadone (3L74), and many MOA-type). Xia's group have also discussed a range of inhibitors [166], including 1SQV (UHDBT), 1SQX (stigmatellin), 1SQP (myxothiazol), and 1SQB (azoxystrobin) from bovine mitochondria. The inclusion of UHDBT makes this a good background for comparison (Fig. 7) Another interesting discussion comes from Hunte's group and a structure binding atovaquone (4PD4) [200]. In all these papers, the authors have extensive discussions of the binding sites of each inhibitor. In *Rhodobacter* complexes from the Xia group, stigmatellin (2QJY [201]; 6NIN [202]; 5KLI (also with antimycin)); azoxystrobin (6NHH [202]); and famoxadone (5KKZ) have been reported in the Q_o-site (Fig. 8).

I should note here that heptyl-HDBT (HHDBT) in 1P84 from Hunte's group (Palsdottir et al., [203]), the other published structure with an HDBT, does not show any amino acid side chain H-bonding directly to the =O across the benzothiazole ring from the 6-OH through which binding to the His-181 of ISP occurs (a bridging water molecule was discussed, see below). However, they identified a pK_a of 6.1 on the inhibitor associated with binding to ISPH His-181, and showed that in their structures, the 6-OH group was dissociated (see also Bowyer et al, who showed a similar pK on UHDBT [120]). Palsdottir et

al. have an extensive discussion of the involvement of different residues in stabilizing the water chain that provides a H^+ exit pathway, to which we will return later.

Examination of these structures shows the configurational adaptability of the proximal volume, and the versatility of roles for the polar residues, E295, Y147, N279 in the putative proton exit pathway. All inhibitors (stigmatellin and UHDBT here) involved in interaction with the ISP through H-bonds to the histidine are constrained to the distal domain; this ligand fixes the ring structures in essentially the same position, so that the ligands across the ring structure (from Glu-271 to stigmatellin, or from was Tyr-131 to UHDBT (in the Esser structure) are also similarly situated. In the Palsdottir HHDBT structure, a water replaced the O of the carboxylate of the glutamate liganding stigmatellin, and provided a bridge to the backbone >NH of the glutamate. However, examination of the orientation of the backbones of the glutamate and the tyrosine molecules in different structures did not change substantially, showing that the change was in all cases by rotation of the sidechain. In each case, the rotation moved the sidechain from a liganding position to a position close to the amide group of the asparagine (N279). In the structures for inhibitors in the proximal domain (azoxystrobin and myxothiazol here), the liganding to the inhibitor involved a H-bond between the methoxy acrylate (or acrylamide) =O and the backbone amide >NH of the glutamate, with the glutamate side chain now rotated so that the sidechain carboxylate, the tyrosine -OH and the asparagine amide were aligned and in H-bonding distance, again with essentially the same backbone configuration in all structures.

A striking feature of the binding of inhibitors in the proximal domain is that all involve a H-bond to the backbone >NH of E295. Although the inhibitors occupy different volumes, the sidechains associated with the water network are also all similarly configured. The binding of famoxadone is subtly different from other proximal lobe inhibitors, shown in the *Rb. sphaeroides* complex in Fig. 8, but discussed at length by Berry and Huang [142] in the context of the avian complex, and described as follow: "…the ISP is held near the *b* position, moving to this position upon soaking the inhibitors into crystals in which it occupied the c_1 position. And there is no H-bond or any other direct contact between the inhibitor and the ISP. This seemed especially surprising since the pharmacophore of these inhibitors … resembles that of the MOA inhibitors, which promote the c_1 position. However, comparing the position of the ISP and its interaction with cyt *b* … shows that the position is not the same as the *b* position induced by stigmatellin. Also, intriguingly, although there is no H-bond from the cluster-liganding His-161 residue of the ISP to the inhibitor, there is an H-bond formed between His-161 and Tyr-279 of cyt *b*…". The tyrosine referred to is the "trap-door" tyrosine that closes the access port through which ISP accesses the Q_o-site occupant when ISP moves away. This same configuration is seen with the equivalent residue, Tyr-302 in the *Rb. sphaeroides* complex, and we will discuss it later. Famoxadone binds in the domain proximal to heme b_L through a H-bond to the backbone >NH of Glu-295 inhibitor. The structure of the pharmacophores and their H-bonding groups are discussed at length in [142], as are the differences in configuration of the protein induced by the packing demanded by the different dispositions of molecular volumes (Berry and Huang [142] have a nice discussion of the different occupancies). The comparison with stigmatellin and azoxystrobin (a typical MOA-inhibitor) in Fig. 8 makes it clear that famoxadone has more in common with the other proximal domain inhibitors than with the distal domain inhibitors, and that the location of ISP at the cyt *b* interface is misleading in comparing classes of inhibitor. In all the distal domain inhibitors, His-161 (His-152 in *Rb. sphaeroides*) H-bonds with the inhibitor, but does not with famoxadone.

Since in MD simulations, this volume of the Q_o-site contains mobile waters, there are many possibilities for configurations involving addition H-bonds to waters, bridging H-bonds to the heme propionates, etc..

All the structures shown are from crystallography, and therefore static, but the take home message here is pretty simple; in addition to more global displacements [84, 142], the sidechain rotations would allow rapid changes in volume in the proximal domain to accommodate occupants, either MOA-type inhibitors or $Q^{\bullet-}$; in addition, rapid exchange of H^+ between the glutamate -COOH/-COO^- and $QH^\bullet$ in the distal domain, and the H-bonded network connecting the asparagine amide to the heme propionates and the exterior P-phase waters would allow for H^+ exit as we had suggested when the first structures came out [129, 204]. The big question is how this network functions in the context of a "working" bc_1 complex, to be addressed later in the context of MD simulation of the formation of an *ES*-complex at the Q_o-site. Although I have emphasized the role of side chain rotations in facilitating rapid changes in volume, achieved without changing the backbone rotations, I should note that substantial displacements of some spans also contribute. Berry and Huang [142] have a perceptive discussion in the context of many different configurations in structures with different inhibitors bound, including the "-PEWY- seesaw" and the "trap-door" tyrosine we discussed earlier [84]. Their discussion of famoxadone binding and the mechanism by which the ISP is held at the cyt *b* interface through interaction with that tyrosine rather than through a bond to the inhibitor is discussed briefly above, and in a more speculative context later.

11. Applications of pulsed EPR to studies of the bc_1 complex

A. Q_o-site structure and atomic features of local radicals important in mechanism

Use of EPR spectroscopy to characterize the properties of $ISPH^\bullet$ through its paramagnetic center has obviously played an important role in studies of the bc_1 complex, with most of the earlier work being performed in other labs. When Dikanov moved to U. of Illinois in the early 2000s, he persuaded me of the importance of pulsed EPR and ESEEM (electron spin echo envelope modulation) arising from the ability to explore the nuclear spins in the neighborhood of a paramagnetic center [205]. In collaboration with Samoilova, we quickly evolved projects exploring the neighborhood of the $ISPH^\bullet$ [137, 159, 161, 165, 175, 206], of the $SQ^\bullet$ species formed in the Q_o-site as an intermediate during QH_2 formation [207-210], and related centers [211-214]. These studies have provided structural information at the atomic level of importance in understanding mechanism, in particular about H-bonds in the liganding shells of the centers studied. Particularly valuable were studies using high resolution variants of ESEEM (3-pulse ESEEM, HYSCORE, etc.). These allow separation of the contributions of nuclear spins to the echo envelope by generation of 2-D spectra. For example, in studies of ISPH from mutant strains, we could distinguish the loss of a single H-bond by comparison of the HYSCORE spectra with those of wild-type [159] to confirm the structural data, and that loss of the bond was the parameter leading to changes of p*K* and E_m. In general, I want to emphasize the utility of these methods. The electron spins are more or less local to a particular redox center, and the spin interactions with neighboring nuclei are felt only a few bonds out. Each interaction has its unique set of parameters, determined by both distance and vector overlap. To the expert in this field, the structural information than can be gleaned from the interactions is exquisitely detailed, and complementary to crystallographic information. However, it obviously requires a paramagnetic center, and a high degree of expertise, limiting the appreciative readership. I am happy to acknowledge my debt to Sergei Dikanov, and his colleague Rimma Samoilova, for the many advances that have come through our collaboration in these studies.

B. Q_i-site structure and mechanism

The quinone reducing site (Q_i-site) in the native structure contains electron density which we have modeled as a bound ubiquinone, which is lost on addition of antimycin. We have previously suggested that the site acts as a two-electron gate and explained the action of antimycin in terms of a displacement of quinone occupant. We proposed a novel mechanism to account for the formation of an

anomalous high potential form of cyt b_H (cyt b-150) on oxidation of quinol at the site, by reversal of the forward reaction to form a $QH^{\bullet}$.ferroheme b_H pair. The mechanism predicts three major contributing factors: the E_m value of heme b_H, the stability of the semiquinone, and a tighter binding of QH_2 than Q. Antimycin induces an oxidation of cyt b-150; the high affinity of antimycin drives oxidation of the ferroheme b_H (b-150) by semiquinone to form quinol, which is displaced by the inhibitor. A detailed analysis of the reaction mechanism has provided new insights into the machinery of the forward reaction, and the effects of mutation on the behavior of the site. This hypothesis is well supported by the new structural information. In collaboration with Dr. Sergei Dikanov, we have investigated the local environment of the semiquinone species formed at the site using high-resolution EPR. By examining the local proton environment using ^{1}H ESEEM and HYSCORE [207-210], and exchangeable protons using ^{2}H exchange, we have identified one weak and two strong H-bonds to the SQ, and identified the N_e-atom of a histidine as a ligand for one of the strong H-bonds, by using ^{13}C methionine generated *in situ*, labelling the ubiquinone specifically in the methyl and methoxy substituents of the head-group. These results support the crystallographic data from Berry's lab. Space and deadlines preclude detailed discussion of interesting recent developments from the Osyczka lab [215-219].

12. Recent developments

A. New information from MD simulation.

When Berry's structures showing the ISP extrinsic domain in different positions first became available, we initiated a collaboration with the Schulten group using molecular dynamics (MD) simulation of the bc_1 complex in a membrane environment to study features of mechanism not readily accessible by spectroscopy [130]. In the renewal of the collaboration using the structures from *Rb. capsulatus* [164], our initial focus was on simulating the formation of the *ES*-complex, based on use of information from our biophysical studies. In the native system, the *ES*-complex is formed only under metastable conditions in which the Q-pool is (partly) reduced and ISP is oxidized. From the redox potentials, this condition cannot occur under equilibrium conditions, hence the metastable character. We set up the metastable state under two different conditions to allow formation of the *ES*-complex [164]. In one of these, His-156 (in *Rb. capsulatus*) of ISP_{ox} was dissociated, so that QH_2 could form a H-bond like that we expected from our model [32, 33, 145, 146, 175, 176, 179, 180]. In the other the histidine was protonated. This allowed us to test the importance of protolytic state of the histidine by using the *ES*-complexes that developed in quantum chemical (QC) simulation of the first electron transfer reaction [167]. In the first state, where the His-156 was initially dissociated, the complex formed with the H-bond expected. However, as already noted above, the H-bond to the other –OH of the quinol ring did not follow the pattern anticipated from our stigmatellin model. Instead of a H-bond to Glu-295, a H-bond to Tyr-147 was found [164]. Although this seemed at variance with our expectation of an important role of the glutamate in H^+ transfer, exploration of the structural database revealed that in one structure with UHDBT [166], the tyrosine equivalent to Y147 formed a similar H-bond to the ring –OH. Furthermore, the dynamics of E295 showed that it would also be able to participate through a secondary H-bond to the OH of Y147. In the second model simulated, a water molecule formed a H-bond to the QH_2 in addition to that to His-156. Barragan and Solov'yov [167] went on to perform quantum chemical calculations involving a minimal set of critical residues on both, abstracted from the MD models, with His-152 either dissociated or associated, and forming the different H-bond to QH_2, and polar sidechains from the neighboring protein including Y147 and E295 in the H-bonding configuration above. The result demonstrated forward chemistry with a reaction energy profile matching that seen experimentally, but only in the model with the *ES*-complex with the dissociated His-152, as expected from the extensive biochemical and spectroscopic data discussed above (Fig. 6).

Our own independent model for MD simulation using the bc_1 complex from *Rb. sphaeroides* which leads to formation of the same *ES*-complex, is discussed later. However, in our model, the E295 sidechain was less frequently in position to association with the Y147 -OH, and the behavior rather emphasized its mobility. However, the rotational range and mobility would allow frequent contacts on the rapid (μs) timescale required for removal of the H^+, rotation to the water chain, and rapid dissociation of $Q^{\bullet-}$.

B. A new intermediate state in the Q_o-site reaction

Several groups had reported that SQ can be detected in the Q_o-site under conditions in which the bifurcated reaction is blocked by inhibition in the low potential chain [143, 144], and, as noted early, we confirmed SQ accumulation under such conditions [139]. In the E295W mutant SQ occupancy was somewhat greater than in the native strain. In these early reports, limitations in mixing constrained the time of freeze-trapping to assay the product state to the >10 ms range. In order to obtain kinetic information appropriate to the ~1 ms turnover of the Q_o-site, we collaborated with the Kenis group to design and construct a micro-fluidic mixer and coupled this to a rapid freezing unit using counter-rotating copper disks kept at 77 K by partial immersion in liq. N_2 (Fig. 9). Using this apparatus, we discovered a new intermediate state, likely $QH^{\bullet}.ISPH^{\bullet}$, suggested to be the immediate product on electron transfer from QH_2 to ISP_{ox} starting in the *ES*-complex [165, 178]. The fate of the intermediate state depends on the availability of acceptors for the electron and the proton. Under conditions in which heme b_L was initially oxidized, no $SQ^{\bullet}$ signal was detected, indicating that the rate of oxidation was much greater than the rate of formation. Turnover leads to formation of the newly identified state only when heme b_L has become reduced, either by redox poising prior to mixing with substrates or by preliminary turnovers of the Q_o-site when heme b_H oxidation is blocked by antimycin, leading to delays in the onset kinetics. We interpret these properties as showing that $SQ^{\bullet}$ is still in the H-bonded complex with His-152 (in *Rb. sphaeroides*) of $ISPH^{\bullet}$. We observed kinetics of formation of the $QH^{\bullet}.ISPH^{\bullet}$ state under different initial conditions consistent with turnover in the range ~70 μs range, which could be well fit by simulation of the conditions in our kinetic model. Although generation of the pre-reaction state, the reaction syringes, and the mixing were all maintained anaerobic, on exit from the mixing chip, the jet and the reaction profile developing while in flight, was in air. The development of the intermediate, and persistence, suggest a limited reactivity with O_2. In that case, its formation may protect against ROS generation under adverse conditions. Since it is formed distal from heme b_L, the distance would also protect against by-pass reactions involving electron exchange with reduced heme b_L. This new complex is discussed in greater detail below.

C. Rapid-mix freeze-quench.

The essential design parameters for the rapid-mix/freeze-quench apparatus are determined by the well-established kinetic properties of the rate-limiting bifurcated reaction at the Q_o-site, - a characteristic time in the 1 ms range. Most previous work on this system has been limited to the >10 ms range by conventional mixing, and by freeze-quench using liquid propane (or isopentane, etc.) cooled to ~ -150° C [139, 143, 144, 220]. However, Zhu et al. [221], in a technical *tour-de-force* in collaboration with Rousseau's group [222], used a silicon based microfluidic rapid mix, fabricated using photolithographic techniques followed by /freeze-quench at liq. N_2 temperature (-196° C) , to determine the kinetics of turnover of the Q_o-site reaction in the 0.05-2 ms range. They concluded from the close match between reduction kinetics of 2Fe-2S and of heme b_L (the immediate acceptors in the two chains) that no intermediate SQ_o was involved, though the result could better be explained by a model in which SQ_o occupancy was kept below detectable levels by rapid removal [139, 175]. We have built on this work to achieve a similar performance using a more easily fabricated mixing device, and an improved freezing

apparatus, and used these to determine the kinetics of SQ_o formation in the bc_1 complex inhibited in the low-potential chain.

a) ***Design and construction of a microfluidic rapid mix/freeze-quench apparatus***. Key features are shown in Fig. 9. The micro fluidics mixing chip was constructed and designed in collaboration with the Kenis group. After calculation of design constraints arising from the experimental parameters and material characteristics associated with potential technologies, we opted to use a polydimethylsiloxane-glass (PDMS-glass) based fabrication for the chip.

This work has been published only in brief [165, 178] because it was unfortunately truncated by Rodney Burton's need to finish his PhD, and a funding famine that prevented us continuing his work. The mixing chip was a simple two input "Z" mixer, with the aperture of the exit channel on an edge. On starting the flow and mixing, a drop would form at the exit, but a quick swipe of a Kleenex tissue allowed a jet to form (20 µm diam., 8 $\mu L.s^{-1}$ flow rate). The jet was directed to the rapid cooling device consisting of counter-rotating copper wheels, half immersed in liq. N_2 and driven by a substantial motor. The jets maintained their integrity for over 10 cm of flight well enough to allow measurement out to ≥4 ms after mixing. The high thermal conductivity of copper meant that the wheels were at close to liq. N_2 temperature (-196 ^oC). The jet was aimed at the rim of the clockwise spinning wheel, with freezing time determined by the in-chip flow distance (~30 µs), and the time of flight. The freezing process for the 20 µm jet was likely faster than the 30 µs minimal time, and therefore not limiting. The wheel with the frozen sample was rapidly rotated to the contact with the counterclockwise wheel, where the force ground the frozen sample to a fine powder, which was collected by a funnel in the liq. N_2 Dewar, emptying into an EPR tube. This all worked as planned. However, the timing was determined in a somewhat Rube Goldberg fashion; a frame mounted above the wheels (not shown) was intended to be a mounting plate for the mixer, but in practice it was easier simply to hold the chip against the plate, aligned against a ruler to allow determination of distance. This introduced some uncertainty in time of flight at short distance, and some scatter of points on kinetic curves generated one point at a time. In general, since substantial dexterity was needed to get everything right, complete kinetic curves were not always obtained. Furthermore, the experiments were costly in time and materials, and dependent on the charity of the Department. Within those constraints, the results were consistent with the kinetic model previously published [139], but there were significant differences from previous measurement of SQ intermediates, including our own.

b) ***Kinetics of SQ_o formation determined using rapid mix/freeze-quench.*** As already noted, the kinetics (Fig. 10) follow the expectations of the Q_o-site reaction model [139]. The initial redox status was established by prior reduction of the sample in an anaerobic vessel by using the quinone analog, OH-decylUQ (idebenone; 2-(10-hydroxydecyl)-5,6-dimethoxy-3-methyl-1,4-benzoquinone), maintained in the reduced state by NADH and a soluble NADH:UQ oxidoreductase (NDH-2) kindly provided by Bob Gennis. Reduction of heme b_H occurred rapidly, but in the absence of mediators, reduction of heme b_L was extremely slow. On mixing with excess ferricyt *c*, the kinetics depended on the initial degree of reduction of the *b*-heme chain. With heme b_H pre-reduced, and antimycin present to block its oxidation, SQ_o appeared as heme b_L became reduced, with the lag time reflecting the fraction of the heme still oxidized, as expected from the kinetic model. The amplitude of the SQ_o signal (Fig. 10, traces on left) are plotted against time (on the right) and fitted by model kinetics. The insert (right) shows early experiments with both *b*-hemes initially oxidized. The low level of SQ_o seen at 1 ms is in line with the lag expected during which heme b_H undergoes reduction, and substantial level seen at 2 ms reflects the formation of SQ_o as reduction of heme b_L goes to completion over the next ms, as seen in the model kinetics. Preliminary data on kinetics under a variety of other conditions and in mutant strains, are available from

work reported in Burton's thesis [223]. Of particular interest are kinetics with the E295Q strain, which showed the rapid initial SQ_o generation without any lag, expected from the model discussed in the closing paragraphs.

c) ***Characterization of the SQ_o species***. The kinetics closely match those expected from the kinetic model [139]. However, other properties of the $SQ^{\bullet}$ species observed in these experiments are surprising, because they differ in several important respects from those previously observed. In comparison with previous reports, interesting new features are seen in our $SQ^{\bullet}$ signal. The signal in the g=2.00 region was not simple; several bands appeared on either side, the signal amplitude was much greater than expected from an $S = ½$ free-radical, and the saturation properties and temperature dependence were quite different from those previously observed. We have suggested that these properties reflect a spin sharing of the $SQ^{\bullet}$ signal with spins from the $ISPH^{\bullet}$, which would suggest a tightly coupled complex (Fig. 10, right). The line shape shows hyperfine "wings" not seen in the symmetrical signal seen in previous work (Fig. 10, left insert), indicating either a modified molecular orbital, or spin interaction with a neighboring paramagnetic species, and the power saturation and temperature dependence also differ (Fig. 11A). The signal saturates only at much higher power, indicating, in support of the above, faster relaxation through spin coupling (Fig. 11A, left). Similar saturation effects are revealed in field-swept ESE spectra taken at different temperatures and times (τ) along the decay curve (center) (Fig. 11A, center). A prominent peak around g=2.06 becomes obvious as the temperature of measurement is lowered from 70 K to 5 K and swamps the $SQ^{\bullet}$ signal at g=2.005. This same component is obvious in the CW spectrum at lower temperatures but is barely detectable at 60 K (Fig. 11A, right).

d) ***Interaction of $SQ^{\bullet}$ with the protein and solvent reaction environment***. In order to explore the possibility of an intermediate product complex that persists so as to control $SQ^{\bullet}$ reactivity, we have used pulsed EPR to look for neighboring nuclear spins that interact with the new species. Fig. 11B (left) shows data obtained from a sample, quenched 2 ms after mixing, which had bc_1 complex at higher concentration to allow the greater signal strength needed for high resolution approaches. The data were obtained using 3-pulse ESEEM with a pulse sequence ($\pi/2$--(τ)--$\pi/2$--(T)--$\pi/2$--(τ)--echo). The stacked plots show spectra at different times T (z-axis), starting at 100ns, and advancing by 16 ns from front to back. The data were measured at the g=2.005 peak of the EPR spectrum. In similar experiments at lower concentration (Fig. 11B, right) both g=2.005 and g=2.06 bands were probed. In both bands, two spin interactions with ^{14}N are observed showing the same frequencies, but with differential evolution in T for the two g-values. This suggests some distinction between spin states probed. Our preliminary work strongly supports the hypothesis that $SQ^{\bullet}$ accumulates only as heme b_L becomes reduced, so this is unlikely to be the spin partner. Although the *c*-hemes were likely oxidized, both would be quite distant, and all the heme species have peaks far removed from this range (cf. [221]). Since only $ISPH^{\bullet}$ has a peak (at g = 2.02) in the region of the new $SQ^{\bullet}$ species, it seems likely that this is both the H-bonding and local spin partner.

e) ***Understanding the high amplitude of the $QH^{\bullet}.ISPH^{\bullet}$ signal***. The ESEEM studies of this $SQ^{\bullet}$ complex revealed perturbation of the $SQ^{\bullet}$ spin by interaction with both ^{14}N and ^{1}H nuclei, with properties consistent with H-bond(s) to histidine, likely His-152 of $ISPH^{\bullet}$. The most straightforward interpretation of the high signal amplitude is spin sharing with a neighboring metal center. In the reduced cluster with S = ½, (Fe(III) has S = 5/2, and Fe(II) has S = 2, the iron spins are antiferromagnetically coupled, the spin of Fe(II) is polarized negatively, and the His ligands are coordinated with Fe(II)). We have suggested that sufficiently strong interaction of the radical spin with S = 2 disturbs antiferromagnetic coupling of two iron spins, and that part of the polarization transfers onto the radical; it might be that all three spins should be considered in analysis of the $QH^{\bullet}.ISPH^{\bullet}$ complex [178]. However, without a detailed QM model, we

have no way to accurately quantify this sharing, and so cannot arrive at a true value for the occupancy of the state.

In summary, the properties show a novel intermediate state differing from those previously reported through the following unique characteristics:

(i) The hyperfine structure in the "wings", indicates additional energy levels in the spin system. These could arise because the molecular orbital of the lone electron has been extended to include additional bonds, or through strong magnetic interaction with a neighboring electron spin, or both.

(ii) Saturation and temperature dependence are different from those previously reported. The signal saturates only at much higher power, indicating faster relaxation through spin coupling. The slowly relaxing SQ seen in previous work trapped at longer times after mixing is in a different state then the more rapidly relaxing species trapped here. A line at g = 2.06 appears in the CW-EPR spectrum when measured at low temperature, with the rapid relaxation characteristics of a metal center, likely involving the spin-coupled partner. No other paramagnetic center in the bc_1 complex matches this line, though the broad g = 2.02 line of [2Fe2S] is close.

(iii) In 3-pulse ESEEM measurements centered at both g = 2.06 and at g = 2.005, we see interactions of the $SQ^{\bullet}$ spin with ^{1}H and ^{14}N, suggesting H bonding, with at least one bond to N. The characteristics suggest N_{ε} of the bridging His-152 from $ISPH^{+}$ to QH_2 as the most likely partner in the H-bond. Since this provides a common path through which the first electron and proton are transferred to the [2Fe2S] cluster, its persistence in the state here strongly suggests a common molecular orbital.

(iv) The most economical hypothesis to account for these properties is that we have trapped an intermediate state in which $QH^{\bullet}.ISPH^{\bullet}$, the products of the first step, are still associated. Although this state dissociates to products rapidly in normal forward chemistry, under the conditions of our experiment, it is clearly persisting into the ms range.

13. The spring-loading of ISP explains longevity in a C. elegans mutant

C. elegans is a nematode worm that provides a model system for studies in a simpler creature of many features of organization in higher animals. In studies of longevity, an important mutation, *isp-1(qm150)*, a P166→S change, close to the cluster, found to extend lifetimes 3-fold, was discovered in the ISP subunit of the mitochondrial bc_1 complex [224]. As part of a wider collaboration to understand this effect, Kaeberlein had set a student, Gholamali Jafari, the task of finding suppressor strains that reversed the longevity. He and colleagues generated 8 strains using selection for faster growth from a population of the *qm150* strain subjected to chemical mutagenesis [225]. All 8 suppressor mutations were in the ISP subunit, but, most surprisingly, in the tethering span, distant in sequence from the original mutation close to the cluster. Since the structure of the ISP was known to be highly conserve, it was obvious from the known structures that the separation in sequence would also represent a physical distance; these features provided no simple explanation for the suppressor effect. However, an obvious conclusion was that the function of ISP in the bc_1 complex must play a role in both longevity and its suppression. In addition to lifespan extension, the *isp-1 (qm150)* phenotype included changes in developmental rate, pharyngeal pumping rate, brood size, body movement, activation of the mitochondrial unfolded protein response reporter, CO_2 production, and inhibition of mitochondrial oxidative phosphorylation, showing that the single-site mutation had ramifications extending deeply into cellular physiology. All these were suppressed in the tether region mutants. On scanning the recent literature, the Kaeberlein group contacted Angela Barragan to seek her advice on the bc_1-complex, and on how the mutations at two widely spaced locations in ISP could affect the function. Angela passed the query on to me, and I recognized that the

suppressor mutations involved the same span of residues previously changed by mutation, mainly from work in Daldal's lab, and studied by Darrouzet et al. [132-136] in an exploration of the tether function. In different mutants, the differential effects suggested that mutations in the tether changed the redox potential of the distant Fe_2S_2 cluster. These, some mutations of our own, and studies of effects of inhibitors on the E_m of ISP, had led us to different interpretation, that the change in E_m of ISP reflected a change in binding affinity with Q_o-site occupants. On that basis we propose a "spring-loaded" mechanism to explain the effect [137], in which the binding forces played off against the change in configuration of the tether span. It then seemed likely that the underlying mechanisms in the this highly conserved complex might be similar. The P to S mutation was on the surface of the ISP protein at the interface with cytochrome *b* close to the opening to the aqueous phase through which ISP accessed QH_2. Since the two subunits were snugly apposed, it seemed likely that the P→S mutation would impede binding, and thus slow the oxidation of QH_2. This would then restrict flux into the complex, implementing a restriction on input of reducing equivalents at the local level analogous to that from dietary restriction at the physiological level, well known to increase longevity. Mutations in the tether region might then relieve the restriction by changing the configurational parameters determining extensibility. In the resulting papers [225, 226], we suggested that this provided an economical explanation not only for the direct effect on longevity, but also for all the more pleotropic effects. We pointed out that this result strongly supported an important role for the bc_1 complex, and specifically the Q_o-site reaction, in aging. Likely, restricting flux into the complex would lower generation of reactive oxygen species, and reduce the cellular damage leading to age related diseases, and the linker span mutations countered that effect. We discussed the energetics of spring-loading in some detail in the SI for [225] and will revisit the discussion later in the context of mechanism.

A. A wider perspective on control

My reason for including this section is that the *C. elegans* results have an obvious and important impact on our understanding of the importance of the ISP in the bc_1 complex and in the wider physiologic context, but the bioenergetics community might possibly have missed the second paper in the on-line journal *Worm* which is focused on *C. elegans*. The 'spring-loaded' model had accounted nicely for the Jafari et al. [225] results at the molecular level, but during their study of tether suppressor mutants, they observed a previously unreported phenotype of *isp-1(qm150)* animals: sensitivity to hyperoxia (100% O_2). *C. elegans* carrying the *isp-1(qm150)* allele were unable to develop past the L2 stage in the presence of hyperoxia, while wild type N2 animals developed normally. As with the other *isp-1(qm150)* phenotypes, this defect was also partially reversed by the tether region suppressors [226].

The mechanistic basis for sensitivity to hyperoxia in *isp-1(qm150)* animals was unclear. Cell culture studies had shown that exposure to 100% O_2 can mimic physiological oxidative stress and reactive oxygen species (ROS) generation [227, 228], and *isp-1(qm150)* animals have been reported to produce a higher level of superoxide (SO) than wild type animals [229]. Thus, one possibility is that both hyperoxia and mutation of *isp-1(qm150)* increase ROS levels independently so as to exceed a threshold consistent with continued development. On the other hand, it seems unlikely from the inhibited rate that the *increase* in ROS comes from complex III, and much more likely that it is associated with complex I, or some other upstream site. In this context, it is worth noting that inhibition at complex III will generate "cross-over" effects [230] such that upstream pools will become over-reduced, and downstream pools over-oxidized. Physiologically, this state is generated when back-pressure from the proton gradient inhibits the low potential chain and is mimicked by inhibition of the Q_i site by antimycin, both conditions leading to generation of ROS. In contrast, the mutation in *isp-1(qm150)* inhibits flux into the Q_o site, reducing ROS.

However, in both cases, over-reduction of the quinone pool will feed-back on complex I, and through that to the metabolic input reactions of the Kreb's cycle.

Hirst and colleagues have suggested that the generation of ROS in complex I is through 1-electron reduction of O_2 to superoxide by the reduced flavin (FMN) of the NAD-binding domain [231]. Under conditions in which flux through complex I is blocked by inhibitors or by reduction of the Q-pool, the reduced flavin can accumulate in the presence of O_2 so as to exacerbate this pathway. Because of the cross-over effect to reduce the quinone pool, these conditions match those showing sensitivity to hyperoxia in *isp-1(qm150)*, accounting for the increased ROS production.

A second interesting twist to this story is the finding that the mitochondrial apoptosis inducing factor, AIF, is a fragment of the NADH-binding subunit of Ndi1, an alternative NADH-Q oxidoreductase in yeast and mammalian mitochondria, homologous to NDH-2 [232, 233]. In *C. elegans*, the worm AIF homologue (WAH-1), has also been identified as a key player in apoptosis [234], and is likely an NDH-2 homologue [232], with a flavoprotein (FAD) in its redox active form. In support of this, expression of yeast Ndi1 in *C. elegans* with impaired complex I function restored respiration and proton-pumping [235]. Although FAD in AIF can form a tight, air-stable charge transfer complex with NADH that is inaccessible to O_2, in its redox active form it shows NADH-Q oxidoreductase activity higher than complex I [232]; when in communication with the Q-pool, the FAD will be kept oxidized as long as the pool is partly oxidized. It seems quite likely that when the pool goes reduced, so will the FAD, which might also be a source of ROS through Hirst's mechanism [231]. Alternatively, accumulation of a ubiquinone SQ intermediate might generate ROS.

Putting these diverse observations together allows for an interesting speculation [226]. Perhaps the NDH-2 class of enzymes serves a "canary" function in detecting conditions threatening the cell's viability. When WAH-1 is appropriately triggered through conversion to the AIF form, this initiates a cascade of apoptotic processes to recycle the defective cells before further damage can occur. Triggering would have to detect the (rare) adverse condition in which the Q-pool is over-reduced in the presence of O_2, and could come from a local effect of ROS, or by formation of the NADH.FADH complex as the mitochondrial NAD-pool becomes reduced, or perhaps both. We note that in vertebrates, these adverse conditions reflect the situation on oxygenation following ischemia in stroke or heart attack, know to lead to tissue damage, and are therefore of considerable medical interest.

This useful transfer of research experience in bacteria to explain an interesting finding in nematode physiology of a mechanism of great medical importance to the health of all of us, is a nice example of the importance of communication between different fields in furthering fundamental research. In particular, our work in determining the mechanism of the Q_o-site in *Rb. sphaeroides* has suggested paths forward to better understand of how the deleterious bypass reactions can be ameliorated in people. At a trivial level, the everyday advice to eat moderately and exercise regularly fits neatly into this understanding of aging at the molecular level.

14. MD simulations in a model using the Rb. sphaeroides bc_1 complex in its native membrane

In some previous MD simulations using the *Rb. capsulatus* structure, problems became apparent as to how the model was set up to deal with a void between the two monomers at the level of heme b_H, apparent in all structures. Clearly, the void does not represent a vacuum; likely disorder in the crystal meant that the occupying material could not be resolved. In [164], it was assumed that "the physics" would find a solution, but unfortunately, instead, the protein collapsed into the void, with some disruption of the structure, most notable of the Q_i-site. In another simulation the strongly hydrophobic volume

became flooded with waters [236]. In neither of these models could further simulation be expected to realistically explore the Q_i-site mechanism, or complete turnover. These responses are not natural. A major interest in MD simulation is the exploration of stochastic processes that might contribute to mechanism. Since structures became available, our picture of the Q_o-site reaction had developed to include several of these, in particular the movement of key players by diffusion, including quinone species and the extrinsic ISP domain, discussed at length above.

Through a failure of communication with our collaborators in the Schulten group, we were unable to ascertain whether or not the problem of the "void" had been dealt with. Since all our work since the collaborations with Kaplan and Gennis groups establishing molecular engineering protocol in1980s had been with the *Rb. sphaeroides* bc_1 complex, Stuart Rose set up from scratch a new model for MD studies based on the higher resolution structures in that background then available [201, 237, 238]. In setting up our model [165, 178], we took pains to construct a membrane with the native constituents, including UQ-10, and this proved important in later studies. To deal with the void, we initially inserted two phosphatidylglycerol (PG) molecules to occupy it, and this prevented distortion. In this model we could demonstrate population of *ES*-complexes at both catalytic sites. At the Q_o-site, we set up an initial state appropriate to formation of the *ES*-complex as indicated from our experimental work, in which ISP_{ox} had N_ε of His-152 dissociated and the Q-pool was partly reduced, and the dynamics spontaneously led to formation of an *ES*-complex (ISP-N_ε--HO-Q-OH--OH-Y147). This included Tyr-147 in H-bonding with the other quinol-OH, as was seen previously in the Barragan et al. work [164]. This configuration had also been the basis of the "functional" model abstracted for quantum chemical studies in [167]. The similarity of the two models suggested either that the void had been corrected in the earlier work, or if not, that collapse had not unduly affected the Q_o-site. In the new model, choice of an occupant for the void was based on crystallographic work from Hunte's group [239, 240] in which headgroups for cardiolipin and phosphatidyl ethanolamine were modeled in the hydrophilic volume (a 'void' in crystallographic structure because the 'tails' are disordered) at the end of the cavity (PDB file 3CX5). *Rb. sphaeroides* can function in mutant strains in which conversion of PG to cardiolipin is blocked, leading to accumulation of the precursor. Since PG also carries a negative charge, it can replace cardiolipin in many functions, including filling the 'void'. At the Q_i-site, an ES complex was formed in excellent agreement with known structures and mutational data. Additional features were revealed in the dynamics not apparent in many structures (but see [203, 239]. These pertain to dynamic water chains which formed when H-bonding to the primary ligands, His-217 and Asp-252, stabilized the complex. The water chains connected liganding sites to the aqueous phase by two different channels to allow H^+ exchanges essential to the chemistry catalyzed. The channel to Asp-252 involved participation of Lys-251 in ionic interaction with a PG molecule at the aqueous interface at the other end, simulating a role of cardiolipin noted earlier by Hunte. In both sites the UQ-10 tails wrapped around the central 2PGs. (It is interesting to note that in the Hunte structures, the ubiquinone tale is excluded from the void, which could have been taken as demonstrating some disordered but constrained occupant.) The new model clearly offers advantages over previous versions in moving forward, and also allows us to examine atomistic features of mechanism in the same protein as studied in our experimental work.

15. Release of protons inside the chromatophore vesicles measured using neutral rad: Identification of partial processes involving H^+ release

Neutral red has been used to measure pH changes inside chloroplasts (cf. 52) and chromatophores [241, 242], but the latter work was not simply interpretable in the context of present mechanistic models. To clarify this situation, Charles Wilson has measured the amplitude and kinetics of H^+ release inside chromatophores under a variety of conditions, and correlated the results with measurement of electron

transfer processes of the Q-cycle and of electrogenic processes [243]. In the presence of myxothiazol, we demonstrated release of H^+ on oxidation of ISPH with kinetics in the 100 μs range as the only significant process, and on oxidation of QH_2 with kinetics in the ms range, consistent with the rate-determining step. In the absence of myxothiazol, the two phases were convoluted. We correlated these measurements with electrogenic reactions associated with reduction of heme b_H in the presence of antimycin, and with flux through the *b*-heme chain to the Q_i-site in the absence of antimycin. All these correlations were consistent with the modified Q-cycle and our deeper understanding of partial processes from subsequent work, in particular the sequence of reactions at the Q_o-site discussed at length above. Charles did preliminary experiments with mutant strains modified at each of the residues discussed in Figs. 7 and 8. Unfortunately, funding constraints prevented completion of this work, though preliminary accounts are available in his thesis [244].

16. Summary

It might be useful to summarize the main conclusions from the above before going on to some more speculative discussion. The modified Q-cycle has become the consensus paradigm for understanding the role of the bc_1 complex in photosynthetic and respiratory chains, but with important extensions following the first complete structures showing the mobility of the extrinsic domain of the Rieske ISP, and its role in catalyzing electron transfer between QH_2 and the high potential chain. From the distances involved, a cycle of movements between docking interfaces at the Q_o-site and at heme c_1 would be needed to catalyze the Q-cycle. MD simulation of this mobility showed the feasibility of such a movement. The MD model also showed a spontaneous population of water chains in the protein from the P-phase into the Q_o-site volume. From analysis of the structures, the stigmatellin binding provided an obvious model for the *ES*-complex. The binding of myxothiazol showed a common ingress path but occupancy of a volume closer to heme b_L. Evaluation of differential effects of mutations in these volumes showed that many mutations that effected myxothiazol binding also inhibited forward electron transfer, suggesting a functional role of this proximal domain. What the structures also showed was an interesting change in configuration of the -PEWY- glutamate between its liganding of stigmatellin through the -COO^- group, to a binding of myxothiazol through the backbone >NH, in which the -COO^- was rotated ~180° to contact the water chain populated in the MD model. From these characteristics and from changes on mutation of the glutamate, we proposed that the glutamate might provide a pathway for exit of the H^+ released on oxidation of the intermediate SQ. Furthermore, since myxothiazol occupied a volume closer to heme b_L, we suggested that movement of the SQ into this volume would increase the rate constant for its oxidation ~1000-fold, and allow the second electron transfer to occur at a much lower occupancy of the intermediate state, and thus reduce the possibility of by-pass reactions involving the SQ.

We noted that the *ES*-complex from which the bifurcated reaction proceeded, likely involved a H-bonded interaction between QH_2 (as proton donor) and His-152 of ISP_{ox}, and our work establishing that the first electron transfer from QH_2 to ISP_{ox} was rate determining, opened the question of why (given the short distance) the rate was so low. That was answered by demonstrating that formation of the H-bond required dissociation of His-152 (pK_{ox1} ~7.6 in the isolated protein, ~6.5 in the *ES*-complex) and a proton-first-then-electron mechanism in which the probability of finding the proton close the histidine was low. We went on to show that the rate constant observed could be described by the Marcus-Brønsted equation proposed, and tested this by characterization of strains mutated at residues stabilizing the Fe_2S_2 cluster of ISP, which led to changes in both E_m and pK_{ox1}.

Analysis of the kinetics of the bifurcated reaction showed that the first electron transfer was strongly endergonic, and that the second electron transfer must be orders of magnitude faster in order to outcompete the backreaction. Analysis of the lag phase of ~120 μs under optimal conditions showed that

~100 μs could be attributed to the high potential chain. Since the intermediate states were formed at the limiting rate (~1000 s^{-1}), the lag ~20 μs remaining limited their occupancy to <0.02. These features strongly supported a mechanism in which movement of the SQ was essential; at that occupancy, and the distance to heme b_L, the calculated rate constant would not allow a fast enough rate, but movement closer to the heme would allow a 1000-fold increase in rate.

Criticism of this model has been based largely on alternatives in which these features were ignored. Models were constrained by localizing all electron transfers involving quinone species to the distal domain occupied by stigmatellin, and by assuming that the rate constants for electron transfer calculated from distances using the Moser-Dutton formalism could be used uncritically for proton-coupled electron transfers. This was clearly not appropriate for the first electron transfer, where it was obvious from the above that the H^+ has a controlling role. On the positive side, the failings of such models do reveal a need for additional complexity through control and gating to prevent by-pass reactions, including generation of reactive oxygen species on 1-electron reduction of Q_o. We pointed out that movement of the SQ provided possibilities for control not allowed in the models proposed. An additional discriminating feature is the role of the -PEWY- glutamate we proposed; it was superfluous to the static models, but essential to models in which mobility of the SQ speeds up the second electron transfer. In this context, a later line of criticism was to point to the diverse range of mutations at the -PEWY- glutamate that could provide a weak electron transfer through the bifurcated reaction, with the implication that glutamate was not essential. Since all such mutations inhibited the observed rate by 85% or more, this was not a strong argument. However, it becomes an absurd argument when account is taken of the fact that all such mutations result in transfer of the rate limiting step from the first to the second electron transfer. Kinetic modeling showed that in wild-type, the strongly endergonic nature of the first electron transfer, and the low occupancy of SQ, mean that to outcompete the backreaction and to match the rate observed (~1000 s^{-1} in wildtype), the rate constant for removal must be >10^7 s^{-1}. From the remaining activity in the mutant strains (v ~40 to 80 s^{-1}), and a measured SQ occupancy of 0.05, an apparent rate constant of ~10^3 s^{-1} was calculated, assumed to be appropriate for electron transfer from SQ trapped in the distal domain. When compared to the uninhibited rate needed, inhibition was almost complete.

On a different theme, we had noted that, given the distances involved, electron transfer across the dimer interface between the b_L hemes would be expected, and tested that hypothesis by looking for the hysteresis on titration using myxothiazol of the rate and amplitude of reduction of heme b_H in the presence of antimycin. If monomers acted independently, linear titration curves would be expected. If electron transfer between hemes b_L could occur at rates in the range <100 ms, the heme b_H in a monomer blocked by myxothiazol could still be reduced by turnover of the Q_o-site of the unblocked monomer. This would be seen as a convex titration curve. We constructed mutants at the tyrosine (Y199) at the axis of asymmetry between the two monomers, which was on the direct path for any transfer across the interface. Somewhat surprisingly, we found strictly linear titration curves for wildtype and all mutant strains. There was no indication of any significant electron transfer across the dimer interface on the timescale of turnover, and the kinetics under a wide variety of conditions could all be explained by a monomeric mechanism.

In this light, it was surprising to see later reports from several labs interpreted as demonstrating electron transfer across the dimer interface at rates comparable to turnover. We successfully reproduced the result of the first such report, but found that the expression system (two copies of cyt *b* joined by a linker span, each carrying different mutations) had facilitated a cross-over recombination to regenerate the wildtype monomeric sequence. In subsequent publications it became apparent that the other labs had encountered similar problems, ameliorated by growing all strains under aerobic conditions under which

the bc_1 complex is not required. If they grew the cells under photosynthetic conditions, they also ended up with strains that had crossed-over to regenerate the wildtype complex. These results, discussed at some length above, and led us to conclude that no report has provided an unambiguous demonstration of significant electron transfer across the dimer interface in the <100 ms range.

In the last section of the paper, I consider more recent work from the perspective of a mechanism that is essentially monomeric (though recognizing that coulombic effects between the two monomers might have a coordinating role). In that context, the most recent work from the lab provides new insights to mechanism especially insofar as these pertain to control functions. In a collaboration with the Kaeberlein group, we were able to account for some interesting *C. elegans* mutant strains, a primary change in ISP near the cluster-binder domain leading to 3-fold increase in lifetimes, and repressor mutations in the linker region, in terms of the 'spring-loading' feature consequent on the ISP movement. Many secondary physiological and cellular changes accompanied the primary mutation, all reversed in the repressor strains, showing an intimate role for the ISP and its action in the aging process. This took on a new interest in the context of our characterization of a new intermediate state identified in rapid-mix/freeze-quench experiments, formed only after heme b_L became reduced under backed-up conditions. The intermediate product, $QH^{\bullet}.ISPH^{\bullet}$, must form from the *ES*-complex in the distal domain, and the spectroscopic data suggest that it is stabilized through a H-bond between ISP and His-152, as in the *ES*-complex, but with quite different properties in the product state. This led to consideration of what difference in the pathway for the second electron transfer could account for the stability under the backed-up condition, and some new ideas on the spring-loading scenario, and the in the role of the -PEWY-glutamate in facilitating dissociation of the intermediate state in normal forward chemistry.

17. Envoi

In this closing section, I want to try to pull together all these rather complex pieces to provide an understanding of the Q_o-site mechanism simple enough to be sensible, or *vice versa*.

A. Formation of the ES-complex.

In Fig. 12, the formation of the *ES*-complex is illustrated to highlight different forces involved in the overall process. Starting with the vacant site, we end up with a site in which both QH_2 and ISP_{ox} are bonded through the H-bond connecting them, and with the QH_2 also stabilized by the H-bond to Tyr-147-OH. Binding of both substrates can in principle occur either by binding QH_2 then ISP_{ox}, or *vice versa*. In the work described above a lot of time was spent estimating the forces involved in formation of these bonds, but in each case, the outcome was to show the same result, an apparent binding constant for formation of the *ES*-complex.

At the top left side of the Fig., the two structures show the change in configuration of the tether region when the ISP head group switches between different states of binding. The tether is stretched out when the head reaches up to bind at the Q_o-site, relaxes to a helical configuration when it is not binding, and stretches in a different direction to bind to the heme c_1 propionate. This is the basis of the "spring-loaded" mechanism discussed above. A sequence of states is shown at the bottom of Fig. 12, constructed from structures which are in different configurations including (from left to right) the "stretched" state (in the stigmatellin bound structure) appropriate to the *ES*-complex, an intermediate state, the "relaxed" state of ISP (in the presence of myxothiazol, and the state bound to a heme c_1 propionate (see [128] and Fig. 2 therein, for details of sources). The scheme is annotated to suggest a plausible reaction cycle. In the relaxed state, the cluster-binding volume of the mobile extrinsic domain is not engaged (the action can be better appreciated in an animated version of this Fig). No forces act on the linker span, which is in helical

configuration. Of course, we are not talking about a mechanical spring; it is a mechanochemical one involving making and breaking of H-bonds, but a helix looks like a spring, so it is important to note the distinction. When ISP is engaged (with stigmatellin here) at the Q_o-site, the linker region is stretched out to an extended chain. All the structures showing this stretching are based on interaction with inhibitors, but a similar configuration must also be needed in formation of the *ES*-complex, or the Q.ISPH complex reported by the g_x=1.800 EPR signal. The change from relaxed to extended configuration (work term *3*) involves the breaking of 10-12 weak H-bonds, requiring work from the binding reaction (work terms *1* + *2*) [225] (the Supplementary Information detailing the H-bonding changes is available here). When the complex dissociates, this work is returned to the "spring". As discussed in detail below, the Darrouzet et al. studies [132-136] provide work terms, $\Delta G_{K_E}^{app}$, associated with the formation of the Q.ISPH complex, which can be calculated from the ΔE_m^{app} via $\Delta G_{K_E}^{app} = -RTlnK_E = -zF\Delta E_m^{app}$, where K_E is the apparent equilibrium constant for a chemical process, and ΔE_m^{app} is the free-energy in electrical units determined from the change in redox potential of ISP on binding (see next section) and for the 'spring' against which binding works.

At the center of the Fig. is a scheme showing the two pathways for forming the *ES*-complex. One can imagine the QH_2 diffusing into the site and the ISP head diffusing up from the relaxed state, and binding (with work term *1*). Alternatively, one can imagine that the QH_2 instead interacts with potential ligand from the protein, for example Y147, to form a stabilizing bond (work term *2*). In either case, to get to the *ES*-complex (the structure top right), the other partner would have to find which ever intermediate state had been formed, and the overall work term will be the sum of *1* and *2*. Pathway *1* involves the process *3*, the extension of the 'spring', - that "diffusion up from the relaxed state" comes at a cost, so the question is, does binding force *1* have enough pull? To my mind, it seems more likely that path *2* would occur first so that force *2* could help in pulling on the tether.

However, we need to consider additional contributions, - since the first structures, it has been recognized that other H-bonds contribute to the stability of the ISP in its docking at the cyt *b* interface [95, 126-128, 130]. We have focused on the H-bond between the occupant and His-152 of ISP because it contributes the major work term.

The peculiar bond from the trap-door tyrosine (Tyr-302 in *Rb. sphaeroides*) in the presence of famoxadone discussed above, which holds the ISP in an intermediate position, clearly shows another possibility [142] (Fig. 8), that of an intermediate state in the transition. We originally identified this tyrosine as part of a coordinated set of structural displacements, the -PEWY- seesaw, associated with changes in occupancy of the Q_o-site, specifically between structures with stigmatellin and myxothiazol [84, 126-128]. As the name implies, the tyrosine closes the access port through which the ISP His-152 makes its H-bond with the occupant; in order for ISP to bind, the port has to open. We now see this residue in a new role. The question of interest then is the strength of the bond. Some indication can be gleaned from the kinetic studies of Millet et al. [141]; the rate constant for reduction of cyt c_1 is changed from 80,000 s^{-1} to 5,400 s^{-1} by addition of famoxadone, but this latter is much faster than the leak around stigmatellin, or even UHDBT. From this, the H-bond from Tyr-302 to His-152 is relatively weak, and could allow a transient binding to aid the transition between the relaxed configuration and that docked with the Q_o-site occupant. As a transient state it would not affect the overall work terms discussed below.

B. The Q.ISPH complex

The spring-loaded idea was originally devised in the context of the Q.ISPH complex (shown by EPR band at g_x 1.800). In that system, the experimental data from binding studies allow us to put values on work term *3* and on work term (*1 + 2*). Most of the data comes from the tether mutants in *Rb.*

capsulatus from Darrouzet, Daldal and colleagues [132-136]. We can start by considering the structure in the presence of myxothiazol; with no extension force applied (represented by the configuration with myxothiazol or azoxystrobin occupying the site), the 'spring' would be fully relaxed; the force required to fully extend the tether from that state would then represent the work done against the spring. In terms of binding, any complex formed at the Q_o-site with a wildtype ISP must, within a small scatter, involve the same extension of the tether. The apparent energy of the H-bond can be estimated by measuring the change in E_m when the tether can be extended without any effort. We assume that in the mutant strain with three extra alanines (the 3A residues introduce ~10 Å) in the tether, there is no need to apply any force to extend it, then $-\Delta G_{spring}$ is zero. The change in E_m (referred to the value with myxothiazol) then shows the work available from binding when none is spent on extension of the spring, $-zF\Delta E_m^{3A} = \Delta G_{K_E}^{3A}$. The measured E_m^{3A} is 460 mV, which when referred to E_m^{myx} at 280 mV gives a difference of 180 mV. Then $-zF\Delta E_m^{3A} = -zF(180) = \Delta G_{K_E}^{app}$ = -17 kJ mol^{-1}. We can think of this as the intrinsic work we could expect from this H-bond.

Let us now suppose that conditions apply in which work is done against the spring, but $\Delta G_{K_E}^{app}$ is measured as zero. Then, $\Delta G_{K_E}^{app} = -zF\Delta E_m^{app} - \Delta G_{spring} = 0$; from which $-zF\Delta E_m^{app} = \Delta G_{spring}$ = -17 kJ mol^{-1}, because the two forces balance. In that case, we can think of the -17 kJ mol^{-1} as a reference value for both bond and extension, and then consider how one or the other (or both) might be changed by additional forces.

In the presence of myxothiazol when there is no binding and no extension, E_m^{myx} = 280 mV. This compares to the intrinsic E_m in the solubilized protein, which is 310 mV. In that case, there is also no spring force; the proteolysis site is immediately after the alanine at which Daldal added residues, so the linker is not attached to anything, and experiences no force. Similarly, the cluster binding domain contacts only waters. We must therefore attributable the difference in E_m to unknown forces associated with the environment if ISP in the bc_1 complex.

Of course, in most circumstances, $\Delta G_{K_E}^{app}$ is not zero. We can measure E_m^{app} with reference to E_m^{myx} to get ΔE_m^{app} in any other strain and use the value to figure how much extra work from bonding (beyond that required to extend the tether) is involved. For example, the E_m^{app} for the Q.ISPH complex (the g_x 1.800 EPR line) is (coincidentally) also 310 mV, higher than the E_m^{myx} = 280 mV in the presence of myxothiazol, giving ΔE_m^{app} = 30 mV and $\Delta G_{K_E}^{app}$ = -3 kJ mol^{-1}. Other departures from these basic values can be attribute to additional forces. These considerations are discussed in detail in the notes to Table 2, which is adapted from a version published in the supplementary information for [225], with some simplification of terms.

C. Mechanistic implications

The work invested in extension of the linker to allow formation of the *ES*-complex must be in the same range as that involved in the other complexes for which we have estimates. The approach through ΔE_m^{app} cannot be applied to formation of the *ES*-complex, but values for $\Delta G_{K_E}^{app}$ ~ -5.8 kJ mol^{-1} can be determined from binding expressed through K_m values as discussed earlier, and applied using the same ΔG_{spring} to give from $\Delta G_{K_E}^{app} = \Delta G_{total}^{occp} - \Delta G_{spring}$, a value for work term (*1 + 2*).

Consideration of these values leads to interesting mechanistic insights. As noted above, in normal forward flux, after the first electron transfer to generate SQ_o, the intermediate is rapidly consumed by formation of Q on transfer of the electron to heme b_L [180]. Somewhere in this process, the bond holding

ISPH at the docking interface is lost. Since the intermediate state is formed of from QH_2.ISP_{ox}, the tension on the 'spring' would not have changed, but would now provide a force favoring dissociation. At the instant of dissociation of the $QH^{\bullet}$.$ISPH^{\bullet}$ complex to liberate $Q^{\bullet-}$, ISPH, and H^+ (rapidly leading to protonation of E295), the work stored in the extended linker would be available to pull the extrinsic domain towards its relaxed configuration, closer to the docking interface with heme c_1. What effect does this have mechanistically? Our detailed kinetic model [139, 180] did not consider this step; it was able to account for the behavior using $\Delta G^{app}_{K_m}$ determined empirically from physicochemical properties represented by the equilibrium constants. However, it was noted that in order to minimize bypass reactions, a more rapid re-oxidation of ISPH was required than expected on the basis of an unbiased diffusion of the extrinsic domain of ISP, implemented in that model by increasing the rate constants for the equilibria for heme c_1 oxidation while maintaining their ratio. We had recognized when the model was published that this was artificial and might alternatively indicate an unrecognized gating process. The 'spring-driven' reconfiguration above would provide such a gating effect quite naturally since it would bias the transition towards the cyt c_1 interface by the substantial work (~-17 kJ mol^{-1}) stored in the spring, to facilitate rapid oxidation to ISP_{ox}. From this, the kinetic model will require substantial revision to deal with contributions of the work term from the "spring".

D. Modelling of the first electron transfer though quantum chemistry

Fig. 13 shows clips from a nice movie generated by my colleagues Angela Barragan and Ilya Solov'yov in an extension of the collaboration with the Schulten group [167]. I can make no claim to have contributed to the calculations, except in terms of the preceding paper [164]. However, in the spirit of "…a picture is worth a thousand words…", the movie will save the reader from yet another few pages of dense argument and make an important point. The two energy landscapes of Fig. 6 show similar profiles for the first electron transfer, one derived from parameters generated from biophysical measurements, and the other from QC calculations on states from MD simulations. The movie shows the progress of the reaction over the activation barrier as seen in the evolution of the highest occupied molecular orbital (HOMO) on transfer of the electron and proton from QH_2 to ISP_{ox}. The QC calculations treat the model as a composite quantum chemical object in a superposition of states. As a consequence, the complexity increases as a power of the number of atoms, and this model is at the extreme of the practicable. The movie expresses at a high level of sophistication the hypothetical mechanism for the first electron transfer introduced 18 years ago [151], fleshed out through the history summarized above, and validated by the similarity of the energy landscapes.

This would be a nice place to close my own chapter on the first electron transfer, except for the fact that the movie appears to leave the $QH^{\bullet}$ component of the intermediate product naked. Since this is the substrate for the second electron transfer, it would be nice to see it clothed, not shown here. The $QH^{\bullet}$ component must have its own unpaired electron, so there should be a new orbital occupancy associated with the state, calculable by similar QC approaches.

It should be noted that there is an important difference between the QM state calculated above, and the $QH^{\bullet}$.$ISPH^{\bullet}$ intermediate seen by EPR in the rapid mix/freeze quench experiments. Barragan et al. [167] noted that electron transfer went to completion only if their reaction model included E295 in carboxylate state as an acceptor for H^+. They could replace Y147 by a bridging water, but either Y147 or the water were needed to serve a relay function to transfer the proton from $QH^{\bullet}$ to E295-COO^- as acceptor. These would all be plausible states associated with rapid forward chemistry in which E295 is initially available in the carboxylate form as H^+ acceptor. However, the $QH^{\bullet}$.$ISPH^{\bullet}$ state accumulates only when heme b_L is reduced. We discuss below a hypothesis that under these circumstances, E295 might be

trapped in its acidic state, perhaps because in the reduced form of the heme, its propionate is protonated, and unavailable as H^+ acceptor. In the $QH^{\bullet}$.$ISPH^{\bullet}$ state there is strong evidence from the magnitude of the EPR signal, for spin sharing between $QH^{\bullet}$ and $ISPH^{\bullet}$, and from ESEEM spectroscopy, that they remain H-bonded through the H-bond with H152 N_{ε}. As discussed above (Section **12 B C**), the complex likely remains in a superposition of quantum states which in principle should be appropriate for calculation of a shared molecular orbitals associated with both product states.

E. The configurational changes in the structure through which transfer of the second electron is implemented

The murkiest part of the whole mechanism is what happens between the generation of the intermediate state and the arrival of an electron on heme b_L. Although the experiments showing the kinetics of formation of $QH^{\bullet}$.$ISPH^{\bullet}$ complex could benefit from higher precision and better reproducibility, with the *provisos* above, the kinetics conform well to the expectations of our model. Indeed, no mechanism for the bifurcated reaction following the pattern for the first electron transfer supported above could proceed without an intermediate state like that proposed. A second thing to bear in mind is that the relatively stable state seen in our rapid mix-freeze experiments is formed only when heme b_L is reduced. We have useful information on kinetics when heme b_L is initially oxidized from the earlier experiments of Zhu et al. [140], who measured the kinetics over first 2 ms of reaction after mixing the oxidized bc_1 complex with 10-fold excess of QH_2, and followed the kinetics of formation of $ISPH^{\bullet}$ and the reduction of heme b_L. When both *b*-hemes were initially oxidized, the two reactions occurred in a small fraction of centers (~10%) apparently simultaneously over the first 200 μs, presumed to show an intermediate process that involved no significant additional reactant. However, from the close match of the kinetics, they concluded that no intermediate SQ species was involved. This conclusion was perhaps too hasty. From our own experiments, a SQ species must have been involved, but the occupancy was so low that that they did not detect it, - the situation shown in our model kinetics. Their data show a lag of ~66 μs before the electron transfer kinetics start, which included a 50 μs 'dead' phase, so that the remaining 16 μs of the lag provides a limited interval for intermediate processes, including binding of QH_2 and formation of the intermediate state. In that context, their data and ours agree, because under their conditions, we saw no intermediate accumulate, and their lag is a little shorter than the 20 μs estimated from our kinetic measurements above. In my view, there is no contradiction between the Zhu et al. data and our own. The kinetics seen in Millett's studies [141] discussed above, also show a similar constraint on occupancy of intermediate states.

The crystallographic data above showing binding of inhibitors were discussed in terms of the participation of residues (Glu-295, Tyr-147, Asn-279) for which changes in behavior in strains mutated at these residues showed functional participation. Data from Glu-295 mutations were interpreted as demonstrating the role of E295 in H^+ transfer out of the site, and a possible role through side chain displacement in facilitating the movement of $Q^{\bullet-}$. In E295W, the mutant with bulkiest side chain, the slow rate might likely have also reflected impediment to movement. The evidence from kinetics studies with these E295 mutant strains was interpreted as showing that both H^+ exit and SQ movement are necessary for normal forward chemistry. [128, 129, 139]. The data from the Tyr-147 mutants of Saribas et al. [198], showed no effect from any of them on binding of Q or stigmatellin with ISPH (as determined by the lines in the EPR spectrum at g_x=1.800 or 1.783, respectively. However, they measured the kinetics as a function of the poise of the Q-pool in this set of Y147 mutants, and observed different shifts in E_h at which the kinetics reached $0.5V_{max}$, from which apparent K_m values could be estimated. These could have been interpreted as changes in binding of QH_2 to form the *ES*-complex dependent on the size and polarity of residue substituted on mutation. However, it is worth noting that the smallest effect was in the Y147F

change, which seemed to show that the -OH of tyrosine was relatively unimportant. The effects of mutation at Asn-279 were less dramatic; as discussed above (Section **10 A),** the rate of heme b_L reduction following a second flash was much slower than in wildtype, interpreted as showing that after the first flash, dissociation of E295-COOH was retarded so that regeneration of the E295-COO^- needed to accept a H^+ after the second flash became limiting; stabilization of the water chain by N279 was important in allowing E295 to cycle through protonation states leading to transfer of H^+ to the exterior.

In general, we suggested a mechanistic scheme in which the transfer of a proton from $QH^\bullet$ to glutamate to form E295-COOH allowed the intermediate complex to dissociate, the rotation of the sidechains, and structural displacements allowed access of the $Q^{\bullet-}$ to the proximal domain to allow rapid electron transfer to heme b_L, and exit of Q, rebinding of QH_2, and regeneration of the E295-COO^- on transfer of H^+ to the water chain completed a cycle allowing the next turnover to occur. The involvement of Y147 in binding meant that the direct involvement of E295 had to be revised, the transfer of a H^+ to the glutamate had to be indirect. The strong inhibition with all E295 mutants showed that it was nevertheless essential, and the N279 mutants were consistent with a role in stabilizing the H^+ bonded network of waters. The structures of Figs 7 and 8 with different inhibitors bound showed the importance of specificity of H-bonding to occupants in reconfiguring the site and highlighted the diversity of interactions allowed by rotational displacement of sidechains, but also brought home the message that, since each structure was necessarily static, they give no information on the dynamics.

I now want to use two other structural models to illustrate the role of some of these residues in proton exit. The first is based on the structure of yeast complex with HHDBT bound (PDB 1P84), and the perceptive discussion by Palsdottir, Hunte and colleagues [203] in the context of the binding of that inhibitor, of a putative water chain to facilitate the proton exit pathway; - the same water chain we had proposed in 1999 [129] on the basis of MD simulation, and they had shown in an earlier structure. Their model is shown in the context of structure in Fig. 14 A. The second model (Fig. 14 B) is a similar view of a frame from an MD simulation of the formation of the *ES*-complex in the *Rb. sphaeroides* bc_1 complex.

With respect to the first model, I cannot do better than refer the reader to the original paper [203]. The authors frame their discussion in terms of the pathway for proton exit inferred from the water chain populated in MD simulation, and the different configurations of the -PEWY- glutamate [129, 130], and developed independently by Hunte et al. in the context of the yeast structure reported shortly thereafter [204]. Their original structure, in which Glu-272 was involved in binding with stigmatellin, revealed a network established by H-bonding of residues Arg-79, Tyr-132, Asn-256, and Tyr-274, with several crystallographically determined waters and their interaction with the heme b_L propionate. In [203], they went on to elaborate the discussion of this network in the context of changes in its configuration in the structure with HHDBT bound. They revealed the anionic nature of the hydroxyl involved in its binding to ISPH, and noted that, compared to the liganding of stigmatellin, the carboxylate group of Glu-272 was not involved in binding HHDBT. The ring >C=O of the inhibitor is H-bonded to a water providing a bridge through a second H-bond to the backbone >NH of Glu-272, and the side chain of the glutamate was dramatically rotated out of the Q_o site, with a water bridged hydrogen bond connecting the carboxylate to the heme propionate. They extended the earlier network, and introduce Tyr-274 and His-253 as additional players, all in the context of specific waters molecules defined in the structure. In constructing Fig. 14A, I simply followed their detailed instructions on how to connect the network. The difference in the configuration of the glutamate in structures with stigmatellin and HHDBT is essentially that which we had noted earlier between stigmatellin and myxothiazol (Fig. 7) structures, from which we had suggested the movement of SQ in the site [129]. However, in contrast with myxothiazol (Fig. 7), or

the MOA-type inhibitor, azoxystrobin (Fig. 8), both binding in the distal lobe, although the glutamate is rotated away from the inhibitor, both UHDBT (see below) and HHDBT are in the distal lobe.

As noted earlier, a very different liganding is seen in the only other structure with a similar molecule, that for UHDBT in the bovine complex (PDB 1SQV, [166]), as seen in Fig. 7, with the H-bond to the ring >C=O provided by Tyr-132. The obvious question is what differences in the two crystals leads to this configurational difference in the binding of HHDBT in the yeast complex. In the yeast structure, as noted above, 6-OH of the benzothiazole ring through which the H-bond to His-161 of ISPH occurs in HHDBT is in the dissociated state. In the bovine structure, as shown in Fig. 7, the >C=O across the benzothiazole ring is involved in the H-bond with Tyr-132, but the state of dissociation of the -OH H-bonding His to ISPH is not discussed. In this structure, Glu-271 (in bovine numbering) is rotate away from inhibitor, and H-bonds with the backbone O of Leu-250, but there is no group H-bonding to the glutamate backbone N, so the link to L250 is the most obvious force stabilizing this configuration.

In Fig. 14 B, a frame from Stuart Rose's MD simulation of formation of the *ES*-complex in the bc_1 complex from *Rb. sphaeroides* is shown, from a trajectory similar to that discussed in [165]. The residues are equivalent to those identified in Fig. 14 A; in *Rb. sphaeroides* numbering, Arg-64, Tyr-147, Asn-276, Glu-295, Tyr-297 of cyt *b*. Also shown is His-152 of ISP, and one of the S-atoms of the cluster. The waters are not crystallographic, but from the simulation and all exchange with the external P-phase (at the bottom) within a few frames of the trajectory, with small changes in position as expected from mobile elements. Those shown here are selected as within 6 Å of the residues above. Inspection of the surfaces of the proteins (Fig. 15) shows that some of the waters near the bottom are outside the cyt *b* protein but are likely connected to the network to the P-phase. Several possible channels are, most prominently, the one identified in [204] running up past Arg-94 and the A propionate of heme b_L (middle), a second channel (left) running up via His-276 (or an aspartate) to Glu-295, and a third less well-populated (furthest right), at the inter dimer interface. (As briefly noted above, His-276 is not conserved in mitochondrial complexes; more commonly, as in bovine and avian complexes, an aspartate is found at this position.) The first two chains might converge in the volume between E295 and N279; depending on the occupant, with small excursions, any of these residues could connect to the network. Note that no waters appear close to the residues involved in binding the QH_2. In the *ES*-complex, the volume around the H-bond between QH_2 and Tyr-147 is insulated from the network by the tyrosine ring, and waters are excluded from the anhydrous volume around the H-bond through which QH_2 interacts with His-152 of ISP and the cluster, where the interface between cyt *b* and ISP proteins is tight (as noted in [82, 161]. However, in the Palsdottir et al. structure, a water provides a bridging H-bond from carbonyl =O of HHDBT to the amide >NH of the E272 backbone.

As discussed elsewhere [165, 178], the MD simulation in which inhibitors were replaced by Q or QH_2 at Q_i- and Q_o-sites, respectively, shows *ES*-complexes at both sites configured as expected from the biophysics of turnover. In the present simulation, the *ES*-complex at the Q_o-site is configured as in the earlier studies in collaboration with the Schulten group on the *Rb. capsulatus* model [164, 167], which provided the initial configuration from which the quantum chemical model and studies discussed in the context of Figs. 6 and 12. This model is therefore in a potentially functional configuration. However, essentially the same *ES*-complex was formed when the Q_i-site was occupied by antimycin (Stuart Rose, unpublished), as in our kinetic studies. In that context, the point of interest is that in general, the sidechain orientations in the Q_o-site fall within the range implicit in the different crystallographic structures in Figs. 7 and 8. The difference from the crystallographic models is that the MD simulation is dynamic and can explore configurations potentially accessible and explore the frequency with which functional configurations are established.

A clear conclusion from this section is that the structures provide evidence for a plasticity of connectivity in the volume in the lobe of the Q_o-site more proximal to heme b_L. This volume includes groups that provide the secondary ligands across their ring structures for inhibitors H-bonded to His-152, and is also the volume in which binding of the MOA-type inhibitors (and similar) occurs. Our earliest analyses after structures became available had shown that mutations effecting binding of these proximal lobe inhibitors, also effected forward function [127]. Another clear conclusion from the diversity of structures, and their locations in this volume is that the protein 'stretches' to accommodate. This is also the volume through which $Q^{\bullet-}$ would have to move to occupy the proximal domain, and in which the cycle of dissociation and association of Glu-295 would have to operate. This plasticity opens up many avenues for speculation, but supplies little in the way of useful constraint.

F. The second electron transfer, from $QH^{\bullet}$ISPH$^{\bullet}$ to heme b_L

The mechanism proposed for the transfer of an electron to heme b_L and a proton to the P-phase requires that E295 is initially in the carboxylate state. What of the other players? In comparing the reaction model with crystallographic structures, it should be borne in mind that in the latter, binding in the distal domain involves an inhibitor, with an H-bond to the reduced ISP *I*, this is also the case on binding Q in the g_x 1.800 complex. In the *ES*-complex, the binding is of QH_2 with the oxidized ISP. There are several important differences.

i) The *ES*-complex forms only under metastable conditions. the redox potentials of QH_2 and ISP_{ox} are such that they can never co-exist under the equilibrium conditions needed for crystal growth. Simulation is our only approach to exploring their structures, and spectroscopic tools the only way to explore the bonds involved.

ii) The H-bonding requirements are quite different; with QH_2, both -OH groups are H-bond donors, but with Q, both =O groups are H-bond acceptors. All things being equal, from the weak effect of mutation to phenylalanine, it was a little surprising that Y147 should be a partner in binding QH_2; however, the QM simulation shows the tyrosine as dissociated, with the $QH^{\bullet}$ -OH group as donor to the H-bond. This opens the possibility for the relay function proposed [164, 167], but begs the question of what promotes the dissociation.

iii) For the electron transfer to occur, the b_L heme must be in the oxidized form. However, since the E_m is pH dependent, on reduction, the heme (or a ligand) must also bind a H^+, likely at one of the heme propionates. Since the charge of the electron is mostly on the Fe, and the carboxyl-group of the propionate A is 6.48 Å distant, the reduction will generate an asymmetric change in the coulombic field compared to any field on the oxidized state.

iv) Other potentially charged groups are Tyr-147, Arg-94 and His-276 (or aspartate in the equivalent position in bovine or avian sequences). As noted above, in E295 mutants, the strong inhibition of electron transfer is partly relaxed at higher pH, showing a p*K* in the range ~8.5, which might reflect dissociation of $QH^{\bullet}$ itself, or of the tyrosine or the histidine as possible alternative acceptors for the H^+ from a $QH^{\bullet}$ with lower p*K*. All these groups are potentially connected to the network of H-bonded waters. However, given that His-276 is replaced by an aspartate in many mitochondrial sequences, it is not a very plausible candidate. In that case, the tyrosine is the most likely contender. As noted above, if the p*K* ~8.5 is associated with dissociation of $QH^{\bullet}$, and if E-295 is the H^+ acceptor, this would demand a dramatic changes in p*K* of the glutamate on cycling between acceptor (from $QH^{\bullet}$) and donor (to the propionate of ferriheme b_L, or to an aqueous phase in the neutral range) functions.

G. Mechanism of the second electron transfer of the bifurcated reaction

With these considerations in mind, we might now sketch out a mechanism.

a) From the rapid mix-freeze experiment (in which excess ferricyt *c* is mixed with the partly reduced complex) we can say that, starting from the *ES*-complex occupying the distal domain of the Q_o-site, the intermediate complex, $ISPH^{\bullet}.QH^{\bullet}$, shows no detectable occupancy when measured at 60 μs when heme b_L is oxidized before mixing. If heme b_H is initially oxidized and antimycin is present to block its oxidation, occupancy is still low at ~1ms, by which time heme b_H is largely reduced and heme b_L is beginning to get reduced in the second turnover of the Q_o-site. In effect, occupancy is delayed until the third turnover when heme b_L is reduced.

b) If heme b_H is initially reduced, the $ISPH^{\bullet}.QH^{\bullet}$ state accumulates in the second turnover as heme b_L gets reduced on the first turnover. Preliminary experiments (R. Burton [223]) show the in the E295Q mutant, the $ISPH^{\bullet}.QH^{\bullet}$ state accumulates without delay in the first turnover even when the *b*-hemes are oxidized, but to a lower amplitude.

c) When turnover is measured in chromatophores, heme b_H starts to go reduced within ~20 μs of the generation of ISP_{ox} (after a ~100 μs lag as electrons are pulled out of the high potential chain); all intermediate processes must therefore be rapid. A similar lag is seen on mixing QH_2 with the oxidized complex [140], or when, with Q/QH_2 reduced by succinate, heme c_1 is rapidly oxidized (1 μs) by photo-oxidation of a ruthenium complex [141].

d) Measurements on flash illumination of the complex *in situ* in chromatophores show that when the H-bonded network for H^+ transfer is slowed by mutation of M270, the reduction of heme b_L on the second turnover of the chain is slowed more than the first. We suggested a possible mechanism in which E295 -COO^- cannot be regenerated rapidly from the -COOH formed on transfer of the H^+ from $QH^{\bullet}$ in the first turnover, because the network is in some way "gummed up". This is consistent with a requirement for the carboxylate form for rapid dissociation on the second turnover.

e) From this, both an oxidized acceptor (ferriheme b_L) and a H^+ acceptor (E295 -COO^-) must be available for rapid oxidation of $ISPH^{\bullet}.QH^{\bullet}$. Oxidation of $ISPH^{\bullet}.QH^{\bullet}$ requires dissociation to $ISPH^{\bullet}$, $Q^{\bullet-}$, and H^+, each processed through its own path, all occurring fast enough in normal forward flux to allow the electrons to reach heme b_H in <20 μs.

Although protolytic reactions are represented only implicitly, all these processes are included in the kinetic model published in 2013 ([139], and see Table 1 and Fig. 9 therein).

f) The *ES*-complex forms with the ISP protein docked at cyt *b*, pulled from the relaxed configuration seen in the presence of myxothiazol, and held in place by the binding force stabilizing it. The intermediate complex forms in the same configuration, held in place by binding of the intermediate state, with a binding force, likely changed, but also working against the "spring" to give $\Delta G_{K_E}^{app,IS} = \Delta G_{total}^{occp} - \Delta G_{spring}$. On dissociation to products, $ISPH^{\bullet}$, $Q^{\bullet-}$, and H^+ in normal forward chemistry, the H-bond providing the binding force is lost, and the retractive force of the spring will pull $ISPH^{\bullet}$ away so that it is free to diffuse over to dock on cyt ferric$_1$.

g) If heme c_1 and cyt c_2 are oxidized (by $2P^+$ generated on flash excitation in chromatophores), $ISPH^{\bullet}$ will be rapidly oxidized. This rapid removal of the product would make the dissociation practically irreversible, and would initiate a subsequent turnover once the Q_o-site is vacated.

h) In the original kinetic model [139] all rate constants were defined with respect apparent equilibrium constants, initially for formation of the *ES*-complex, $\Delta G_{K_E}^{app}$, and for the limiting first electron transfer, with ratios of forward and reverse rate constants as appropriate, and with values derived from kinetic measurements. In the published version, the modelling kinetics were extended to simulate up to three turnovers of the Q_o-site when antimycin blocked oxidation of heme b_H. This version is available on request as a Dynafit model. Stuart Rose has versions of the model in MatLab, and an implementation of the Gillespie algorithm also in MatLab, which gave, in effect the same outcome. However, none of these versions have been modified to deal with the spring-loaded scenario. Apart from the treatment of the

diffusion of SQ, no complexity associated with specific partial processes in the second electron transfer was attempted; the limitation associated with mutation of E295 was simulated by lowering the diffusion step.

In order to include dynamics of the spring in the kinetic model, it needs to be revised to take account of the action. The equilibrium constant for formation of the *ES*-complex ($QH_2.ISP_{ox}$) must be deconvoluted as implicit in the terms in $\Delta G_{K_E}^{app,ES} = \Delta G_{total}^{occp} - \Delta G_{spring}$, including the contribution of additional forces in the two terms on the right. After formation of $ISPH^{\bullet}.QH^{\bullet}$ in the first electron transfer, the ISP protein must remain docked at cyt *b*, but now with $ISPH^{\bullet}$ as H-bonding partner, with a similar set of terms for the intermediate state (IS) involving $\Delta G_{K_E}^{app,IS}$, in which the second H-bond to Y147 contributes a different ΔG_{extra}^{occp} to ΔG_{total}^{occp}. To generate the same output, the overall values for the binding constants must remain the same. This is not a trivial exercise, and I have not attempted this revision, because I am in no position to explore the validity of any change by new experiments. However, I invite others to the fray. In the original model, we found that the rate constant for oxidation of the high potential chain had to be artificially large to get the observed kinetics. It seems likely that this artificiality would be eliminated by including the action of the "spring".

H. Parameters for participation of Glu-295

The story so far explains the rapid forward chemistry in terms of processes that we can justify from direct experimental measurements. However, there are several partial processes that can be inferred.

a) Given the distances involved, and the rate constants required, the $Q^{\bullet-}$ liberated on dissociation must move ~5.5 Å from the distal to the proximal domain to be oxidized rapidly. Side chain rotations (1-10 ns) [245], and 1-D diffusion along the constrained path (<100 ns) allow estimation of a value for k_{diff} in the range 10^6 to 10^8 s^{-1}, and in our kinetic model [139], values in this range generate observed kinetic behavior. Given the high $k_{forward}$ for electron transfer from $Q^{\bullet-}$ to heme b_L at the distance involved, this movement becomes limiting at the low end of this range.

b) The next question to consider is the cycle of processes involving E295 leading to proton exit, including a role of the heme. Our perspective on this cycle depends on the pK values of the groups involved in H^+ exchange. Rich and Bendall [246] have a useful Table of values for physicochemical parameters for a wide range of Q/QH_2 couple, including ubiquinone, from which for dissociation of $QH^{\bullet}$ has p*K* 5.9 in solution, compared to the p*K* of glutamic acid at ~4.3. I have discussed the dissociation of $QH^{\bullet}$ above in the context of the p*K* ~8.5 determining the rate in E295 mutants, and pointed out that a more plausible candidate is Tyr-132. Although p*K* values for dissociable groups can be displaced over a very wide range by local chemistry of the protein, in the Q_o-site, it does not seem plausible that the p*K* values for either the intermediate $QH^{\bullet}$ or E295 could be shifted this far. The simplest model for the chemistry would have both $QH^{\bullet}$ and E295-COOH with operational p*K* values close, and in the range below the p*K* of ~6.5 observed for the overall rate. The following sequence then seems likely: after the first electron transfer, with $QH^{\bullet}.ISPH^{\bullet}$ still bound, the -COO^- sidechain of E295rotates so as accept the proton from $QH^{\bullet}$ (either directly or via Y132), allowing the intermediate complex to dissociate. E295-COOH then rotates away, allowing transfer of the H^+ to the network, and opening the volume into which $Q^{\bullet-}$ can move. The rotation makes the E295 backbone >NH accessible as H-bond donor, likely to the >C=O of $Q^{\bullet-}$, leaving the >C-O^- close to ferriheme b_L for rapid electron transfer. On reduction, a heme propionate likely becomes protonated. Transfer of the H^+ to the heme propionate would then represent a coordinated transfer of the electron and the proton to the heme. The H-bonded water network of Palsdottir et al. [203] has E295 H-bonded to the propionate A of heme b_L through a bridging water. Transfer on

reduction, and then release on re-oxidation, would all occur in <20 μs in normal forward chemistry. E295 is also directly H-bonded to H276 (using *Rb. sphaeroides* numbering), but that residue is not conserved; in most mitochondrial bc_1 complexes, including bovine and avian, an aspartate is found, but the histidine in yeast is also found in the *Rhodobacter*.

c) In the condition in which the $QH^{\bullet}.ISPH^{\bullet}$ state accumulates, the heme b_L is reduced. Perhaps reduction of the heme freezes the network in some way, so that E295 -COOH cannot dissociate and the proton cannot exit. The propionate would be unavailable as H^+ acceptor, and this might be reason enough to account for the inhibition, or perhaps in the carboxylic state, the H-bonding potential of E295 is different enough that the Palsdottir network has a different configuration. In normal forward chemistry, the cycle of E295 protolytic states, dissociation on oxidation of $QH^{\bullet}.ISPH^{\bullet}$, and movement of $Q^{\bullet-}$, discussed above must of course be speculative, but for any cycle, the network will re-open within the <20 μs time for transient reduction and oxidation of heme b_L, insignificant with respect to the limiting first electron transfer. In revising the kinetic model, it will be necessary to include the E295 cycle through explicit processes, and include a role for the heme propionate, and for Arg-94, its H-bonding partner in the oxidized heme.

d) The water chains connect the volume to the Q_o-site to the P-phase, but there are two channels, one leading to Arg-94 and the propionate and the other to H276. How are these involved? At present, we can only guess, but the many different configurations offered in crystallographic structures, and more so in MD simulation, offer plenty of room for speculation. Maybe since the histidine is not conserved, we can discount a specific role for that channel. The arguments above suggest that this largess might be further constrained by additional experiments and computational modeling. Unfortunately, the lack of funding also killed off any further progress in the prodigious efforts made by Stuart Rose in improving and exploiting both our models from MD simulations, and those from kinetic modelling.

I. Protection against SO^- generation

The final question I want to address is that of protection against SO^- generation. In the forward reaction sketched out above, our kinetic model shows that SQ is accumulated to significant occupancy only under backed-up conditions. Under "open" conditions it is removed so rapidly that participation in such bypass reactions is minimal. When SQ does accumulate, it is trapped in the $QH^{\bullet}.ISPH^{\bullet}$ complex at the distal domain, and therefore removed enough from the reduced heme b_L that rate constants are at least 10^3-fold lowered. In the 2013 model, this separation of SQ from interaction with ferroheme b_L was implemented by introducing a coulombic bias in the forward and reverse rate constants for SQ diffusion. This somewhat artificial bias would now be unnecessary since the stability of the $QH^{\bullet}.ISPH^{\bullet}$ state provides the same function.

Since the time of flight in the mixing experiments is through free air, but the $QH^{\bullet}.ISPH^{\bullet}$ state does not decay, it is apparently also unreactive with O_2 on this time scale when bound, and this therefore protects against SO^- generation.

This two provisions, the separation by distance from heme b_L, and the lack of reactivity with O_2, would provide the fix to the Q-cycle sought by Osyczka et al. [177].

The mechanistic model above depends heavily on the validity of the rapid mix/freeze quench experiments, sadly truncated by funding failure. I hope that others will revisit this approach. The Osyczka group [217, 247, 248] have found an $ISPH^{\bullet}.QH^{\bullet}$ state with quite different, but also complex EPR spectra, formed over a longer time scale, and so unlikely to be an intermediate of interest in normal forward chemistry. However, they invoke the state as protective against SO^- generation. Neither of these states shows the symmetrical SQ signal shown in earlier experiments [139, 143, 144]. It would be

interesting to compare the protocols under which the states are trapped. Rapid freezing at liq. N_2 temperatures in our experiments seems to be the main difference; there are accounts of changes in the physical state of waters bound in protein over the temperature range of the different freezing protocols [249] that might explain the different properties. In addition, kinetic resolution depends on the rate of cooling; with the spinning wheels, the dimensions of the jet lead to freezing to liq. N_2 temperatures in the low μs time range. With injection into freezing mixtures, the rate depends strongly on droplet size; with heterogeneity in the population, rates can cover a wide range, extending to the 10 ms range.

Acknowledgements

I am grateful for funding over the years from the National Institutes of Health NIGMS PHS 5 RO1 GM35438, NIGMS PHS 5 RO1 GM62954, NIH Shared Instrument Grant 1 S10 RR025438; from Fogarty International Research Collaboration Award 1 RO3 TW001495; from USDA NRI AG 98-35306-7009; from NATO Collaborative Linkage Grant 977132; and from Department of Energy DE-FG02-08ER15960

References

[1] J.B. Chappell, A.R. Crofts, Calcium Ion Accumulation and Volume Changes of Isolated Liver Mitochondria: Calcium Ion-Induced Swelling. , Biochem. J., 95 (1965) 378-386.
[2] J.B. Chappell, A.R. Crofts, Gramicidin and Ion Transport in Isolated Liver Mitochondria. , Biochem. J., 95 (1965) 393-402.
[3] J.B. Chappell, A.R. Crofts, The Effect of Atractylate and Oligomycin on the Behavior of Mitochondria Towards Adenine Nucleotides. , Biochem. J., 95 (1965) 707-716.
[4] A.R. Crofts, J.B. Chappell, Calcium Ion Accumulation and Volume Changes of Isolated Liver Mitochondria: Reversal of Calcium Ion-Induced Swelling. , Biochem. J., 95 (1965) 387-392.
[5] J.B. Chappell, A.R. Crofts, Ion Transport and Reversible Volume Changes of Isolated Mitochondria. In: Regulation of Metabolic Processes in Mitochondria,, in: J.M. Tager, S. Papa, E. Quagliariello, E.C. Slater (Eds.), Elsevier Publishing Co., Amsterdam, Holland., 1966, pp. 293-316.
[6] P. Mitchell, Coupling of phosphorylation to electron and hydrogen transfer by a chemi-osmotic type of mechanism, Nature, 191 (1961) 144-148.
[7] A.R. Crofts, Uptake of Ammonium Ion by Chloroplasts, and the Mechanism of Amine Uncoupling, Biochem. Biophys. Res. Commun., 24 (1966) 127-134.
[8] A.R. Crofts, Uptake of Ammonium Ion by Chloroplasts and its Relation to Photophosphorylation, Biochem. Biophys. Res. Commun., 24 (1966) 725-731.
[9] A.R. Crofts, Amine Uncoupling of Energy Transfer in Chloroplasts. I. Relation to Ammonium Ion Uptake., J. Biol. Chem., 242 (1967) 3352-3359.
[10] A.R. Crofts, Ammonium Ion Uptake by Chloroplasts and the High-Energy State, in: J. Jarnefelt (Ed.) Regulatory Functions of Biological Membranes, Elsevier Publishing Co., Amsterdam, Holland., 1968, pp. 248-263.
[11] A.R. Crofts, D.W. Deamer, L. and Packer, Mechanisms of Light-Induced Structural Change in Chloroplasts. II. The Role of Ion Movements in Volume Changes, Biochim. Biophys. Acta, 131 (1967) 97-118.
[12] A.R. Crofts, The Chromatophore as a Functional Unit, in: J.M. Tager, S. Papa, E. Quagliariello, E.C. Slater (Eds.) Electron Transport and Energy Conservation., Adriatica Editrice, Bari, Italy., 1970, pp. 221-228.
[13] J.B. Jackson, A.R. Crofts, Bromothymol Blue and Bromocresol Purple as indicators of pH changes in chromatophores of *Rhodospirillum rubrum*, Eur. J. Biochem., 10 (1969) 226-237.
[14] J.B. Jackson, A.R. Crofts, The high energy state in chromatophores from *Rhodopseudomonas spheroides*, FEBS Lett., 4 (1969) 185-189.
[15] J.B. Jackson, A.R. Crofts, The kinetics of light induced carotenoid changes in *Rhodopseudomonas spheroides* and their relation to electrical field generation across the chromatophore membrane, Eur. J. Biochem., 18 (1971) 120-130.
[16] J.B. Jackson, A.R. Crofts, L.-V. Von Stedingk, Ion Transport Induced by Light and Antibiotics in Chromatophores from *Rhodospirillum rubrum*, Eur. J. Biochem., 6 (1968) 41-54.
[17] J.B. Jackson, P.L. Dutton, The kinetic and redox potentiometric resolution of the carotenoid shifts in *Rhodopseudomonas spheroides* chromatophores: Their relationship to electric field alterations in electron transport and energy coupling, Biochim. Biophys. Acta - Bioenergetics, 325 (1973) 102-113
[18] E.H. Evans, R.J. Cogdell, A.R. Crofts, H^+-Uptake and the Carotenoid Shift in *Rhodopseudomonas capsulata* Chromatophores Induced by Repeated Saturating Flashes, Biochem. Soc. Trans., 2 (1974) 538-540.
[19] E.H. Evans, A.R. Crofts, *In situ* Characterization of Photosynthetic Electron Transport in *Rhodopseudomonas capsulata*, Biochim. Biophys. Acta, 357 (1974) 89-102.
[20] E.H. Evans, A.R. Crofts, A Thermodynamic Characterization of the Cytochromes of Chromatophores from Rhodopseudomonas capsulata, Biochim. Biophys. Acta, 357 (1974) 78-88.
[21] R.J. Cogdell, A.R. Crofts, H^+-uptake by Chromatophores from *Rhodopseudomonas sphaeroides*. The Relation Between Rapid H^+-uptake and the H^+ Pump, Biochim. Biophys. Acta, 247 (1974) 264-272.

[22] R.J. Cogdell, J.B. Jackson, A.R. Crofts, The Effect of Redox Potential on the Coupling Between Rapid H^+-binding and Electron Transport in Chromatophores from *Rhodopseudomonas spheroides*, J. Bioenergetics, 4 (1972) 211-227.
[23] R.J. Cogdell, R.C. Prince, A.R. Crofts, Light Induced H^+-uptake Catalysed by Photochemical Reaction Centres from *Rhodopseudomonas spheroides* R26, FEBS Lett., 35 (1973) 204-208.
[24] R.C. Prince, A. Baccarini-Melandri, G.A. Hauska, B.A. Melandri, A.R. Crofts, Asymmetry of an Energy Transducing Membrane. The Location of Cytochrome c_2 in *Rhodopseudomonas sphaeroides* and *Rps. capsulata*, Biochim. Biophys. Acta, 387 (1975) 212-227.
[25] R.C. Prince, R.J. Cogdell, A.R. Crofts, Light-Induced Proton Uptake by Bacterial Reaction Centres, Biochem. Soc. Trans., 2 (1974) 162-164.
[26] R.C. Prince, A.R. Crofts, Photochemical Reaction Centres from *Rhodopseudomonas capsulata*, FEBS Lett., 35 (1973) 213-216.
[27] R.C. Prince, G.A. Hauska, A.R. Crofts, A. Melandri, B.A. Melandri, Asymmetry of an Energy-Coupling Membrane. The Immunological Localisation of Cytochrome c_2 in *Rhodopseudomonas sphaeroides*, in: M. Avron (Ed.) Proc. Third International Cong. on Photosynthesis, Elsevier Publishing Co., Amsterdam, The Netherlands., 1974, pp. 769-776.
[28] N.G. Holmes, A.R. Crofts, The Carotenoid Shift in *Rhodopseudomonas sphaeroides*; Change Induced Under Continuous Illumination, Biochim. Biophys. Acta, 461 (1977) 141-150.
[29] N.G. Holmes, A.R. Crofts, The Carotenoid Shift in Rhodopseudomonas sphaeroides; the Flash-Induced Change, Biochim. Biophys. Acta, 459 (1977) 492-505.
[30] N.G. Holmes, C.N. Hunter, R.A. Niederman, A.R. Crofts, Identification of the pigment pool responsible for the flash-induced carotenoid band shift in *Rhodopseudomonas sphaeroides* chromatophores, FEBS Lett., 115 (1980) 43-48.
[31] A.R. Crofts, D. Crowther, J. Bowyer, G.V. Tierney, Electron Transport Through the Antimycin Sensitive Site in Rhodopseudomonas capsulata, in: K. van Dam, B.F. Gelder (Eds.) Structure and Function of Energy Transducing Membranes,, Elsevier/North Holland, Amsterdam, The Netherlands., 1977, pp. 139-155.
[32] A.R. Crofts, D. Crowther, H. Celis, S. Alvanza de Celis, G. Tierney, Proton Pumps in Bacterial Photosynthesis, Biochem. Soc. Trans., 5 (1977) 491-495.
[33] A.R. Crofts, D. Crowther, G.V. Tierney, Electrogenic Electron Transport in Photosynthetic Bacteria, in: E. Quagliariello, S. Papa, F. Palmieri, E.C. Slater, N. Siliprandi (Eds.) Electron Transfer Chains and Oxidative Phosphorylation, North-Holland Publishing Co., Amsterdam, The Netherlands., 1975, pp. 233-241.
[34] W. Junge, Protons, proteins and ATP, in: Govindjee, J.T. Beatty, H. Gest, J.F. Allen (Eds.) Discoveries in Photosynthesis, Springer, Dordrecht, The Netherlands, 2005, pp. 571-595.
[35] W. Junge, H.T. Witt, On the ion transport system of photosynthesis - investigations on a molecular level, Z. Naturforsch., 23b (1968) 244-254.
[36] B. Chance, A.R. Crofts, M. Nishimura, B. Price, Fast Membrane H+ Binding in the Light-Activated State of Chromatium Chromatophores. , Eur. J. Biochem., 13 (1970) 364-374.
[37] N. Murata, K. Sugahara, Control of excitation transfer in photosynthesis. III. Light-induced decrease in chlorophyll *a* fluorescence related to photophosphorylation system in spinach chloroplasts, Biochim. Biophys. Acta, 189 (1969) 182–192.
[38] A. Hager, Lichtbedingte pH-Erniedrigung in einem Chloroplasten-Kompartiment als Ursache der enzymatischen Violaxanthin-Zeaxanthin-Umwandlung; Beziehungen zur Photophosphorylierung, Planta, 89 (1969) 224-243.
[39] H. Yamamoto, Biochemistry of the violaxanthin cycle in higher plants, Pure and Appl. Chem., 51 (1979) 639-648.
[40] B. Demmig-Adams, Carotenoids and photoprotection in plants: A role for the xanthophyll zeaxanthin, Biochim. Biophys. Acta, 1020 (1990) 1-24.
[41] A.R. Crofts, C.T. Yerkes, A Molecular Mechanism for Q_E-quenching, FEBS Lett., 352 (1994) 265-270.

[42] C.A. Wraight, A.R. Crofts, Delayed Fluorescence and the High-Energy State of Chloroplasts, Eur. J. Biochem., 19 (1971) 386-397.
[43] A.R. Crofts, C.A. Wraight, D.E. Fleischman, Energy Conservation in the Photochemical Reactions of Photosynthesis and its Relation to Delayed Fluorescence, FEBS Lett., 15 (1971) 89-100.
[44] C.A. Wraight, A.R. Crofts, Energy-Dependent Quenching of Chlorophyll a Fluorescence in Isolated Chloroplasts, Eur. J. Biochem., 17 (1970) 319-327.
[45] L.N.M. Duysens, The Photochemical Apparatus; Its Structure and Function, in: Brookhaven Symp. Biol. 11, Brookhaven National Laboratory, 1958.
[46] S. Saphon, A.R. Crofts, Protolytic Reactions in Photosystem II. A New Model for the Release of Protons Accompanying the Photooxidation of Water, Z. Naturforsch., 32c (1977) 617-626.
[47] B. Kok, B. Forbush, M.P. McGloin, Cooperation of charges in photosynthetic O_2 evolution I. A linear four step mechanism, Photochem. Photobiol., 11 (1970) 457 - 475.
[48] J.M. Bowes, A.R. Crofts, Interactions of Protons with Transitions of the Water-splitting Enzyme of Photosystem II as Measured by Delayed Fluorescence, Z. Naturforsch., 33c (1978) 271-275.
[49] J.M. Bowes, A.R. Crofts, Binary Oscillations in the Rate of Reoxidation of the Primary Acceptor of Photosystem II, Biochim. Biophys. Acta, 590 (1980) 373-384.
[50] J.M. Bowes, A.R. Crofts, The Role of pH and Membrane Potential in the Reactions of Photosystem II as Measured by Effects on Delayed Fluorescence, Biochim. Biophys. Acta., 637 (1981) 464-472.
[51] J.M. Bowes, A.R. Crofts, S. Itoh, Effects of pH on Reactions on the Donor Side of Photosystem II, Biochim. Biophys. Acta, 547 (1979) 336-346.
[52] P. Abbyad, W. Childs, X. Shi, S.G. Boxer, Dynamic Stokes shift in green fluorescent protein variants, Proc. Natl. Acad. Sci. (U. S. A), 104 (2007) 20189-20194.
[53] P. Mitchell, Proton motive redox mechanism of the cytochrome b-c_1 complex in the respiratory chain: Proton motive ubiquinone cycle., FEBS Lett., 56 (1975) 1-6.
[54] M.K.F. Wikström, J.A. Berden, Oxidoreduction of cytochrome b in the presence of antimycin, Biochim. Biophys. Acta, 283 (1972) 403-420.
[55] P. Mitchell, Possible molecular mechanisms of the protonmotive function of cytochrome systems, J. Theor. Biol., 62 (1976) 327-367.
[56] J.R. Bowyer, A.R. Crofts, Inhibition of Electron Transport in *Rps. capsulata* by a Ubiquinone Analogue, in: P.L. Dutton, J. Leigh, A. Scarpa (Eds.) Frontiers of Biological Energetics, Academic Press, New York, NY., 1978, pp. 326-333.
[57] J.R. Bowyer, G.V. Tierney, A.R. Crofts, Cytochrome c_2 - Reaction Centre Coupling in Chromatophores, FEBS Lett., 101 (1979) 207-212.
[58] J.R. Bowyer, P.L. Dutton, R.C. Prince, A.R. Crofts, The role of the Rieske iron-sulfur center as the electron donor to ferricytochrome c2 in Rhodopseudomonas sphaeroides, Biochimica et Biophysica Acta (BBA) - Bioenergetics, 592 (1980) 445-460.
[59] S.W. Meinhardt, A.R. Crofts, Kinetic and thermodynamic resolution of cytochrome c_1 and cytochrome c_2 from *Rps. sphaeroides*, FEBS Lett., 149 (1982) 223-227.
[60] P.M. Wood, Do photosynthetic bacteria contain cytochrome c_1?, Biochem. J., 189 (1980) 385-391.
[61] P.M. Wood, The interrelation of the two c-type cytochromes in *Rhodopseudomonas sphaeroides* photosynthesis, Biochem. J., 192 (1980) 761-764.
[62] S.W. Meinhardt, A.R. Crofts, The Role of Cytochrome b_{566} in the Electron Transfer Chain of *Rps. sphaeroides*, Biochim. Biophys. Acta, 723 (1983) 219-230.
[63] E.G. Glaser, S.W. Meinhardt, A.R. Crofts, Reduction of cytochrome b_{561} through the antimycin-sensitive site of the ubiquinol:cytochrome c_2 oxidoreductase complex of *Rps. sphaeroides*, FEBS Lett., 178 (1984) 336-342.
[64] E.G. Glaser, A.R. Crofts, A new electrogenic step in the ubiquinol: Cytochrome c2 oxidoreductase complex of Rhodopseudomonas sphaeroides, Biochimica et Biophysica Acta (BBA) - Bioenergetics, 766 (1984) 322-333.
[65] J.R. Bowyer, A.R. Crofts, On the Mechanism of Photosynthetic Electron Transfer in *Rps. capsulata* and *Rps. sphaeroides*, Biochim. Biophys. Acta, 636 (1981) 218-233.

[66] B.L. Trumpower, C.A. Edwards, Purification of a reconstitutively active iron-sulfur protein (oxidation factor) from succinate . cytochrome c reductase complex of bovine heart mitochondria, J. Biol. Chem., 254 (1979) 8697-8706.
[67] S.W. Meinhardt, A.R. Crofts, The site and mechanism of action of myxothiazol as an inhibitor of electron transfer in *Rhodopseudomonas sphaeroides*, FEBS Lett., 149 (1982) 217-222.
[68] W.F. Becker, G. Von Jagow, T. Anke, W. Steglich, Oudemansin, Strobolurin A, Strobolurin B and Myxothiazol: new inhibitors of the bc_1 segment of the respiratory chain with an E-*β*-methoxyacrylate system as a common structural element, FEBS Lett., 132 (1981) 329-333.
[69] G. von Jagow, T. Ohnishi, The chromone inhibitor stigmatellin - binding to the ubiquinol oxidation center at the C-side of the mitochondrial membrane, FEBS Lett., 185 (1985) 311-315.
[70] A.R. Crofts, The Q-cycle, - a personal perspective, Photosynth. Res., 80 (2004) 223-243
[71] P.B. Garland, R.A. Clegg, D. Boxer, J.A. Downie, B.A. Haddock, Proton-translocating nitrate reductase of *Escherichia coli*, in: E. Quagliariello, S. Papa, F. Palmieri, E.C. Slater, N. Siliprandi (Eds.) Electron Transfer Chains and Oxidative Phosphorylation, North-Holland Publishing Co., Amsterdam, The Netherlands., 1975, pp. 351-358. .
[72] A.R. Crofts, S.W. Meinhardt, A Q-cycle Mechanism for the Cyclic Electron Transfer Chain of Rps. sphaeroides Biochem. Soc. Trans., 10 (1982) 201-203.
[73] A.R. Crofts, S.W. Meinhardt, M. Snozzi, K.R. Jones, A Q-cycle Mechanism for Cyclic Electron Transport in *Rps. sphaeroides*, in: 2nd EBEC Short Reports, 1982, pp. 327-328.
[74] A.R. Crofts, S.W. Meinhardt, K.R. Jones, M. Snozzi, The role of the quinone pool in the cyclic electron-transfer chain of *Rhodopseudomonas sphaeroides*: A modified Q-cycle mechanism, Biochim. Biophys. Acta, 723 (1983) 202-218.
[75] A.R. Crofts, The mechanism of Ubiquinol:cytochrome c Oxidoreductases of Mitochondria and of *Rhodopseudomonas sphaeroides*, in: A.N. Martonosi (Ed.) In: The Enzymes of Biological Membranes, Plenum Publ. Corp., New York., 1985, pp. 347-387.
[76] A.R. Crofts, Reaction center and UQH_2:cyt c_2 oxidoreductase act as independent enzymes in *Rps. sphaeroides*, J. Bioenerg. Biomemb., 18 (1986) 437-446.
[77] M. Snozzi, A.R. Crofts, Electron transport in chromatophores from Rhodopseudomonas sphaeroides GA fused with liposomes, Biochimica et Biophysica Acta (BBA) - Bioenergetics, 766 (1984) 451-463.
[78] M. Snozzi, A.R. Crofts, Kinetics of the c-cytochromes in chromatophores from *Rps. sphaeroides* as a function of the concentration of cytochrome c_2: Influence of this concentration on the oscillation of the secondary acceptor of the reaction center, Q_B., Biochim. Biophys. Acta, 809 (1985) 260-270.
[79] G. Venturoli, J.G. Fernandez-Velasco, A.R. Crofts, B.A. Melandri, Demonstration of a collisional interaction of ubiquinol with the ubiquinol-cytochrome c_2 oxidoreductase complex in chromatophores from *Rhodobacter sphaeroides*, Biochimica et Biophysica Acta (BBA) - Bioenergetics, 851 (1986) 340-352.
[80] G. Venturoli, J.G. Fernandez-Velasco, A.R. Crofts, B.A. Melandri, The effect of the size of the quinone pool on the electrogenic reactions in the UQH_2:cyt c_2 oxidoreductase of *Rhodobacter capsulatus*. Pool behavior at the quinone reductase site, Biochim. Biophys. Acta, 935 (1988) 258-272.
[81] A.R. Crofts, Z. Wang, How rapid are the internal reactions of the ubiquinol:cytochrome c_2 oxidoreductase?, Photosynth. Res., 22 (1989) 69-87.
[82] A.R. Crofts, Proton-coupled electron transfer at the Q_o-site of the bc_1 complex controls the rate of ubihydroquinone oxidation, Biochim. Biophys. Acta, 1655 (2004) 77-92.
[83] A.R. Crofts, The cytochrome bc_1 complex – function in the context of structure, Annu. Rev. Physiol., 66 (2004) 689-733.
[84] A.R. Crofts, M. Guergova-Kuras, R. Kuras, N. Ugulava, J. Li, S. Hong, Proton-coupled electron transfer at the Q_o-site: what type of mechanism can account for the high activation barrier?, Biochim. Biophys. Acta, 1459 (2000) 456-466.
[85] A.R. Crofts, V.P. Shinkarev, D.R.J. Kolling, S. Hong, The modified Q-cycle explains the apparent mismatch between the kinetics of reduction of cytochromes c_1 and b_H in the bc_1 complex, J. Biol. Chem., 278 (2003) 36191-36201.

[86] J. Deisenhofer, O. Epp, K. Miki, R. Huber, H. Michel, X-Ray structure analysis of a membrane protein complex: Electron density map at 3 Å resolution and a model of the chromophores of the photosynthetic reaction center from *Rhodopseudomonas viridis*., J. Mol. Biol., 180 (1984) 385 -398.
[87] W.R. Widger, W.A. Cramer, R.G. Herrmann, A. Trebst, Sequence homology and structural similarity between cytochrome b of mitochondrial complex III and the chloroplast b6-f complex: Position of the cytochrome b hemes in the membrane, Proc. Natl. Acad. Sci. USA, 81 674-678.
[88] M. Saraste, Location of haem-binding sites in the mitochondrial cytochrome b, FEBS Lett., 166, (1984) 367-372.
[89] A.R. Crofts, H.H. Robinson, K. Andrews, S. Van Doren, E. Berry, Catalytic sites for reduction and oxidation of quinones. , in: S. Papa, B. Chance, L. Ernster (Eds.) Cytochrome Systems: Molecular Biology and Bioenergetics, Plenum Publ. , New York, 1987, pp. 617-624.
[90] H.R. Mahler, P.S. Perlman, in: A.N. Martonosi (Ed.) The enzymes of biological membranes, Plenum Press, 1985, pp. 195-234.
[91] N. Howell, K. Gilbert, Mutational analysis of the mouse mitochondrial cytochrome *b* gene, J. Mol. Biol., 203 (1988) 607-618.
[92] C.-H. Yun, A.R. Crofts, R.B. Gennis, Assignment of the histidine axial ligands to the cytochrome b_H and cytochrome b_L components of the bc_1 complex from *Rb. sphaeroides* by site-directed mutagenesis, Biochemistry, 30 (1991) 6747-6754.
[93] C.-H. Yun, S.R. Van Doren, A.R. Crofts, R.B. Gennis, The Use of Gene Fusions to Examine the Membrane Topology of the L-Subunit of the Photosynthetic Reaction Center and of the Cytochrome b Subunit of the bc_1 Complex from *Rhodobacter sphaeroides*, J. Biol. Chem., 266 (1991) 10967-10973.
[94] D. Xia, C.-A. Yu, H. Kim, J.-Z. Xia, A.M. Kachurin, L. Zhang, L. Yu, J. Deisenhofer, Crystal Structure of the Cytochrome bc_1 Complex from Bovine Heart Mitochondria, Science, 277 (1997) 60-66.
[95] Z. Zhang, L.-S. Huang, V.M. Shulmeister, Y.-I. Chi, K.-K. Kim, L.-W. Hung, A.R. Crofts, E.A. Berry, S.-H. Kim, Electron transfer by domain movement in cytochrome bc_1, Nature (Lond.), 392 (1998) 677-684.
[96] A.R. Crofts, Z. Wang, Y. Chen, S. Manalingham, C.-H. Yun, R.B. Gennis, Function, steady state turn-over, and structure of the UQH_2:cyt c_2 oxidoreductase of *Rb. sphaeroides*, in: G. Lenaz, O. Barnabei, A. Rabbi, M. Battino (Eds.) Highlights in Ubiquinone Research, Taylor & Francis, Ltd, London, 1990, pp. 98-103.
[97] A.R. Crofts, B. Hacker, B. Barquera, C.-H. Yun, R. Gennis, Structure and function of the *bc*-complex of *Rhodobacter sphaeroides*, Biochim. Biophys. Acta, 1101 (1992) 162-165.
[98] T.J. Donohue, A.G. McEwan, S. Kaplan, Cloning, DNA sequence, and expression of the *Rhodobacter sphaeroides* cytochrome c_2 gene, J. Bacteriol., 168 (1986) 962-972.
[99] N. Gabellini, W. Sebald, Nucleotide sequence and transcription of the fbc operon from *Rhodopseudomonas sphaeroides*. Evaluation of the deduced amino acid sequences of the FeS protein, cytochrome *b* and cytochrome c_1, Eur. J. Biochem., 154 (1986) 569-579.
[100] E. Davidson, F. Daldal, fbc Operon, encoding the Rieske Fe□S protein cytochrome b, and cytochrome c1 apoproteins previously described from Rhodopseudomonas sphaeroides, is from Rhodopseudomonas capsulata, Journal of Molecular Biology, 195 (1987) 25-29.
[101] C.-H. Yun, R. Beci, A.R. Crofts, S. Kaplan, R.B. Gennis, Cloning and DNA Sequencing of the fbc Operon Encoding the Cytochrome bc_1 complex from *Rb. sphaeroides*: Characterization of fbc Deletion Mutants, and Complementation by a Site-Specific Mutational Variant, Europ. J. Biochem., 194 (1990) 399-411.
[102] B. Hacker, B. Barquera, A.R. Crofts, R.B. Gennis, Characterization of mutations in the cytochrome *b* subunit of the bc_1 complex of *Rhodobacter sphaeroides* that affect the quinone reductase site (Q_c), Biochemistry, 32 (1993) 4403-4410.
[103] B. Hacker, B. Barquera, R.B. Gennis, C. A.R., Site-directed mutagenesis of arginine-114 and tryptophan-129 in the cytochrome *b* subunit of the bc_1 complex of *Rhodobacter sphaeroides* : two highly conserved residues predicted to be near the cytoplasmic surface of putative transmembrane helices B and C, Biochemistry, 33 (1994) 13022-13031.

[104] S.R. Van Doren, R.B. Gennis, B. Barquera, A.R. Crofts, Site-Directed Mutations of Conserved Residues of the Rieske Iron-Sulfur Subunit of the Cytochrome bc_1 Complex of *Rhodobacter sphaeroides* Blocking or Impairing Quinol Oxidation, Biochemistry, 32 (1993) 8083-8091.
[105] S.R. Van Doren, C.-H. Yun, A.R. Crofts, R. Gennis, Assembly of the Rieske iron-sulfur subunit of the cytochrome bc_1 complex in *Escherichia coli* and *Rhodobacter sphaeroides* membranes independent of the cytochrome b and c_1 subunits, Biochemistry, 32 (1993) 628-636.
[106] C.-H. Yun, Z. Wang, A.R. Crofts, R.B. Gennis, Examination of the functional roles of five highly conserved residues in the cytochrome *b* subunit of the *bc*1 complex of *Rhodobacter sphaeroides*, J. Biol. Chem., 67 (1992) 5901-5909.
[107] K.M. Andrews, A.R. Crofts, R.B. Gennis, Large scale purification and characterization of a highly active four-subunit cytochrome bc_1 complex from *Rb. sphaeroides*, Biochemistry, 29 (1990) 2645-2651.
[108] M. Guergova-Kuras, R. Salcedo-Hernandez, G. Bechmann, R. Kuras, R.B. Gennis, A.R. Crofts, Expression and one-step purification of a fully active polyhistidine-tagged cytochrome bc_1 complex from *Rhodobacter sphaeroides*, Protein Expression and Purification, 15 (1999) 370-380.
[109] K.R. Popper, Objective Knowledge: An Evolutionary Approach, Clarendon Press, Oxford, 1972.
[110] M. Snozzi, A.R. Crofts, Diffusion Controlled Rates in Bacterial Photosynthetic Electron Transport as Studied by Fusion of Chromatophores of *Rps. sphaeroides* with Liposomes, in: C. Sybesma (Ed.) Advances in Photosynthesis Research, Martinus Nijhoff/Dr. W. Junk Publishers, The Hague., 1984, pp. 755-758.
[111] C.C. Moser, Page, C.C., Farid, R. and Dutton, P.L., Biological electron transfer, J. Bioenerg. Biomembranes, 27 (1995) 263-274.
[112] C.C. Moser, P.L. Dutton, Engineering protein structure for electron transfer function in photosynthetic reaction centers, Biochimica et Biophysica Acta, 1101 (1992) 171-176.
[113] C.C. Moser, C.C. Page, X. Chen, P.L. Dutton, Biological electron tunneling through native protein media, Journal of Biological Inorganic Chemistry, 2 (1997) 393-398.
[114] A.R. Crofts, S. Rose, Marcus treatment of endergonic reactions: a commentary, Biochim. Biophys. Acta, 1767 (2007) 1228-1232.
[115] H. Ding, C.C. Moser, D.E. Robertson, M.K. Tokito, F. Daldal, P.L. Dutton, Ubiquinone pair in the Q_o site central to the primary energy conversion reactions of cytochrome bc_1 complex, Biochemistry, 34 (1995) 15979-15996.
[116] H. Ding, D.E. Robertson, F. Daldal, P.L. Dutton, Cytochrome bc_1 complex [2Fe-2S] cluster and its interaction with ubiquinone and ubihydroquinone at the Q_o site: a double-occupancy Q_o site model, Biochemistry, 31 (1992) 3144-3158.
[117] H.G. Ding, D.E. Robertson, F. Daldal, P.L. Dutton, Cytochrome bc_1 Complex 2Fe-2S Cluster and Its Interaction with Ubiquinone and Ubihydroquinone at the Q_o Site - a Double-Occupancy Q_o Site Model, Biochemistry, 31 (1992) 3144-3158.
[118] B.L. Trumpower, Function of the iron-sulfur protein of the cytochrome b-c1 segment of the respiratory chain, Biochim Biophys Acta, 639 (1981) 129-155.
[119] J.R. Bowyer, and Trumpower, B.L., Pathways of electron transfer in the cytochrome b-c_1 complexes of mitochondria and photosynthetic bacteria, in: V.P. Skulachev, and Hinkle, P.C. (Ed.) Chemiosmotic Proton Circuits in Biological membranes, Addison-Wesley Publ. Co., Reading, Mass., 1981, pp. 105-122.
[120] J.R. Bowyer, C.A. Edwards, T. Ohnishi, B.L. Trumpower, An analogue of ubiquinone which inhibits respiration by binding to the iron-sulfur protein of the cytochrome bc_1 segment of the mitochondrial respiratory chain., J. Biol. Chem., 257 (1982) 8321-8330.
[121] R.D. Britt, K. Sauer, M.P. Klein, D.B. Knaff, A. Kriauciunas, C.-A. Yu, R. Malkin, Electron Spin Echo Envelope Modulation Spectroscopy Supports the Suggested Coordination of Two Histidine Ligands to the Rieske Fe-S Centers of the Cytochrome b_6f Complex of Spinach and the Cytochrome bc_1 Complexes of *Rhodospirillum rubrum*, *Rhodobacter sphaeroides* R-26 and Bovine Heart Mitochondria. , Biochemistry, 30 (1991) 1892-1901.

[122] R.J. Gurbiel, Ohnishi, T., Robertson, D., Daldal, F. and Hoffman, B.M., Q-Band ENDOR spectra of the Rieske protein from *Rhodobacter capsulatus* ubiquinol-cytochrome c oxidoreductase show two histidines coordinated to the [2Fe-2S] cluster., Biochemistry, 30 (1991) 11579–11584.
[123] S. Iwata, Saynovits, M., Link, T.A. and Michel, H., Structure of a water soluble fragment of the Rieske iron sulfur protein of the bovine heart mitochondrial cytochrome bc_1 complex determined by MAD phasing at 1.5 Å resolution, Structure, 4 (1996) 567-579.
[124] C.-A. Yu, J.-Z. Xia, A.M. Kachurin, L. Yu, D. Xia, H. Kim, J. Deisenhofer, Crystallization and preliminary structure of beef heart mitochondrial cytochrome-bc_1 complex, Biochim. Biophys. Acta, 1275 (1996) 47-53.
[125] A.R. Crofts, B. Hacker, B. Barquera, C.-H. Yun, R.B. Gennis, Structure and Function of the *bc*-complex of *Rhodobacter sphaeroides*, in: N. Murata (Ed.) Research in Photosynthesis, Kluwer Academic Publishers, Dordrecht., 1992, pp. 463-470.
[126] A.R. Crofts, S. Hong, Z. Zhang, E.A. Berry, Physicochemical aspects of the movement of the Rieske iron sulfur protein during quinol oxidation by the bc_1 complex, Biochemistry, 38 (1999) 15827-15839.
[127] A.R. Crofts, B. Barquera, R.B. Gennis, R. Kuras, M. Guergova-Kuras, E.A. Berry, Mechanism of ubiquinol oxidation by the bc_1 complex: the different domains of the quinol binding pocket, and their role in mechanism, and the binding of inhibitors, Biochemistry, 38 (1999) 15807-15826.
[128] A.R. Crofts, M. Guergova-Kuras, L.-S. Huang, R. Kuras, Z. Zhang, E.A. Berry, The mechanism of ubiquinol oxidation by the bc_1 complex: the role of the iron sulfur protein, and its mobility, Biochemistry, 38 (1999) 15791-15806.
[129] A.R. Crofts, S.J. Hong, N. Ugulava, B. Barquera, R. Gennis, M. Guergova-Kuras, E.A. Berry, Pathways for proton release during ubihydroquinone oxidation by the bc_1 complex, Proc. Natl. Acad. Sci. (U.S.A.), 96 (1999) 10021-10026.
[130] S. Izrailev, A.R. Crofts, E.A. Berry, K. Schulten, Steered molecular dynamics simulation of the Rieske subunit motion in the cytochrome bc_1 complex, Biophys. J., 77 (1999) 1753-1768.
[131] S.J. Hong, N. Ugulava, M. Guergova-Kuras, A.R. Crofts, The energy landscape for ubihydroquinone oxidation at the Q_o-site of the bc_1 complex in *Rhodobacter sphaeroides*, J. Biol. Chem., 274 (1999) 33931-33944.
[132] E. Darrouzet, Valkova-Valchanova, M., and Daldal, F., The [2Fe-2S] cluster E_m as an indicator of the iron-sulfur subunit position in the ubihydroquinone oxidation site of the cytochrome bc_1 complex, J. Biol. Chem, 277 (2002) 3464-3470.
[133] E. Darrouzet, F. Daldal, Protein-protein interactions between cytochrome *b* and the Fe-S protein subunits during QH_2 oxidation and large-scale domain movement in the bc_1 complex, Biochemistry, 42 (2003) 1499-1507.
[134] E. Darrouzet, C.C. Moser, P.L. Dutton, F. Daldal, Large scale domain movement in cytochrome bc_1: a new device for electron transfer in proteins, Trends Biochem.Sci., 26 (2001) 445-451.
[135] E. Darrouzet, M. Valkova-Valchanova, F. Daldal, Probing the role of the Fe-S rubunit hinge region during Q_o site catalysis in *Rhodobacter capsulatus* bc_1 complex, Biochemistry, 39 (2000) 15475-15483.
[136] E. Darrouzet, M. Valkova-Valchanova, C.C. Moser, P.L. Dutton, F. Daldal, Uncovering the [2Fe2S] domain movement in cytochrome bc_1 and its implications for energy conversion, Proc. Natl. Acad. Sci. U. S. A., 97 (2000) 4567-4572.
[137] A.R. Crofts, V.P. Shinkarev, S.A. Dikanov, R.I. Samoilova, D. Kolling, Interactions of quinone with the iron-sulfur protein of the bc_1 complex: is the mechanism spring-loaded?, Biochim. Biophys. Acta, 1555 (2002) 48-53.
[138] V.P. Shinkarev, D.R.J. Kolling, T.J. Miller, A.R. Crofts, Modulation of the Midpoint Potential of the [2Fe-2S] Rieske Iron Sulfur Center by Q_o Occupants in the bc_1 Complex, Biochemistry, 41 (2002) 14372-14382.
[139] D. Victoria, R. Burton, A.R. Crofts, Role of the -PEWY- glutamate in catalysis at the Q_o-site of the cyt bc_1 complex, Biochim. Biophys. Acta, 1827 (2012) 365-386.

[140] J. Zhu, T. Egawa, S.R. Yeh, L. Yu, C.-A. Yu, Simultaneous reduction of iron-sulfur protein and cytochrome b_L during ubiquinol oxidation in cytochrome bc_1 complex., Proc. Natl. Acad. Sci. U. S. A., 104 (2007) 4864-4869.
[141] F. Millett, J. Havens, S. Rajagukguk, B. Durham, Design and use of photoactive ruthenium complexes to study electron transfer within cytochrome bc1 and from cytochrome bc1 to cytochrome c, Biochimica et Biophysica Acta (BBA) - Bioenergetics, 1827 (2013) 1309-1319.
[142] E.A. Berry, L.-S. Huang, Conformationally linked interaction in the cytochrome bc_1 complex between inhibitors of the Q_o site and the Rieske iron–sulfur protein, Biochim. Biophys. Acta, 1807 (2011) 1349-1363.
[143] J.L. Cape, M.K. Bowman, D.M. Kramer, A semiquinone intermediate generated at the Q_o site of the cytochrome bc_1 complex: Importance for the Q-cycle and superoxide production, Proc. Natl. Acad. Sci. (U.S.A.), 104 (2007) 7887-7892.
[144] H. Zhang, A. Osyczka, P.L. Dutton, C.C. Moser, Exposing the complex III Q_o semiquinone radical, Biochim. Biophys. Acta, 1767 (2007) 883-887.
[145] N.B. Ugulava, A.R. Crofts, CD-monitored redox titration of the Rieske Fe-S protein of *Rhodobacter sphaeroides*: pH dependence of the mid-point potential in isolated bc_1 complex and in membranes, FEBS Lett., 440 (1998) 409-413.
[146] Y. Zu, M.M.-J. Couture, D.R.J. Kolling, A.R. Crofts, L.D. Eltis, J.A. Fee, J. Hirst, The reduction potentials of Rieske clusters: the importance of the coupling between oxidation state and histidine protonation state, Biochemistry, 42 (2003) 12400-12408.
[147] K.-L. Hsueh, W.M. Westler, J.L. Markley, NMR investigations of the Rieske protein from *Thermus thermophilus* support a coupled proton and electron transfer mechanism, J. Am. Chem. Soc., 132 (2010) 7908-7918.
[148] A.R. Crofts, E.A. Berry, R. Kuras, M. Guergova-Kuras, S. Hong, N. Ugulava, Structures of the bc_1 complex reveal dynamic aspects of mechanism, in: G. Garab (Ed.) Photosynthesis: Mechanisms and Effects, Kluwer Academic Publ., Dordrecht/Boston/London., 1998, pp. 1481-1486.
[149] J.P. Kirby, J.A. Roberts, D.G. Nocera, Significant fffect of salt bridges on electron transfer, J. Am. Chem. Soc., 119 (1997) 9230-9236.
[150] J.A. Roberts, J.P. Kirby, S.T. Wall, D.G. Nocera, Electron transfer within ruthenium(II) polypyridyl-(salt bridge)-dimethylaniline acceptor-donor complexes, Inorg. Chim. Acta, 263 (1997) 395-405.
[151] A.R. Crofts, M. Guergova-Kuras, N. Ugulava, R. Kuras, S. Hong, Proton processing at the Q_o-site of the bc_1 complex of *Rhodobacter sphaeroides*, in: Proc. XIIth Congress of Photosynthesis Research, Brisbane, Australia, 2002, pp. S
[152] R.A. Marcus, N. Sutin, Electron transfers in chemistry and biology, Biochim. Biophys. Acta, 811 (1985) 265-322
[153] D.V. Matyushov, Protein electron transfer: is biology (thermo)dynamic?, J. Phys.: Condens. Matter (2015) (24pp), 27 (2015) 473001-473025.
[154] R.C. Prince, P.L. Dutton, Further studies on the Rieske iron-sulfur center in mitochondrial and photosynthetic systems: A p*K* on the oxidized form, FEBS Lett., 65 (1976) 117-119.
[155] T.A. Link, Two pK values of the oxidised 'Rieske' [2Fe-2S] cluster observed by CD spectroscopy, Biochim. Biophys. Acta, 1185 (1994) 81-84.
[156] T.A. Link, W.R. Hagen, A.J. Pierik, C. Assmann, G. von Jagow, Determination of the redox properties of the Rieske [2Fe-2S] cluster of bovine heart bc_1 complex by direct electrochemistry of a water-soluble fragment, Eur. J. Biochem., 208 (1992) 685-691.
[157] M. Guergova-Kuras, R. Kuras, N. Ugulava, I. Hadad, A.R. Crofts, Specific mutagenesis of the Rieske iron sulfur protein in *Rhodobacter sphaeroides* shows that both thermodynamic gradient and the pK of the oxidized form determine the rate of quinol oxidation by the bc_1 complex, Biochemistry, 39 (2000) 7436-7444.
[158] G.M. Ullmann, L. Noodleman, D.A. Case, Density functional calculation of pK_a values and redox potentials in the bovine Rieske iron-sulfur protein, J. Biol. Inorg. Chem., 7 (2002) 632–639.

[159] S. Lhee, D.R. Kolling, S.K. Nair, S.A. Dikanov, A.R. Crofts, Modifications of protein environment of the [2Fe-2S] cluster of the bc_1 complex: effects on the biophysical properties of the Rieske iron-sulfur protein and on the kinetics of the complex, J. Biol. Chem., 285 (2010) 9233-9248.
[160] S.A. Dikanov, D.R.J. Kolling, B. Endeward, R.I. Samoilova, T.F. Prisner, S.K. Nair, A.R. Crofts, Identification of Hydrogen Bonds to the Rieske Cluster through the Weakly Coupled Nitrogens Detected by Electron Spin Echo Envelope Modulation Spectroscopy, J. Biol. Chem., 281 (2006) 27416-27425.
[161] D.R. Kolling, R.I. Samoilova, A.A. Shubin, A.R. Crofts, S.A. Dikanov, Proton environment of reduced Rieske iron-sulfur cluster probed by two-dimensional ESEEM spectroscopy, J. Phys. Chem. A, 113 (2009) 653-667.
[162] D.J. Kolling, J.S. Brunzelle, S. Lhee, A.R. Crofts, S.K. Nair, Atomic resolution structures of rieske iron-sulfur protein: role of hydrogen bonds in tuning the redox potential of iron-sulfur clusters, Structure, 15 (2007) 29-38.
[163] D.L. Gatti, S.W. Meinhardt, T. Ohnishi, A. Tzagoloff, Structure and function of the mitochondrial bc_1 complex. A mutational analysis of the yeast Rieske iron-sulfur protein, J. Mol. Biol., 205 (1989) 421-435.
[164] A.M. Barragan, A.R. Crofts, K. Schulten, I.A. Solov'yov, Identification of ubiquinol binding motifs at the Q_o-site of the cytochrome bc_1 complex, J. Phys. Chem. B, 119 (2015) 433-447.
[165] A.R. Crofts, S.W. Rose, R.L. Burton, A.V. Desai, P.J.A. Kenis, S.A. Dikanov, The Q-Cycle Mechanism of the bc_1 Complex: A Biologist's Perspective on Atomistic Studies, The Journal of Physical Chemistry B, 121 (2017) 3701-3717.
[166] L. Esser, B. Quinn, Y.-F. Li, M. Zhang, M. Elberry, L. Yu, C.-A. Yu, D. Xia, Crystallographic studies of quinol oxidation site inhibitors: A modified classification of Inhibitors for the cytochrome bc_1 complex, J. Mol. Biol., 341 (2004) 281-302.
[167] A.M. Barragan, K. Schulten, I.A. Solov'yov, Mechanism of the primary charge transfer reaction in the cytochrome bc_1 complex, J. Phys. Chem. B, 120 (2016) 11369-11380.
[168] A. Osyczka, H. Zhang, C. Mathé, P.R. Rich, C.C. Moser, P.L. Dutton, Role of the PEWY Glutamate in Hydroquinone-Quinone Oxidation-Reduction Catalysis in the Q_o Site of Cytochrome bc_1, Biochemistry, 45 (2006) 10492-10503.
[169] P. Brzezinski, A.-L. Johansson, Variable proton-pumping stoichiometry in structural variants of cytochrome c oxidase, Biochim. Biophys. Acta - Bioenergetics, 1797 (2010) 710-723.
[170] M. Wikström, M.I. Verkhovsky, The D-channel of cytochrome oxidase: An alternative view, Biochimica et Biophysica Acta (BBA) - Bioenergetics, 1807 (2011) 1273-1278.
[171] A. Boveris, Determination of the production of superoxide radicals and hydrogen-peroxide in mitochondria, Methods Enzymol., 105 (1984) 429-435.
[172] A. Boveris, B. Chance, The mitochondrial generation of hydrogen peroxide. General properties and effect of hyperbaric oxygen, Biochem. J., 134 (1973) 707-716.
[173] F. Muller, The nature and mechanism of superoxide production by the electron transport chain: Its relevance to aging, J. Am. Aging Assoc., 23 (2000) 227-253.
[174] F. Muller, A.R. Crofts, D.M. Kramer, Multiple Q-cycle bypass reactions at the Q_o-site of the cytochrome bc_1 complex, Biochemistry, 41 (2002) 7866-7874.
[175] A.R. Crofts, J.T. Holland, D. Victoria, D.R. Kolling, S.A. Dikanov, R. Gilbreth, S. Lhee, R. Kuras, M.G. Kuras, The Q-cycle reviewed: How well does a monomeric mechanism of the bc_1 complex account for the function of a dimeric complex?, Biochim. Biophys. Acta., 1777 (2008) 1001-1019.
[176] A.R. Crofts, S. Lhee, S.B. Crofts, J. Cheng, S. Rose, Proton pumping in the bc_1 complex: A new gating mechanism that prevents short circuits, Biochim. Biophys. Acta, 1757 (2006) 1019-1034.
[177] A. Osyczka, Moser, C.C., and Dutton, P.L., Fixing the Q-cycle, Trends Biochem. Sci., 30 (2005) 176-182.
[178] A.R. Crofts, C.A. Wilson, S.W. Rose, S.A. Dikanov, R.L. Burton, The bc_1 Complex: A Physicochemical Retrospective and an Atomistic Prospective, in: M. Wikström (Ed.) Mechanisms of Primary Energy Transduction in Biology, The Royal Society of Chemistry, Cambridge, U.K., 2017, pp. 161-191.

[179] A.R. Crofts, The bc_1 complex: what is there left to argue about?, in: M. Wikström (Ed.) Biophysical and Structural Aspects of Bioenergetics, Royal Society of Chemistry Publishing, Cambridge, 2005, pp. 123-155.
[180] A.R. Crofts, S. Hong, C. Wilson, R. Burton, D. Victoria, C. Harrison, K. Schulten, The mechanism of ubihydroquinone oxidation at the Q_o-site of the cytochrome bc_1 complex, Biochim. Biophys. Acta, 1827 (2013) 1362-1377.
[181] M. Wikström, M.I. Verkhovskya, G. Hummer, Water-gated mechanism of proton translocation by cytochrome c oxidase, Biochim. Biophys. Acta, 1604 (2003) 61- 65.
[182] S. Ransac, N. Parisey, J.-P. Mazat, The loneliness of the electrons in the bc_1 complex, Biochim. Biophys. Acta, 1777 (2008) 1053-1059.
[183] S. Ransac, J.-P. Mazat, How does antimycin inhibit the bc_1 complex? A part-time twin, Biochim. Biophys. Acta, 1797 (2010) 1849-1857.
[184] D.T. Gillespie, Exact Stochastic Simulation of Coupled Chemical Reactions, J. Phys. Chem., 81 (1977) 2340–2361.
[185] N. Kim, M.O. Ripple, R. Springett, Measurement of the mitochondrial membrane potential and pH gradient from the redox poise of the hemes of the bc_1 complex, Biophys. J., 102 (2012) 1194-1203.
[186] M. Rocha, R. Springett, Measuring the functionality of the mitochondrial pumping complexes with multi-wavelength spectroscopy, Biochimica et Biophysica Acta (BBA) - Bioenergetics, (2018).
[187] V.P. Shinkarev, C.A. Wraight, Intermonomer electron transfer in the bc_1 complex dimer is controlled by the energized state and by impaired electron transfer between low and high potential hemes, FEBS Lett., 581 (2007) 1535-1541.
[188] S. Hong, D. Victoria, A.R. Crofts, Inter-monomer electron transfer is too slow to compete with monomeric turnover in bc_1 complex Biochim. Biophys. Acta, 1817 (2012) 1053-1062.
[189] R. Covián, Trumpower, B. L., Rapid electron transfer between monomers when the cytochrome bc_1 complex dimer is reduced through center N, J. Biol. Chem., 280 (2005) 22732-22740.
[190] R. Covián, B.L. Trumpower, Regulatory interactions in the dimeric cytochrome bc1 complex: The advantages of being a twin, Biochim. Biophys. Acta, 1777 (2008) 1079-1091.
[191] A. Kröger, and Klingenberg, M., The kinetics of the redox reactions of ubiquinone related to the electron-transport activity in the respiratory chain, Eur. J. Biochem., 34 (1973) 358-368.
[192] A. Kröger, M. Klingenberg, Further Evidence for the Pool Function of Ubiquinone as Derived from the Inhibition of the Electron Transport by Antimycin, . Europ. J. Biochem., 39 (1973) 313-323.
[193] V.P. Shinkarev, A.R. Crofts, C.A. Wraight, The electric field generated by photosynthetic reaction center induces rapid reversed electron transfer in the bc(1) complex, Biochemistry, 40 (2001) 12584-12590.
[194] M. Świerczek, E. Cieluch, M. Sarewicz, A. Borek, C.C. Moser, P.L. Dutton, A. Osyczka, An electronic bus bar lies in the core of cytochrome bc_1, Science, 329 (2010) 451-454.
[195] P. Lanciano, D.-W. Lee, H. Yang, E. Darrouzet, F. Daldal, Intermonomer Electron Transfer between the Low-Potential *b* Hemes of Cytochrome bc_1, Biochemistry, 50 (2011) 1651–1663.
[196] M. Castellani, R. Covian, T. Kleinschroth, O. Anderka, B. Ludwig, B.L. Trumpower, Direct Demonstration of Half-of-the-sites Reactivity in the Dimeric Cytochrome bc_1 Complex, J. Biol. Chem., 285 (2010) 502–510.
[197] M. Czapla, A. Borek, M. Sarewicz, A. Osyczka, Enzymatic activities of isolated cytochrome bc_1-like complexes containing fused cytochrome *b* subunits with asymmetrically inactivated segments of electron transfer chains, Biochemistry, 51 (2012) 829-835.
[198] A.S. Saribas, H. Ding, P.L. Dutton, F. Daldal, Tyrosine 147 of cytochrome *b* is required for efficient electron transfer at the ubihydroquinone oxidase site (Q_o) of the cytochrome bc_1 complex, Biochemistry, 34 (1995) 16004-16012.
[199] J.L. Yuly, P. Zhang, C.E. Lubner, J.W. Peters, D.N. Beratan, Universal free-energy landscape produces efficient and reversible electron bifurcation, Proc. Natl. Acad. Sci. (U.S.), 117 (2020) 21045-21051.

[200] D. Birth, W.-C. Kao, C. Hunte, Structural analysis of atovaquone-inhibited cytochrome bc_1 complex reveals the molecular basis of antimalarial drug action, Nature Commun., 5 (2014) 4029.
[201] L. Esser, M. Elberry, F. Zhou, C.-A. Yu, L. Yu, D. Xia, Inhibitor complexed structures of the cytochrome bc_1 complex from the photosynthetic bacterium *Rhodobacter sphaeroides*, J. Biol. Chem., 283 (2008) 2846-2857.
[202] L. Esser, F. Zhou, C.-A. Yu, D. Xia, Crystal structure of bacterial cytochrome bc_1 in complex with azoxystrobin reveals a conformational switch of the Rieske iron–sulfur protein subunit, J. Biol. Chem., 294 (2019) 12007-12019.
[203] H. Palsdottir, C.G. Lojero, B.L. Trumpower, C. Hunte, Structure of the Yeast Cytochrome bc1 Complex with a Hydroxyquinone Anion Qo Site Inhibitor Bound, J. Biol. Chem., 278 (2003) 31303-31311.
[204] C. Hunte, J. Koepke, C. Lange, T. Roßmanith, H. Michel, Structure at 2.3 Å resolution of the cytochrome bc_1 complex from the yeast *Saccharomyces cerevisiae* co-crystallized with an antibody F_v fragment, Structure, 8 (2000) 669-684.
[205] S.A. Dikanov, A.R. Crofts, Electron Paramagnetic Resonance Spectroscopy (Chapter 3) in: D.R. Vij (Ed.) Handbook on Applied Solid State Spectroscopy, Springer, Berlin, 2006, pp. 97-149.
[206] R.I. Samoilova, D. Kolling, T. Uzawa, T. Iwasaki, A.R. Crofts, S.A. Dikanov, The interaction of the Rieske iron sulfur protein with occupants of the Q_o-site of the bc_1 complex, probed by 1D and 2D Electron Spin Echo Envelope Modulation, J. Biol. Chem., 277 (2002) 4605-4608.
[207] D.R.J. Kolling, R.I. Samoilova, J.T. Holland, E.A. Berry, S.A. Dikanov, A.R. Crofts, Exploration of ligands to the Q_i-site semiquinone in the bc_1 complex using high resolution EPR, J. Biol. Chem., 278 (2003) 39747–39754.
[208] S.A. Dikanov, R.I. Samoilova, D.R.J. Kolling, J.T. Holland, A.R. Crofts, Hydrogen bonds involved in binding the Q_i-site semiquinone in the bc_1 complex identified through deuterium exchange using pulsed EPR, J. Biol. Chem., 279 (2004) 15814-15823.
[209] S.A. Dikanov, J.T. Holland, B. Endeward, D.R. Kolling, R.I. Samoilova, T.F. Prisner, A.R. Crofts, Hydrogen bonds between nitrogen donors and the semiquinone in the Q_i-site of the bc_1 complex, J Biol Chem, 282 (2007) 25831-25841.
[210] S. Hong, W.B. de Almeida, A.T. Taguchi, R.I. Samoilova, R.B. Gennis, P.J. O'Malley, S.A. Dikanov, A.R. Crofts, The semiquinone at the Q_i site of the bc_1 complex explored using HYSCORE spectroscopy and specific isotopic labeling of ubiquinone in *Rhodobacter sphaeroides* via ^{13}C methionine and construction of a methionine auxotroph, Biochemistry, 53 (2014) 6022-6031.
[211] T. Iwasaki, A. Kounosu, D.R.J. Kolling, A.R. Crofts, S.A. Dikanov, A. Jin, T. Imai, A. Urushiyama, Characterization of the pH-Dependent Resonance Raman Transitions of Archaeal and Bacterial Rieske [2Fe-2S] Proteins, J. Am. Chem. Soc., 126 (2004) 4788-4789.
[212] T. Iwasaki, Kounosu, A., Kolling, D.R.J., Lhee, S., Crofts, A.R., Dikanov, S.A., Uchiyama, T., Kumasaka, T., Ishikawa, H., Kono, M, Imai, T. and Urushiyama, A. , Resonance Raman characterization of archaeal and bacterial Rieske protein variants with modified hydrogen bond network around the [2Fe-2S] center, Protein Science, 15 (2006) 2019-2024.
[213] S.A. Dikanov, R.I. Samoilova, R. Kappl, A.R. Crofts, J. Hüttermann, The reduced [2Fe-2S] clusters in adrenodoxin and *Arthrospira platensis* ferredoxin share spin density with protein nitrogens, probed using 2D ESEEM, Phys. Chem. Chem. Phys., 11 (2009) 6807-6819.
[214] R.I. Samoilova, A.R. Crofts, S.A. Dikanov, Reaction of superoxide radical with quinone molecules, J. Phys. Chem. A, 115 (2011) 11589-11593.
[215] S. Bhaduri, V. Stadnytskyi, S.D. Zakharov, S. Saif Hasan, Ł. Bujnowicz, M. Sarewicz, S. Savikhin, A. Osyczka, W.A. Cramer, Pathways of Transmembrane Electron Transfer in Cytochrome *bc* Complexes: Dielectric Heterogeneity and Interheme Coulombic Interactions, J. Phys. Chem. B, 121 (2017) 975-983.
[216] P. Kuleta, M. Sarewicz, P. Postila, T. Róg, A. Osyczka, Identifying involvement of Lys251/Asp252 pair in electron transfer and associated proton transfer at the quinone reduction site of *Rhodobacter capsulatus* cytochrome bc_1, Biochim. Biophys. Acta (Bioenergetics), 1857 (2016) 1661-1668.

[217] R. Pietras, M. Sarewicz, A. Osyczka, Distinct properties of semiquinone species detected at the ubiquinol oxidation Q_o site of cytochrome bc_1 and their mechanistic implications., J. R. Soc. Interface, 13 (2016).
[218] P.A. Postila, K. Kaszuba, P. Kuleta, I. Vattulainen, M. Sarewicz, A. Osyczka, T. Róg, Atomistic determinants of co-enzyme Q reduction at the Q_i-site of the cytochrome bc_1 complex, Scientific Reports, 6 (2016) 33607.
[219] S. Pöyry, O. Cramariuc, P.A. Postila, K. Kaszuba, M. Sarewicz, A. Osyczka, I. Vattulainen, T. Róg, Atomistic simulations indicate cardiolipin to have an integral role in the structure of the cytochrome bc_1 complex., Biochim. Biophys. Acta, 1827 (2013) 769-778.
[220] P.R. Vennam, N. Fisher, M.D. Krzyaniak, D.M. Kramer, M.K. Bowman, A caged, destabilized free radical intermediate in the Q-Cycle, Chem. Biochem., 14 (2013) 1745-1753.
[221] J. Zhu, T. Egawa, S.R. Yeh, L. Yu, C.-A. Yu, Simultaneous reduction of iron-sulfur protein and cytochrome b_L during ubiquinol oxidation in cytochrome bc_1 complex., Proc Natl Acad Sci U S A., 104 (2007) 4864-4869.
[222] Y. Lin, G.J. Gerfen, D.L. Rousseau, S.-R. Yeh, Ultrafast microfluidic mixer and freeze-quenching device, Anal. Chem., 75 (2003) 5381-5386.
[223] R.L. Burton, Q_o site of the bc_1 complex; unlocking the gate of the electron transport chain. PhD thesis, in: Biochemistry, University of Illinois at Urbana-Champaign, Urbana, Illinois, 2015.
[224] J. Feng, F. Bussiere, S. Hekimi, Mitochondrial electron transport is a key determinant of life span in *Caenorhabditis elegans*, Dev. Cell, 1 (2001) 633-644.
[225] G. Jafari, B.M. Wasko, A. Tong, N. Schurman, C. Dong, Z. Li, R. Peters, E.-B. Kayser, J.N. Pitt, P.G. Morgan, M.M. Sedensky, A.R. Crofts, M. Kaeberlein, Tether mutations that restore function and suppress pleiotropic phenotypes of the *C. elegans isp-1(qm150)* Rieske iron-sulfur protein, Proc. Natl. Acad. Sci., U.S.A., 112 (2015) E6148-E6157.
[226] G. Jafari, B.M. Wasko, M. Kaeberlein, A.R. Crofts, New functional and biophysical insights into the mitochondrial Rieske iron-sulfur protein from genetic suppressor analysis in *C. elegans*, Worm, 10.1080/21624054.2016.1174803 (2016).
[227] D. Jamieson, B. Chance, E. Cadenas, A. Boveris, The relation of free radical production to hyperoxia, Annu Rev Physiol, 48 (1986) 703-719.
[228] J.J. Gille, H. Joenje, Cell culture models for oxidative stress: superoxide and hydrogen peroxide versus normobaric hyperoxia, Mutat Res, 275 (1992) 405-414.
[229] W. Yang, S. Hekimi, A mitochondrial superoxide signal triggers increased longevity in Caenorhabditis elegans, PLoS biology, 8 (2010) e1000556.
[230] B. Chance, G.R. Williams, The respiratory chain and oxidative phosphorylation, Adv. Enzymol., 17 (1956) 65-134.
[231] K.R. Pryde, J. Hirst, Superoxide Is Produced by the Reduced Flavin in Mitochondrial Complex I, Journal of Biological Chemistry, 286 (2011) 18056-18065.
[232] M.M. Elguindy, E. Nakamaru-Ogiso, Apoptosis-inducing factor (AIF) and its family member protein, AMID, are rotenone-sensitive NADH:ubiquinone oxidoreductases (NDH-2), J. Biol. Chem., 290 (2015) 20815-20826.
[233] M.D. Miramar, P. Costantini, L. Ravagnan, L.M. Saraiva, D. Haouzi, G. Brothers, J.M. Penninger, M.L. Peleato, G. Kroemer, S.A. Susinc, NADH Oxidase Activity of Mitochondrial Apoptosis-inducing Factor, J. Biol. Chem., 276 (2001) 16391-16398.
[234] X. Wang, J. Wang, K. Gengyo-Ando, L. Gu, C.-L. Sun, C. Yang, Y. Shi, T. Kobayashi, Y. Shi, S. Mitani, X.-S. Xie, D. Xue, C. elegans mitochondrial factor WAH-1 promotes phosphatidylserine externalization in apoptotic cells through phospholipid scramblase SCRM-1, Nat Cell Biol, 9 (2007) 541-549.
[235] A. DeCorby, D. Gášková, L.C. Sayles, B.D. Lemire, Expression of Ndi1p, an alternative NADH:ubiquinone oxidoreductase, increases mitochondrial membrane potential in a *C. elegans* model of mitochondrial disease, Biochim. Biophys. Acta, 1767 (2007) 1157-1163.

[236] D.R. Martin, D.N. LeBard, D.V. Matyushov, Coulomb soup of bioenergetics: Electron transfer in a bacterial bc_1 complex, J. Phys. Chem. Lett. , 4 (2013) 3602−3606.
[237] L. Esser, M. Elberry, F. Zhou, C.A. Yu, L. Yu, D. Xia, Crystal structure of *Rhodobacter sphaeroides* double mutant with stigmatellin and UQ2, J Biol Chem 283 (2008) 2846-2857.
[238] D. Xia, L. Esser, W.-K. Tang, F. Zhou, Y. Zhou, L. Yu, C.-A. Yu, B. Meunier, Structural analysis of cytochrome bc_1 complexes: Implications to the mechanism of function, Biochim. Biophys. Acta, 1827 (2013) 1278-1294.
[239] C. Hunte, H. Palsdottir, B.L. Trumpower, Protonmotive pathways and mechanisms in the cytochrome bc_1 complex, FEBS Lett., 545 (2003) 39-46.
[240] S.R.N. Solmaz, C. Hunte, Structure of complex III with bound cytochrome *c* in reduced state and definition of a minimal core interface for electron transfer, J. Biol. Chem., 283 (2008) 17542-17549.
[241] W. Junge, W. Ausländer, A. Mcgeer, T. Runge, The buffering capacity of the internal phase of thylakoids and the magnitude of the pH changes inside under flashing light, Biochim. Biophys. Acta, 546 (1979) 121-141.
[242] A.Y. Mulkidjanian, W. Junge, Calibration and time resolution of luminal pH-transients in chromatophores of *Rhodobacter capsulatus* following a single turnover flash of light: Proton release by the cytochrome bc_1-complex is strongly electrogenic, FEBS Letters, 353 (1994) 189-193.
[243] C.A. Wilson, A.R. Crofts, Dissecting the pattern of proton release from partial process involved in ubihydroquinone oxidation in the Q-cycle, Biochimica et Biophysica Acta (BBA) - Bioenergetics, 1859 (2018) 531-543.
[244] C.A. Wilson, Identifying the mechanism of second proton release from the bc_1 complex Q_o-site, in: Center for Biophysics and Quantitative Biology, University of Illinois at Urbana-Champaign, Urbana, Illinois, 2017.
[245] Y. Xu, M. Havenith, Perspective: Watching low-frequency vibrations of water in biomolecular recognition by THz spectroscopy, J. Chem. Phys., 143 (2015) 170901-170907.
[246] P.R. Rich, D.S. Bendall, The kinetics and thermodynamics of the reduction of cytochrome c by substituted *p*-benzoquinols in solution, Biochim. Biophys. Acta, 592 (1980) 506-518.
[247] M. Sarewicz, Ł. Bujnowicz, S. Bhaduri, S.K. Singh, W.A. Cramer, A. Osyczka, Metastable radical state, nonreactive with oxygen, is inherent to catalysis by respiratory and photosynthetic cytochromes bc1/b6f, Proc. Natl. Acad. Sci. (U. S. A), 114 (2017) 1323-1328.
[248] M. Sarewicz, M. Dutka, S. Pintscher, A. Osyczka, Triplet State of the Semiquinone–Rieske Cluster as an Intermediate of Electronic Bifurcation Catalyzed by Cytochrome bc1, Biochemistry, 52 (2013) 6388-6395.
[249] Y. Akiyama, M. Shinose, H. Watanabe, S. Yamada, Y. Kanda, Cryoprotectant-free cryopreservation of mammalian cells by superflash freezing, Proceedings of the National Academy of Sciences of the United States of America, 116 (2019) 7738-7743.
[250] B.L. Trumpower, J.C. Haggerty, Inhibition of electron transfer in the cytochrome b-c, segment of the mitochondrial respiratory chain by a synthetic analogue of ubiquinone, J Bioenerg Biomembr, 12 (1980) 151-164.

Table 1. Rates of electron transfer in the *b*-heme chain in mutants interfering with H^+ exit. Reduction of heme b_H was measured on the first flash, that of heme b_L on the second flash.

Residue Asn-279	heme b_H red ($e/bc_1/s^{-1}$)	% of wildtype	heme b_L red ($e/bc_1/s^{-1}$)	% of heme b_H rate
Wildtype	500	100	334	67
N279D	179	35.8	83	46.4
N279I	200	40	32	16
N279F	112	22.4	31	27.7

Table 2. Estimated values for the work terms associated with interaction of ISP with the Q_o-site for changes between different states of occupancy or on mutation.

Configuration	$E_{m,7}^{intr}$ mV (a)	$E_{m,7}^{app}$ *mV (b)*	$\Delta E_{m,7}^{app}$ *mV (c)*	ΔG_{total}^{occp} kJ/mol (d)	ΔG_{spring} kJ/mol (e)	$\Delta G_{K_E}^{app}$ kJ/mol (c)
in situ, wildtype myxothiazol	310	280	0	0 + 0	0	0
Q.ISPH		310	30	-17 + (-3)	-17	-3
stigmatellin.ISPH		540	260	-17 + (-25)	-17	-25
UHDBT.ISPH		350	90	-17 +(-8.7)	-17	-8.7
ES-complex (f) $QH_2.ISP_{ox}$	not applicable			-17 + (-5.8)	-17	-5.8
hinge mutants A46T		386	106	-17	-6.75	-10.25
2A		410	130	-17	-4.6	-12.6
3A		460	180	-17	0	-17
interface mutant (g) *isp*-P→S		280	0	-17 + 8	-17	8

Notes:

The exercise here is necessarily over simplified but will give a flavor of the forces at work. The principle is to assume that extension of the tether region from the relaxed helix of the "spring" costs the same work in all structures in which the head group H-bonds to an occupant, and that H-bond has a value in the same range so that, in the net, forces cancel. Then we add or subtract from these values by additional work terms to account for specific instances.

(a) The $E_{m,7}$ value of the Fe_2S_2 cluster in the proteolyzed extrinsic domain of wildtype, taken as an intrinsic property in the absence of protein contacts.

(b) The apparent $E_{m,7}$ measured *in situ*, $E_{m,7}^{app}$. The $E_{m,7}$ in the presence of myxothiazol is taken as the reference for $\Delta E_{m,7}^{app}$ in calculating affinity values. The difference from the intrinsic value (a) is attributable to the location for ISP in the complex, and a constrained local environment that differs from the free aqueous environment for measurement in the soluble extrinsic domain.

(c) Values calculated from $\Delta G_{K_E}^{app} = -zF\Delta E_{m,7}^{app}$, using data from the literature, as follows: UHDBT [58], stigmatellin [69], myxothiazol [132, 137], Q.ISPH [82, 137], $QH_2.ISP_{ox}$ [82]. The value comes from subtraction of column (e) from column (d).

(d) ΔG_{total}^{occp} is contributed by the sum of Δ_{H-bond}^{occp} and ΔG_{extra}^{occp}. The first term is the part of the binding of the occupant attributable to the H-bond, and the second term is attributable to additional terms. The sum acts against the "spring" and subtraction of the spring force leaves $\Delta G_E^{app} = -RTlnK_E^{app}$. The division between contributions from each term is somewhat arbitrary but reflects an assumption that the H-bond to H161 N_ε has the same strength in all complexes. Likely in the stigmatellin complex, the H-bond to E272 accounts for much of the additional ΔG_{extra}^{occp}= -25 kJ.ml^{-1} value contributing to K_E^{app}. With Q as occupant, we assume that extra forces have negative ΔG (are favorable), except in mutants in which no g_x=1.80 line (from Q.ISPH) is seen. Then the contribution to binding is a positive ΔG, but the value shown is somewhat arbitrary. Mutations in the docking surface of ISP will hinder binding, and lessen the total, and are included as a positive contribution to ΔG_{extra}^{occp}.

(e) $\Delta G_{H-bond}^{hinge}$ and ΔG_{extns}^{hinge} are terms associated with ΔG_{spring}. With no extension force applied (represented by the configuration with myxothiazol or azoxystrobin occupying the site), the "spring" would be fully relaxed; the work done against the spring, assumed here to be the same (-17 kJ/mol) for all configurations. Any extra work would then represent a complex with ISP formed at the Q_o-site. In the linker mutants, ΔG_{spring} is lessened by a positive ΔG_{extns}^{hinge}. The minimal binding energy can then be equated with the value for $\Delta G_{K_E}^{app}$ when binding can occur without any extension. Here we assume that when no extension is required (3 alanines introduce a slack of ~10 Å), $\Delta G_{K_E}^{app} = \Delta G_{spring} =$ -17 kJ/mol. For all configurations in which the linker is fully extended, this work term is balanced by the binding free-energy, with the difference given by $\Delta G_{K_A}^{app}$ (see notes (b, c)).

(f) $\Delta G_{K_A}^{app}$ is estimated from the either the change in E_m of Q/QH_2 from that in the pool ($\Delta E_{m,7}$ = 30 mV, $\Delta G_{K_A}^{app} = -zF\Delta E_m = -5.8$ kJ/mol) or from the change in pK^{app} of ISP_{ox} (ΔpK ~1, $\Delta G_{K_A}^{app} = -2.303RT\Delta pK = -5.8$ kJ/mol). See for further discussion [82].

(g) Allocation of the change in binding to the spring or binding free energies is somewhat arbitrary.

Figures

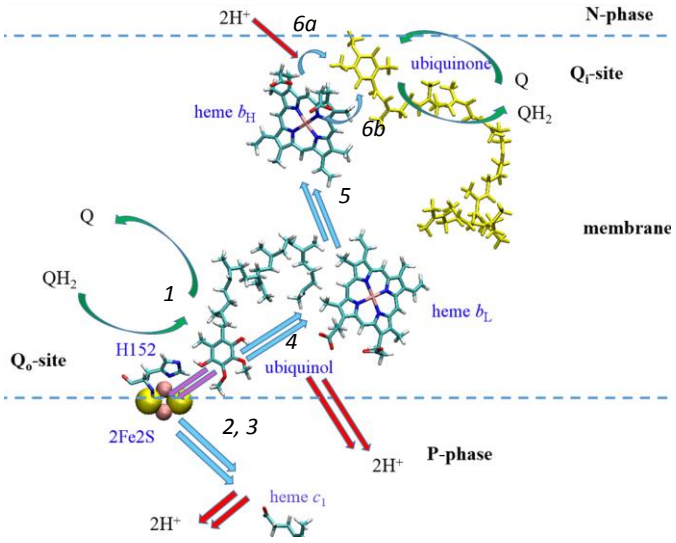

Formation of ES_1-complex

(1) $Eb_Hb_L \ldots ISP_{ox} + QH_2 \rightleftharpoons Eb_Hb_L.QH_2.ISP_{ox}$

1st e⁻ transfer (to high potential chain)

(2a) $Eb_Hb_L.QH_2.ISP_{ox} \rightleftharpoons ISPH^{\bullet}.QH^{\bullet}.Eb_Hb_L$

(2b) $ISPH^{\bullet}.QH^{\bullet}.Eb_Hb_L \rightleftharpoons ISPH^{\bullet}(mobile) + Eb_Hb_L.QH^{\bullet}$

(3) $ISPH^{\bullet}.heme\ c_1^+ \rightleftharpoons ISP_{ox}.c_1 + H_P^+$

2nd e⁻ transfer (to low potential chain)

(4) $Eb_Hb_L.QH \rightleftharpoons Eb_Hb_L^- + Q + H_P^+$

(5) $Eb_Hb_L^- \rightleftharpoons Eb_H^-b_L$

Q_i-site reaction

(6a) $Eb_H^-b_L + Q + H_N^+ \rightleftharpoons Eb_Hb_LQ^{\bullet-}(H^+)$ or

(6b) $Eb_H^-b_L.Q^{\bullet-}(H^+) + H_N^+ \rightleftharpoons Eb_Hb_L + QH_2$

Fig. 1 The modified Q-cycle. The structure of prosthetic groups involved is taken from a molecular dynamics (MD) simulation of the *Rb. sphaeroides* bc_1 complex, in which ubiquinone has been modeled at the Q_o-site (as QH_2) and at the Q_i-site (as Q). The ISP is modeled as in the oxidized state, with the N_ε of His-152 dissociated. This modeling leads to formation of an *ES*-complex as discussed in the text.

Numbered reactions in the scheme (left) correspond to reaction numbers (right). Each of these main processes may involve several partial reactions, as represented in the kinetic model. N and P subscripts refer to aqueous phases of negative and positive proton potential (N-phase and P-phase in scheme).

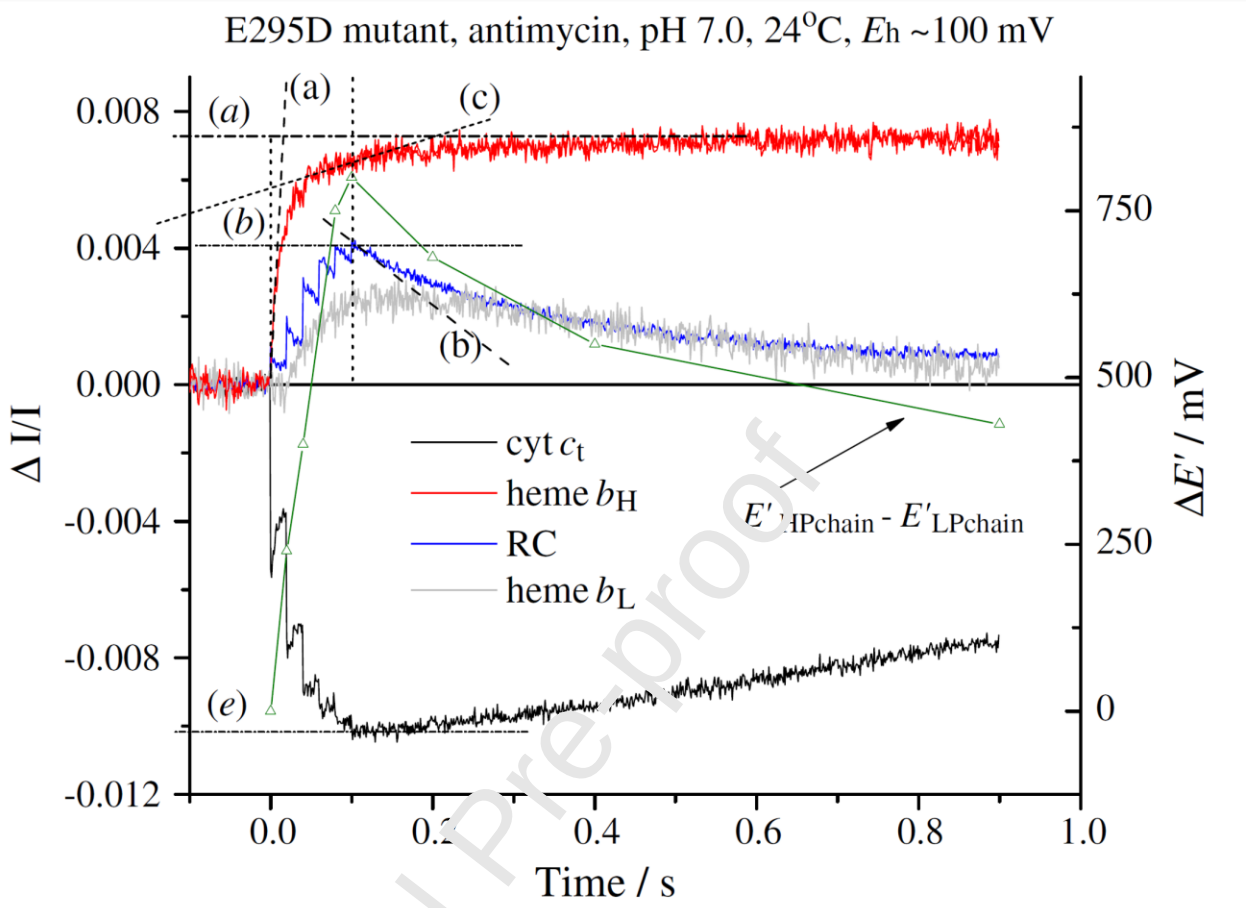

Fig. 2. Kinetic traces to illustrate protocols used to assay different partial processes. Chromatophores from E295D mutant were suspended in a medium containing 100 mM KCl, 50 mM MOPS buffer at pH 7.0, with mediators to catalyze equilibration of redox centers with the ambient redox potential, Eh, poised at 100 mV. Under these conditions, the ubiquinone pool was ~30% reduced, and the *ES*-complex close to saturated. The *b*-hemes of the bc_1 complex, and the quinone acceptors of the reaction center (RC) were oxidized, and the high potential chain, and the RC donor, were reduced. The reaction mixture in an anaerobic cuvette was stirred, except during data acquisition. Turnover was initiated by a group of six saturating flashes (~5 μs at half-height), spaced 20 ms apart. Each flash activated >90% of open RCs to generate the substrates of the bc_1 complex. The traces show the kinetics in the presence of antimycin. Traces are colored as follows: red, heme b_H reduction (ΔA561–569); black, heme c_1+c_2 (cyt c_t) (ΔA551–542); blue, RC P^+ (ΔA542); gray, heme b_L (ΔA566–575–0.5(ΔA561–569) with small additional corrections for P^+ and cyt c_t depending on relative stoichiometry). The rates of different partial processes were determined from the slopes and amplitudes *(italics)* labeled as follows: (a) initial rate of reduction of heme b_H. In the presence of antimycin, with allowance for small lags (not apparent on this time scale) this assays the rate of QH_2 oxidation through the bifurcated reaction. *(a)* Maximal amplitude of heme b_H absorbance change in the presence of antimycin (1 heme/bc_1 monomer), allowing normalization of rate. (b) Rate of reduction of P^+, the oxidized RC donor, immediately after the 6th flash, which assays the pseudo-steady state flux from processes leading to relaxation of the system. *(b)* Maximal amplitude of P^+ absorbance change to assay total RC, allowing normalization of rate. (c) Rate of the heme b_H reduction through the bifurcated reaction immediately after the 6th flash (to allow correction of bypass rates). This assays the rate in bc_1 complexes in which reduction of heme b_H is incomplete. Subtraction of this rate

from that measured in (b) allows assay of bypass reactions. Rate of reduction of heme b_L, and maximal amplitude of heme b_L absorbance change can be similarly measured. At the E_h and pH of this experiment, reduction of heme b_L occurred on the second flash because heme b_H was substantially reduced after the first flash (e) Rate of reduction of cyt c_t immediately after the 6th flash. This flux must be added to that determined in (b) to obtain the total flux through the high potential chain. *(e)* Maximal amplitude of cyt c_t absorbance change to allow normalization.

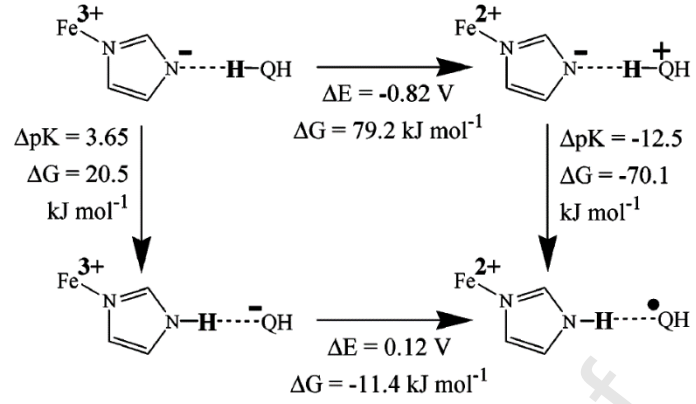

Fig. 3. Thermodynamic square for coupled proton and electron transfer between the Rieske cluster and bound QH_2. The histidine (His-152 in *Rb. sphaeroides*) is one of the ligands to Fe2 of the Fe_2S_2 cluster of ISP. The reaction begins with the top, left species upon binding of the deprotonated Rieske protein and finishes with the bottom, right species, and the dissociation of the protonated and reduced Rieske protein (taken from [84, 146]).

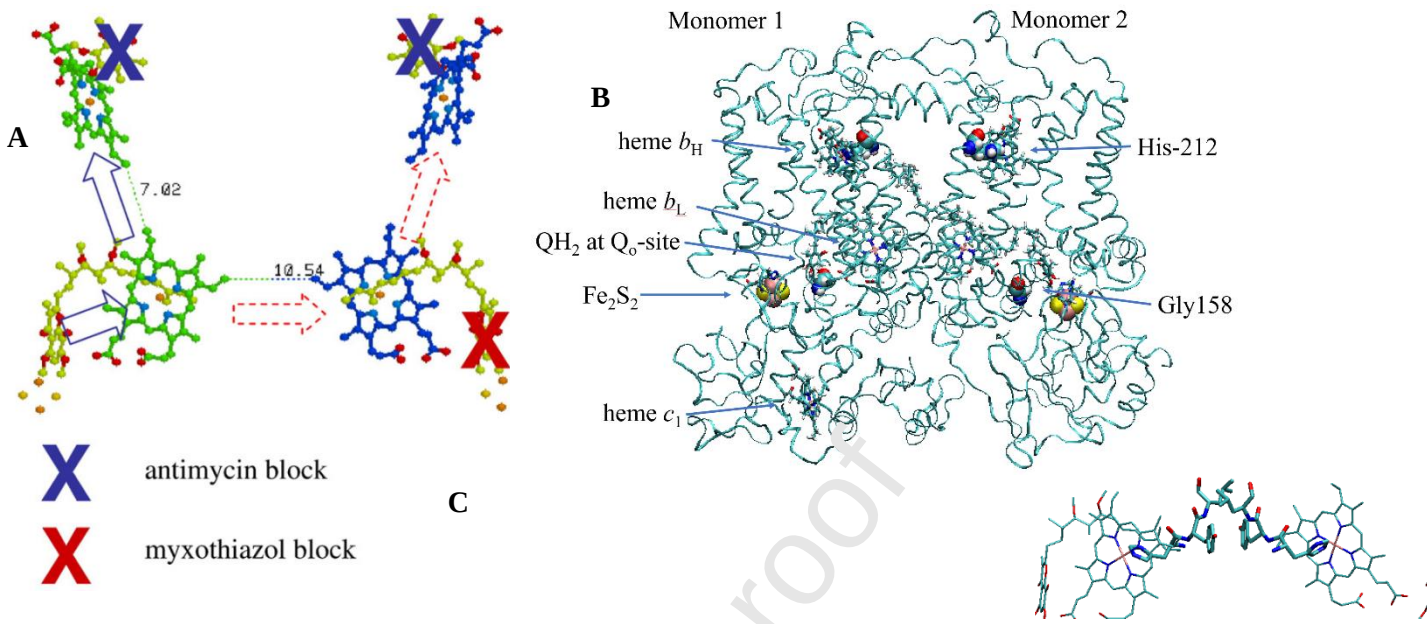

Fig. 4. Scheme to show potential electron transfer pathways involved in electron equilibration between monomers at the level of heme b_L. A. The redox centers of the dimer are shown, and the Q_o-sites are occupied by stigmatellin (to represent QH_2), and the Q_i-sites by antimycin. The scheme shows the dimer with the Qi-site blocked in both monomers by antimycin (blue crosses), and the Q_o-site of one monomer blocked by myxothiazol (red cross). Under these conditions, if electron transfer between the two hemes b_L could occur, both hemes b_H could be reduced by turnover of the uninhibited Q_o-site (broken red arrows). **B.** A slice through the *Rb. sphaeroides* bc_1 complex in the plane of the b-hemes, with location of residues mutated to test inter monomer electron transfer. On mutation of Gly-158 to tryptophan (W), the bulk of the ring occupies the volume occupied by the ubiquinone ring and blocks access to the Q_o-site; mutation of His-212 to asparagine (N) removes a ligand for heme b_H. **C.** View of the dimer interface in a similar orientation to **A**, showing the shortest through bond path across the dimer interface. The path starts with His-198, the ligand to the Fe of the heme, then Tyr-199, the residue mutated, then a jump through space to the Tyr-199 and His-198 from the other monomer, and so to the other heme b_L. Also shown are Leu-200 from each monomer, the two hemes b_L, and stigmatellin in the monomer on the left to show the position in which the *ES*-complex forms (stereo pair for crossed-eye viewing).

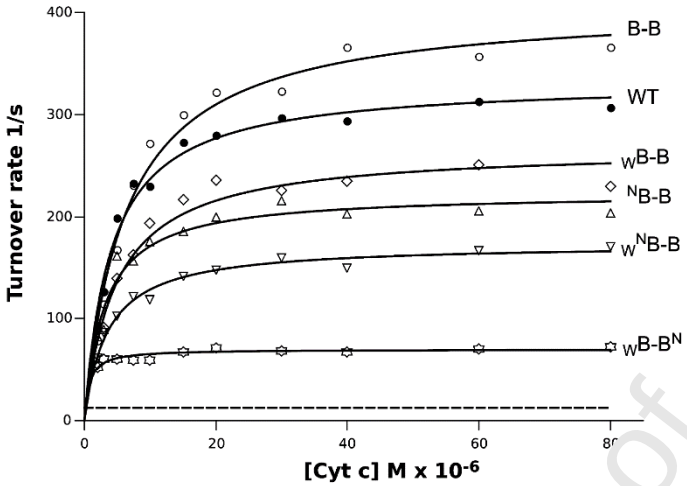

Fig. 5 Comparison of enzymatic activities of cytochrome bc_1 in various B−B complexes (from [197]). Plots show dependence of the turnover rate measured in a DBH_2: cyt *c* reductase assay vs concentration of cytochrome *c* (Cyt c). The nomenclature of the different complexes is explained in the text.

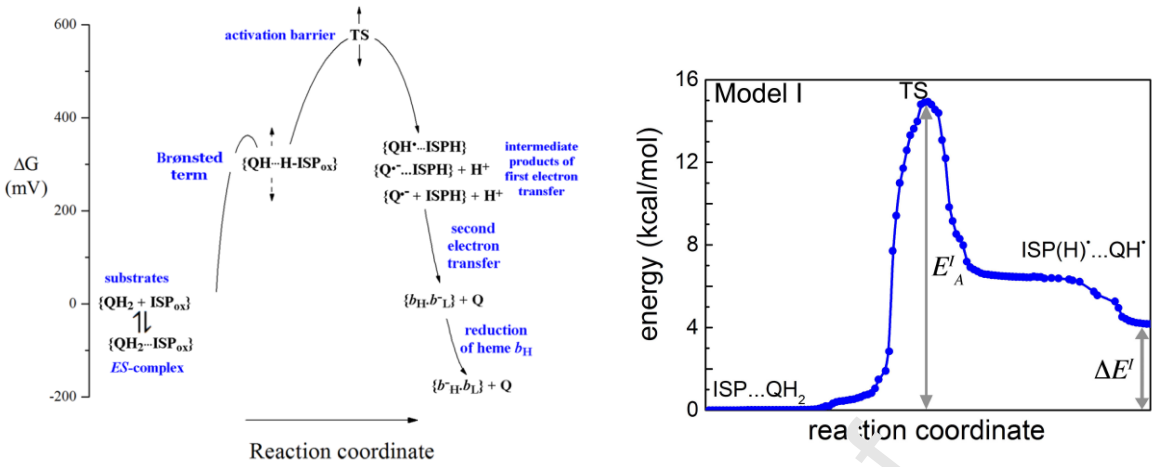

Fig. 6. Left. Energy profile of the Q_o-site reaction. Values for ΔG are calculated from experimental data. The vertical dotted arrows show limits on estimated values (from [165]). **Right. Energy profile from QM calculation.** The model [167] was set up with the *ES*-complex (ISP...QH_2) as starting state in which QH_2 is H^+ donor to H152 N_ε in the H-bond, so that the reaction follows the path expected from the Marcus-Brønsted approach. The calculated profile (right) shows the main features gleaned from experiment (left, the state after the first electron transfer).

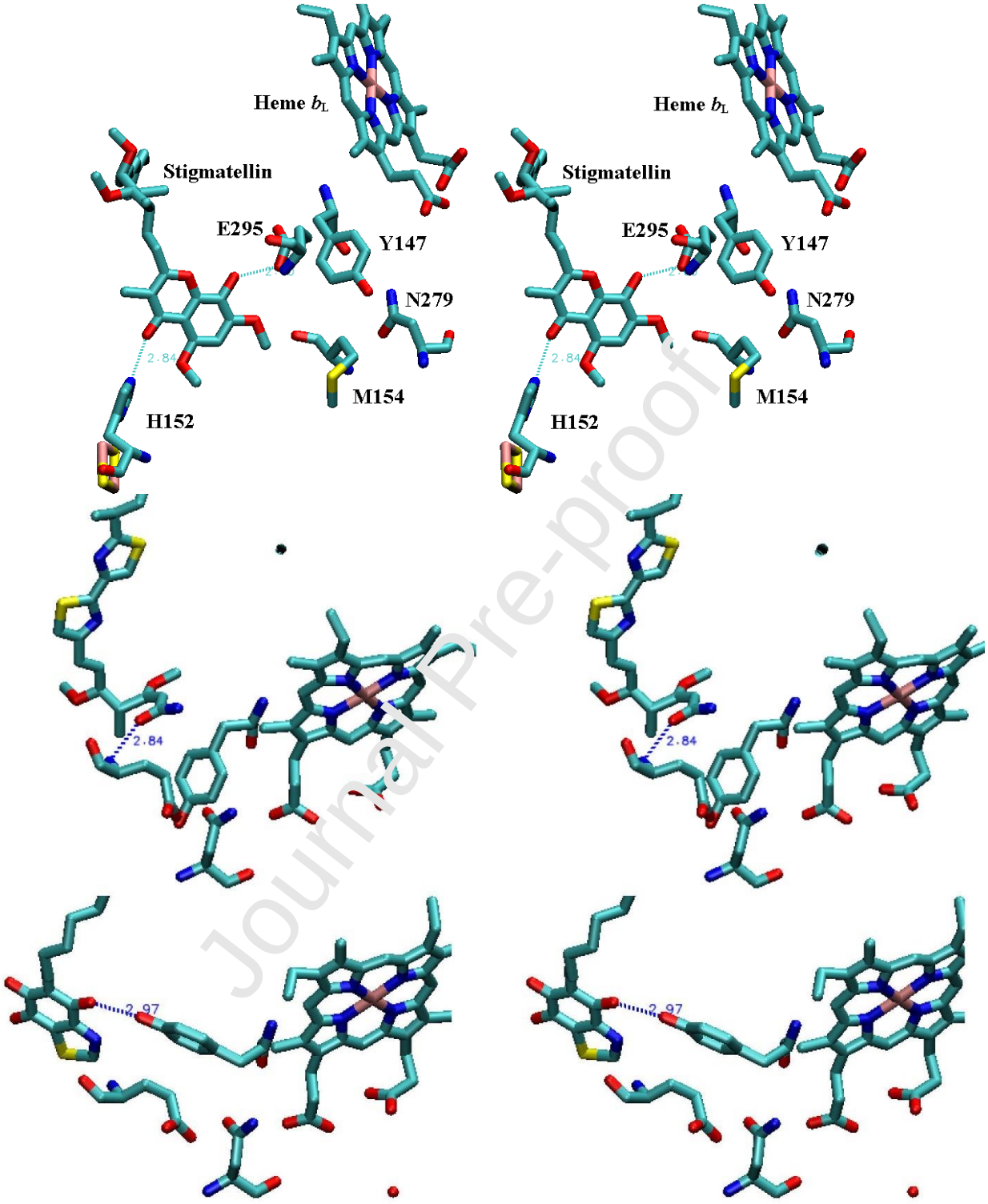

Fig. 7. Comparison of the binding of stigmatellin (top), myxothiazol (middle) and UHDBT (bottom). Top. *Rb. sphaeroides* (2QJY): Structure around stigmatellin annotated to show layout of the residues involved and numbering. **Middle and bottom**. **Bovine structures (1SQP) (1SQV).** Binding of myxothiazol (view is tilted to get a better view) and of UHDBT (tilted similarly). The dimeric structure would show the ligand to the ISP histidine but is not available in the data bank. UHDBT, (pK_a 6.5) [250], is normally ionized. (Note that perspective in the stigmatellin structure is rotated compared to that of the myxothiazol and UHDBT structures. The binding of stigmatellin in the *Rb. sphaeroides* complex (Fig. 8, top) provides a more comparable perspective.)

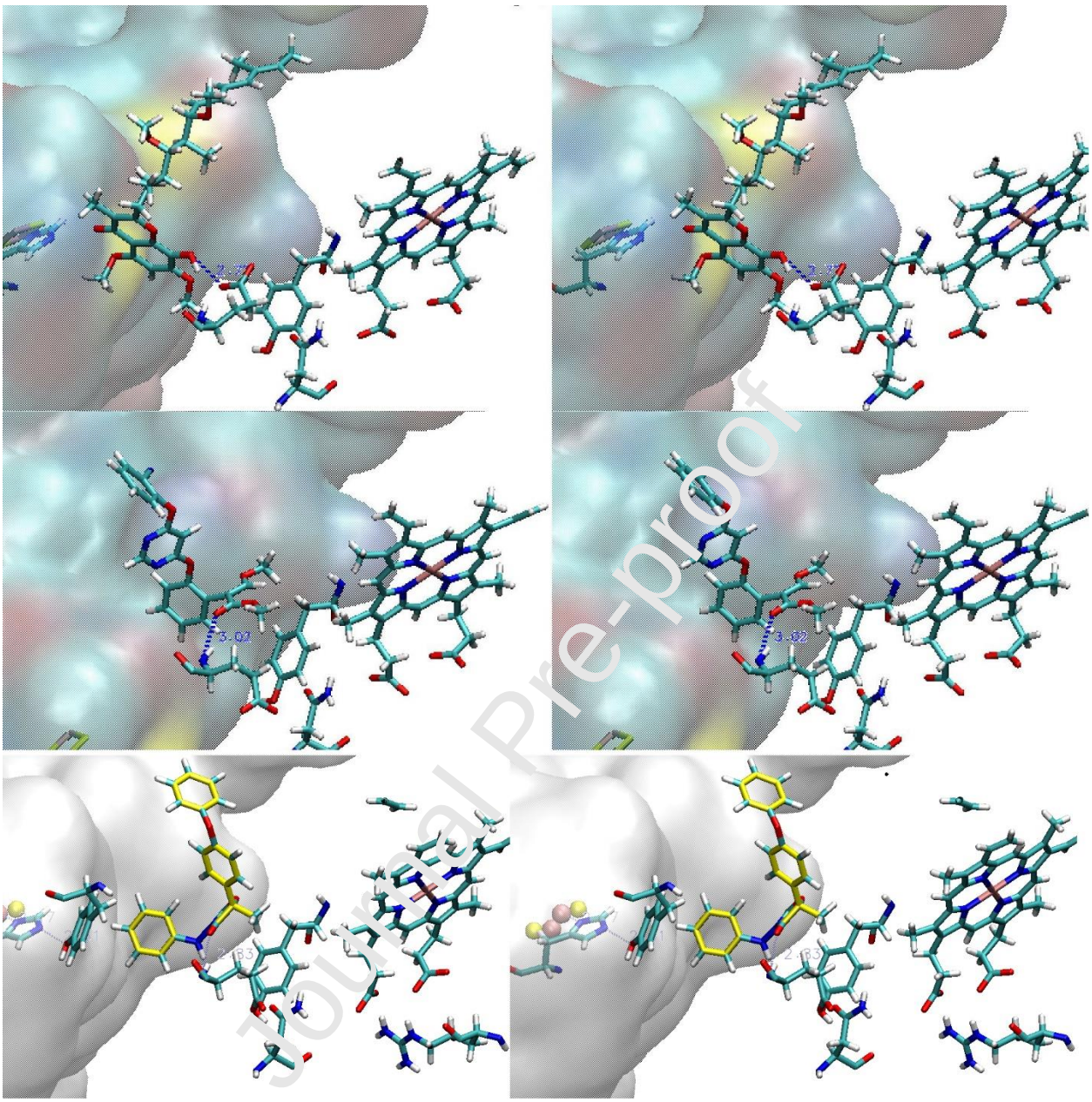

Fig. 8 Structures of the *Rb. sphaeroides* bc_1 complex showing the relation to ISP and the Fe_2S_2 cluster with different inhibitors. Top, with stigmatellin. The transparent surface shown to the left is the ISP, with His-152 of ISP, a ligand to Fe2 of the cluster (hidden behind the histidine), H-bonded to the carbonyl O of stigmatellin. Glu-295 forms another H-bond to the -OH across the chromone ring from the =O. **Middle, with azoxystrobin.** In the azoxystrobin structure, the ISP is rotated do the relaxed position, and the cluster binding domain is no longer involved in liganding. Glu-295 is rotated away from the inhibitor, allowing the backbone -NH to form a H-bond with the carbonyl O of the methoxy-acrylate group of the inhibitor. All inhibitors occupying the domain close to heme b_L (the proximal domain) make a similar H-bond [126-128]. (Stereo pairs for crossed-eye viewing.). **Bottom, with famoxadone.** Here,

the ISP is close to the position with stigmatellin, but the H-bond to His-152 comes from the "trap-door" tyrosine, Tyr-302 in *Rb. sphaeroides*. The famoxadone (with C-atoms in yellow) is liganded by a H-bond to the backbone >NH of Glu-295 (as in the azoxystrobin structure), but the ring structure of famoxadone occupies a different volume so the local structure has to accommodate, which then positions Tyr-302 in a position to H-bond to ISP His-152, which holds the ISP at the cyt *b* interface.

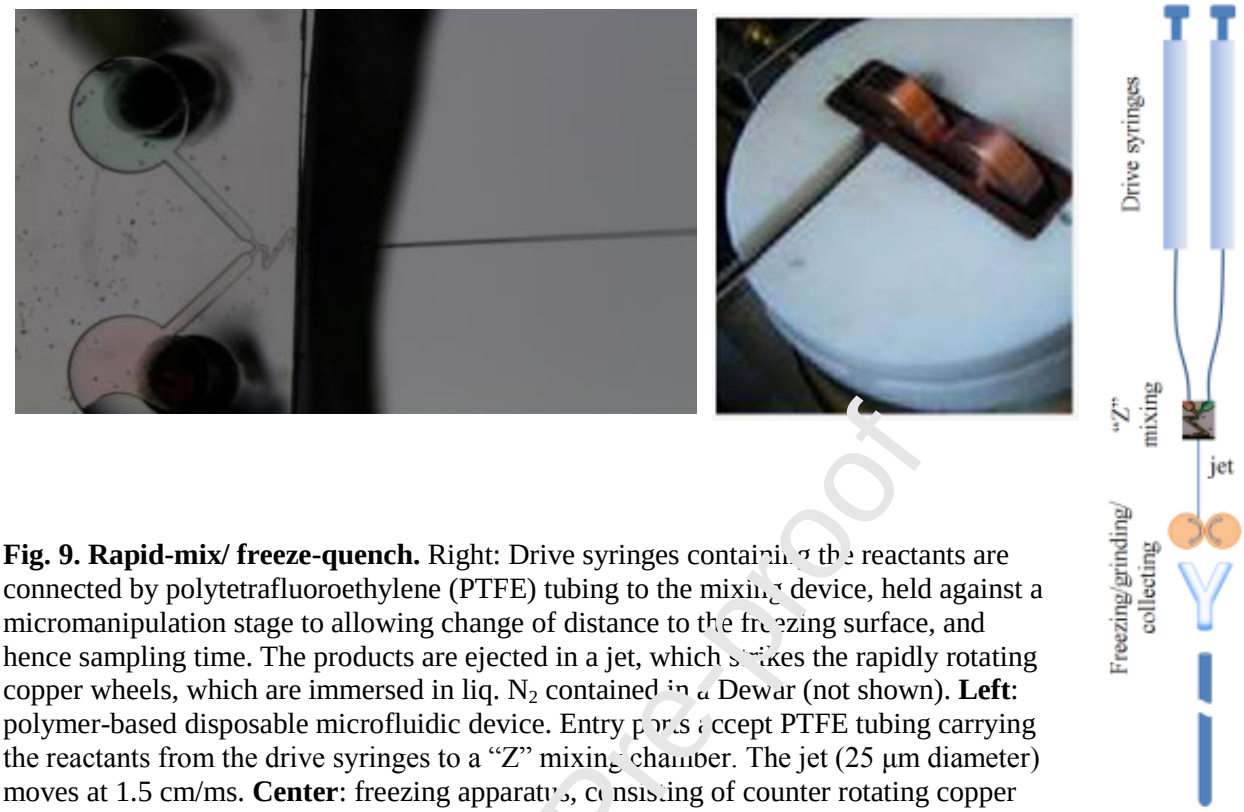

Fig. 9. Rapid-mix/ freeze-quench. Right: Drive syringes containing the reactants are connected by polytetrafluoroethylene (PTFE) tubing to the mixing device, held against a micromanipulation stage to allowing change of distance to the freezing surface, and hence sampling time. The products are ejected in a jet, which strikes the rapidly rotating copper wheels, which are immersed in liq. N_2 contained in a Dewar (not shown). **Left**: polymer-based disposable microfluidic device. Entry ports accept PTFE tubing carrying the reactants from the drive syringes to a "Z" mixing chamber. The jet (25 μm diameter) moves at 1.5 cm/ms. **Center**: freezing apparatus, consisting of counter rotating copper wheels, driven by geared coupling, mounted in a Teflon housing that sits at the top of the Dewar. The geared coupling improves efficiency of pulverization to generate a powder, collected in a funnel (in cross-section here) for packing into the EPR tube. Freezing time is ~ 10 μs. **Right**: schematic of the complete apparatus.

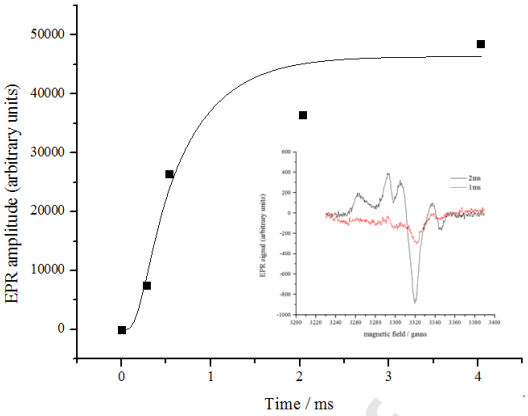

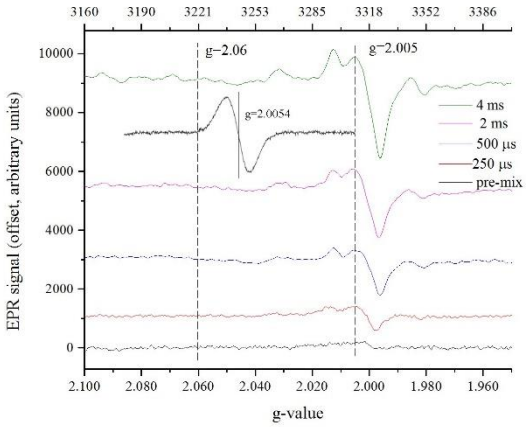

Fig. 10. Kinetics of SQ_o formation. **Left**: CW-EPR spectra of the ISPH•.QH• complex obtained from (bottom) the pre-mix sample (bc_1 complex in the presence of antimycin, poised by excess QH_2 so that heme b_H was fully reduced but heme b_L oxidized), and samples at the times shown after mixing with excess oxidized cyt *c*. The insert shows the spectrum of the SQ species reported in earlier studies [143, 144] at a similar amplitude scale, but offset on the g-scale. **Right**: the kinetic data taken from the traces on the left fit by a kinetic curve derived from the model of Victoria et al. [139]. The insert shows spectra at two different times after mixing from a separate experiment in which heme b_H was initially oxidized. The spectrum at 1 ms shows little ISPH•.QH• signal, that at 2 ms a much larger signal, interpreted as showing that the complex forms only after heme b_L is reduced (see text).

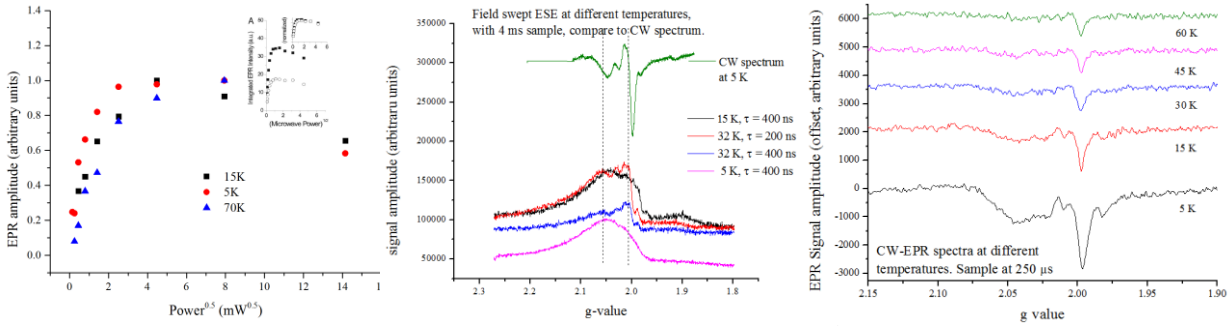

Fig. 11A. Power saturation temperature dependence. Left: Signal amplitude was determined as a function of microwave power at three temperatures. Saturation onset occurred at lower power at 5 K than at 15 K, both peaking at $\sqrt{P}$ ~4, and peaked at higher power at 70 K ($\sqrt{P}$ ≥8). However, saturation at all temperatures was much less marked than that observed in previous work on the conventional SQ_o signal. The insert shows for comparison the saturation characteristics of the SQ_o species detected in earlier experiments (peaking at $\sqrt{P}$ ~1) [143]. **Center**: Field-sweep ESE spectra at different temperatures and times (τ) after the pulse, compared to the CW spectrum of the 4 ms sample at 5 K (top trace). **Right**: Temperature dependence of CW spectrum at 250 μs.

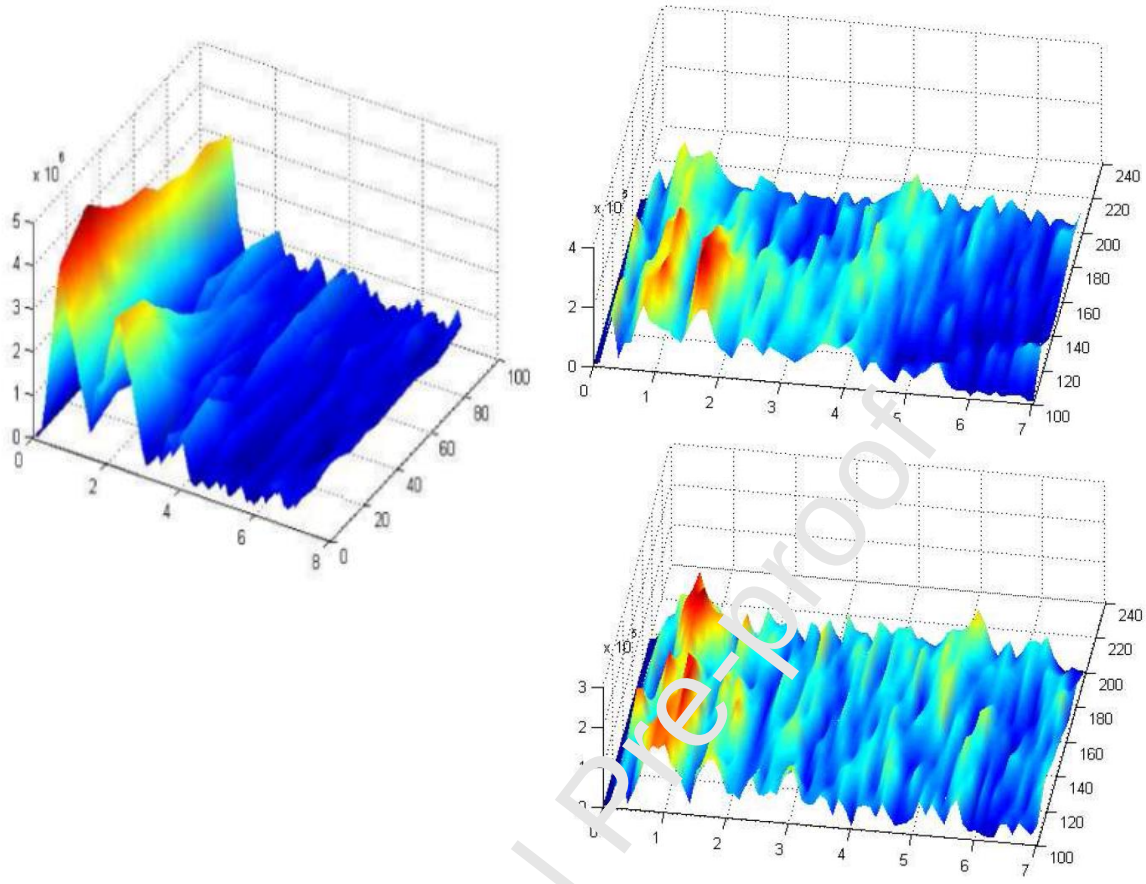

Fig. 11B. 3-pulse ESEEM spectra to identify interactions with nuclear spins in the immediate environment. Left: Stacked plot showing two distinct peaks for ^{14}N, at ~1.6 and 0.7-0.9 MHz, in spectra taken at g=2.005, seen in the sample collected 2 ms after mixing (see Fig. 10, right). In the region ~15 MHz (not shown), at least one ^{1}H interaction was also seen. Right: Results at lower bc_1 complex concentration revealed similar spectra from a sample at 4 ms after mixing taken at g=2.005 (near the peak of the CW-spectrum (top), and at g=2.06 (in the region where the ISPH$^{\bullet}$ has a significant band in the conventional (uncomplexed) spectrum) (bottom) (unpublished data, Burton, R. L., Desai, A. V., Kenis, P. J., Crofts, A. R., Dikanov, S. A.). (For the position of these g-values in the CW spectrum, see dashed vertical lines in Fig. 10, left.)

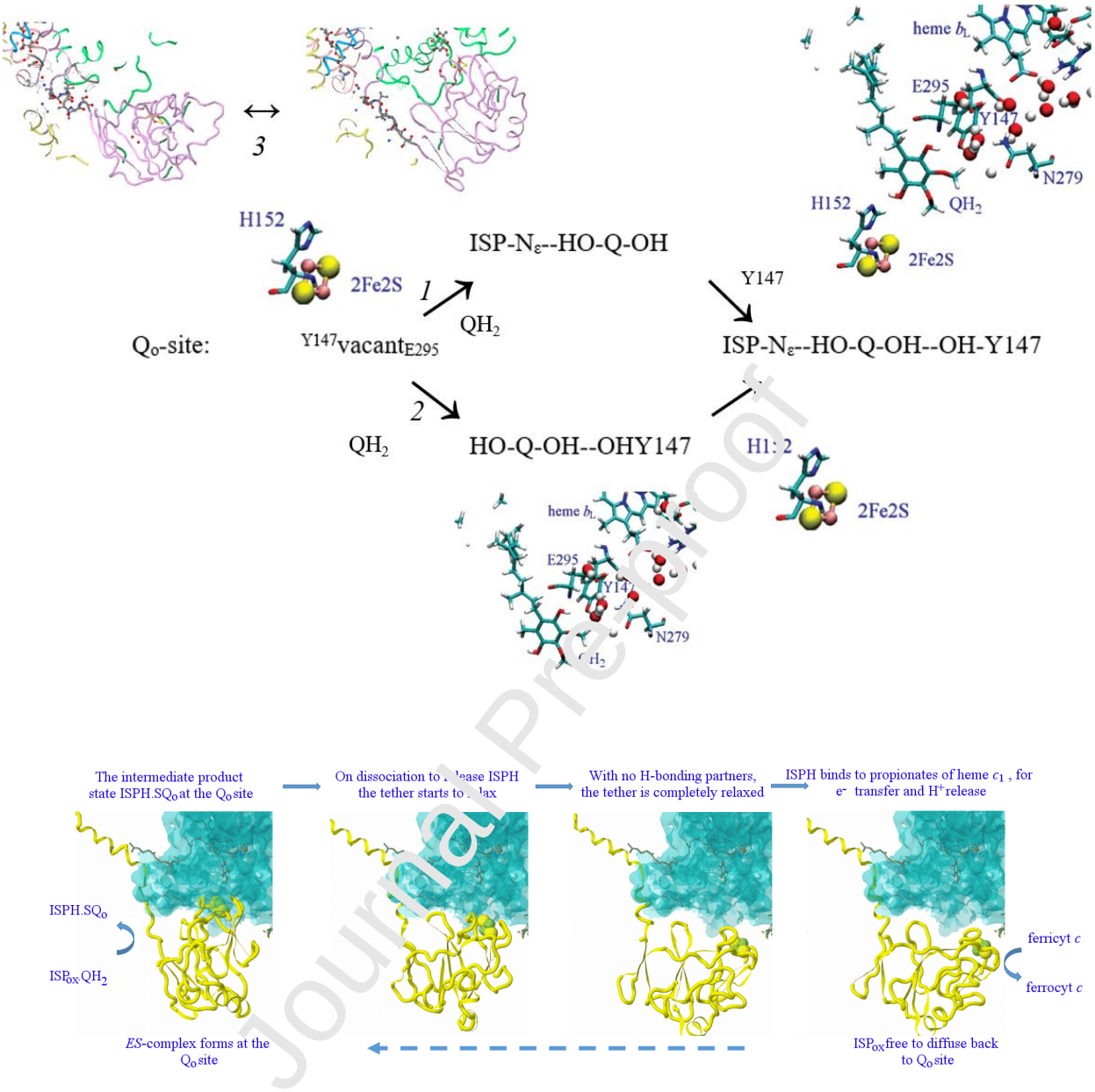

Fig. 12. Scheme showing the formation of the *ES*-complex and the different work terms involved. Top. The different chemical processes and the mechanochemical involvement of the configuration of the linker span. **Bottom.** The different configurations of the "spring" seen in structures, used to illustrate the involvement in formation of the *ES*-complex.

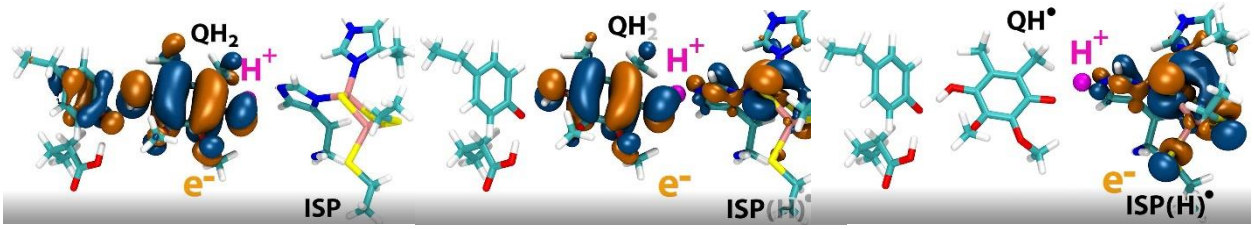

Fig. 13. Frames from a movie showing a QM simulation of the 1st electron and proton transfer. The movie features selected configurations of the Q_o-site taken from quantum chemical geometry optimizations, performed with the use of the B3LYP/6-311G(d) method. The significant residues where the action occurs in each frame, abstracted from a more complete model complex, are, in each of the three frames, Tyr-147 (on the left), QH_2 or $QH^{\bullet}$ (in the middle), and the Fe_2S_2 cluster with its histidine ligands, His-156 (*Rb. capsulatus* numbering), which H-bonds to QH_2, and His-135 (the other ligand) (right). The evolution of the highest occupied molecular orbital (HOMO), obtained for each configuration, shows (left to right) the progress of the electron transfer from the QH_2 donor to the Fe_2S_2 cluster acceptor of the ISP subunit. The proton transfer is depicted by the moving magenta sphere (labeled H^+) going from QH_2 towards the His-156 residue of the ISP. In the initial frame, the HOMO is shared between the tyrosine and QH_2, and the histidine N_ε shows no occupancy of the H; the H^+ is on the QH_2 -OH but is mostly hidden. In the second frame, the H^+ is not yet fully on N_ε, but apparently almost there. The electronic component of the HOMO is lost from the tyrosine, and now shared with the cluster and its ligands. This frame is relatively late in the movie. In the final frame, the HOMO has completely transferred to the cluster and its ligands. As shown, after transfer of an electron and a proton, the QH_2 is now $QH^{\bullet}$, but we are not seeing any of the orbital occupancy reflecting that state. In principle, this is the substrate for the second electron transfer. The movie can be downloaded from the ACS website.

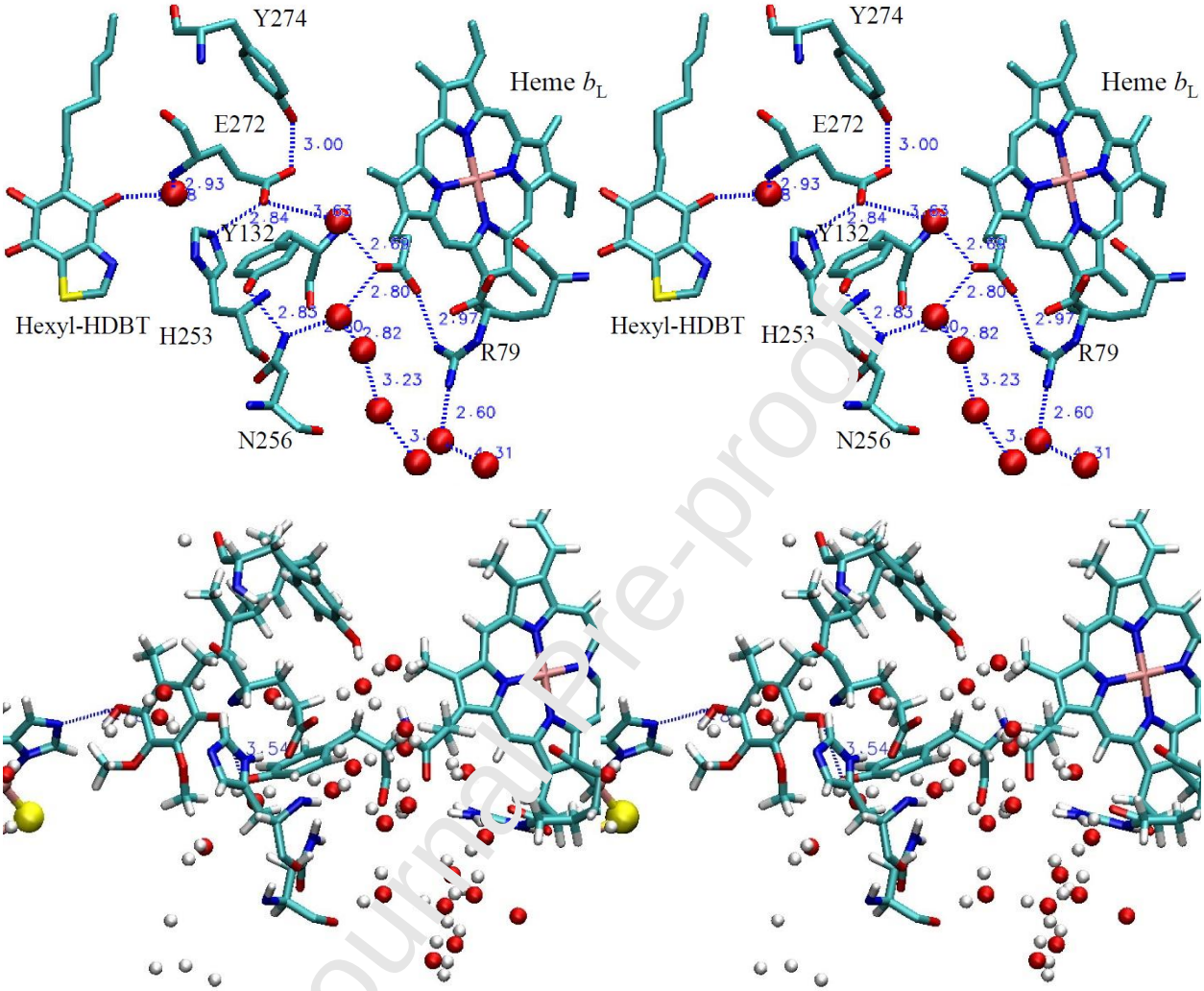

Fig. 14. Putative H^+ exit pathway in yeast bc_1 complex. A. Residues identified as contributing to the proton exit pathway from mutagenesis studies and biophysical and structural analysis [126-129, 180, 203]. The structure is from 1P84, and the role of crystallographic H_2O molecules is taken from the excellent discussion by Palsdottir et al. [203]. **B**. **The pathway seen in an MD simulation of the *ES*-complex in *Rb. sphaeroides* bc_1 complex.** The players shown are those in **A**, but with the inhibitor replaced by QH_2, and crystallographic waters replaced by simulated waters within 6 Å of the residues, equivalent to those labeled in **A.** above, Arg-64, Tyr-147, Asn-276, Glu-295, Tyr-297 of cyt *b*, and His-152 of ISP, also shown (on the left). See text for further discussion. The ISP was in the oxidized form, with His-152 dissociated. With QH_2 present, this represents the metastable condition under which the *ES*-complex can form, as seen here.

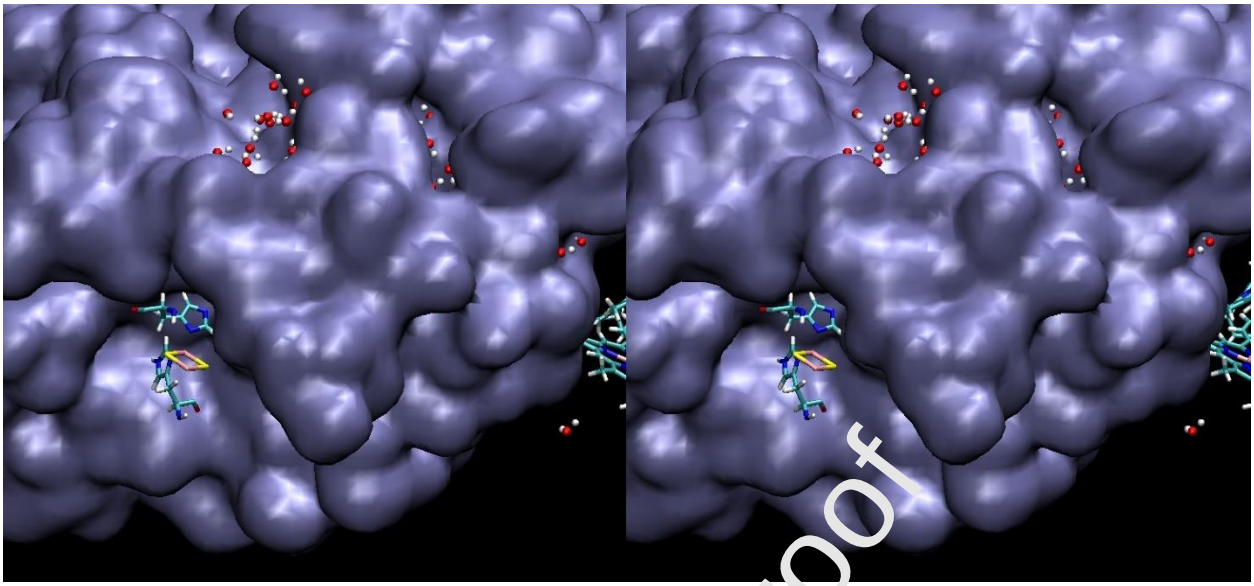

Fig. 15. Looking at the surface of cyt *b* from the perspective of the ISP protein. The Fe_2S_2 cluster and the His-152 though which QH_2 is bound are seen mid-left; the -OH of QH_2 can be seen through the entry port. The visible waters are outside the protein but are connected to the H-bonded network of the Q_o-site in the volume more proximal to the heme. The left-hand cluster reaches up past the His-276 residue, and the right-hand cluster reaches up along the heme propionate A to Glu-295. Note that the volume around the H-bond from His-152 of ISP_{ox} to QH_2, which provides the main force stabilizing the *ES*-complex, is anhydrous. (Compared to Fig. 14, the view is rotated ~-90^o around the *x*-axis, and then ~90^o around the *y*-axis.). As noted in the text, the residue equivalent to His-276 is an aspartate in most mitochondrial complexes, also surface located; it is not obvious whether the location, the polarity or the dissociable character are of importance mechanistically, but it seems unlikely that as surface residue, aspartate would have a p*K* as high as the p*K* ~8.5 seen as controlling the rate of turnover in Glu-295 mutant strains.

Declaration of competing interest

The author declares that he has no conflicts of interest associated with this publication.